



NTNU – Trondheim
Norwegian University of
Science and Technology

Experimental analysis of the pressure characteristic curve of a forced convection boiling flow in single horizontal channel

Dejan Doder

Master of Energy and Environmental Engineering

Submission date: Januar 2013

Supervisor: Carlos Alberto Dorao, EPT

Co-supervisor: Ezequiel Manavela Chiapero, EPT

Norwegian University of Science and Technology
Department of Energy and Process Engineering

EPT-M-2012-26

MASTER THESIS

For Dejan Doder

Stud.techn.
Fall 2012*Experimental analysis of the pressure characteristic curve of a forced convection boiling flow in horizontal channel***Background and objective**

Heat exchangers used in the oil and gas industry, nuclear reactors and power plants operate in the two-phase flow region. When operating in the two-phase region flow boiling instabilities are an undesirable phenomenon and can be a cause of concern. Flow boiling instabilities can be divided into two groups: static and dynamic. They modify the hydrodynamics of the flow, introduce structural vibrations, generate acoustic noise, and can jeopardize the structural integrity of the heat exchanger. Whether some flow instabilities (pressure drop oscillations and Ledinegg instability) occur during forced convective flow boiling depends on total pressure drop versus the mass flux through a channel, and this relationship is called the pressure characteristics curve.

There is a need to do experimental work in the laboratory for comparing experimental results with results from an existing parametric study on the characteristic curve in a boiling channel. The aim of this master's project is to perform experimental work on the effects the inlet pressure, inlet temperature, heating power and heating power distribution has on the pressure characteristic curve for a forced convection two-phase flow in a horizontal channel.

The following task should be considered in the project work:

- A literature study on the behaviour of the pressure characteristic curve and instabilities in forced convection boiling flow.
- Familiarization with the experimental facility and calibration of its equipment.
- Experimental work.
- Error analyse of experimental work.
- Compare experimental results with results from the parametric study

Within 14 days of receiving the written text on the master thesis, the candidate shall submit a research plan for his project to the department.

When the thesis is evaluated, emphasis is put on processing of the results, and that they are presented in tabular and/or graphic form in a clear manner, and that they are analyzed carefully.

The thesis should be formulated as a research report with summary both in English and Norwegian, conclusion, literature references, table of contents etc. During the preparation of the text, the candidate should make an effort to produce a well-structured and easily readable report. In order to ease the evaluation of the thesis, it is important that the cross-references are correct. In the making of the report, strong emphasis should be placed on both a thorough discussion of the results and an orderly presentation.

The candidate is requested to initiate and keep close contact with his/her academic supervisor(s) throughout the working period. The candidate must follow the rules and regulations of NTNU as well as passive directions given by the Department of Energy and Process Engineering.

Pursuant to "Regulations concerning the supplementary provisions to the technology study program/Master of Science" at NTNU §20, the Department reserves the permission to utilize all the results and data for teaching and research purposes as well as in future publications.

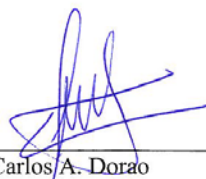
One – 1 complete original of the thesis shall be submitted to the authority that handed out the set subject. (A short summary including the author's name and the title of the thesis should also be submitted, for use as reference in journals (max. 1 page with double spacing)).

Two – 2 – copies of the thesis shall be submitted to the Department. Upon request, additional copies shall be submitted directly to research advisors/companies. A CD-ROM (Word format or corresponding) containing the thesis, and including the short summary, must also be submitted to the Department of Energy and Process Engineering

Department of Energy and Process Engineering, 4.Oktober 2012



Olav Bolland
Department Head



Carlos A. Dorao
Academic Supervisor



Ezequiel M. Chiapero
Co-Supervisor

Preface

This master thesis was written during the final semester of my Energy and Environmental Engineering Master Programme at the Norwegian University of Science and Technology.

First I want to thank the Natural Gas Technology Group at the Department of Energy and Process Engineering for making it possible for me to write a master thesis on this exciting topic. Also, thanks to Statoil for supporting the Two-Phase Instability Project this master thesis is a part of.

I would like to thank my supervisor, prof. Carlos A. Dorao, for the guidance and feedback you has given me through both my master- and project thesis. The care you have for your students is highly appreciated. Thanks to my co-supervisor, Ezequiel M. Chiapero, for always taking time to talk with me and sharing your knowledge with me. I have learnt a lot from you during this master thesis.

Thanks to my father, Nebojša, and my mother, Dunja, for the support you have given me throughout my studies. Your love and encouragement means so much to me - I couldn't have asked for better parents. I am also grateful to my sister, Dina, and the rest of my family for always being there for me.

To all the friends I have made in Trondheim, I want to thank you for the good times we have spent together. I cherish the memories I have with you, and I will always keep them with me. A special thanks to my very good friend and housemate, Andreas, for always staying positive.

Finally, thanks to Vega for making sure that Saturday nights never get boring in Trondheim.

Abstract

Forced convection boiling flow, often referred to as two-phase flow, is a common phenomenon which occurs in many industrial processes. The relationship between the total pressure drop in a channel containing two-phase flow and the mass flux of the flow is known as the pressure characteristic curve. If any part of pressure characteristic curve contains a negative slope, flow instabilities might occur in the channel. Flow instabilities are unwanted because they can reduce the efficiency of the industrial process.

In this study experimental work has been done to analyze the behavior of the pressure characteristic curve in two-phase flow by applying a sensitivity analysis. The parameters which were analyzed in the sensitivity analysis were inlet pressure, subcooling temperature, total heating power and heating power distribution. Also, experimental results from this study were compared with the results from a numerical study of the characteristic pressure curve of two-phase flow [1].

The experimental study showed that all the analyzed parameters influence the behavior of the pressure characteristics curve. The comparison with the numerical study showed the same trends for behavior for the pressure characteristic curve for all analyzed parameters except for the total heating power.

From the analyzed parameters it was shown that the inlet pressure has the largest relative influence on the behavior of the pressure characteristic curve compared to the other parameters. Lowering the inlet pressure leads to the largest change in the mass flux range where flow instabilities can occur. Lowering the inlet pressure also leads to the largest change in the negative slope the pressure characteristic curve.

Sammendrag

Fordampning ved tvungen konveksjon, ofte kalt tofasestrømning, er et fenomen som finnes i mange industrielle prosesser. Forholdet mellom det totale trykkfallet i en kanal med tofasestrømning og massefluksen til strømmingen er kjent som den karakteristiske trykkkurven. Dersom den karakteristiske trykkkurven inneholder et negativ stigningstall, kan strømningsustabiliteter oppstå i kanalen. Strømningsustabiliteter er uønsket fordi de reduserer effektiviteten til den industrielle prosessen.

I dette prosjektet har eksperimentelt arbeid blitt gjort for å analysere oppførselen til den karakteristiske trykkkurven i tofasestrømning ved en følsomhetsanalyse. Parameterne som ble analysert under følsomhetsanalysen var inngangstrykket, underkjølingstemperaturen, den total varmetilførselen og varmefordelingen. De eksperimentelle resultatene ble sammenlignet med resultatene fra et numerisk studium av tofasestrømning[1].

De eksperimentelle resultatene viste at alle de analyserte parameterne påvirket oppførselen til den karakteristiske trykkkurven. Sammenligningen med det numeriske studiet viste de samme trendene for oppførsel til den karakteristiske trykkkurven for alle de analyserte parameterne med unntak av den total varmetilførselen.

Av de analyserte parameterne ble det vist at inngangstrykket har den største relative påvirkningen på oppførselen til den karakteristiske trykkkurven sammenliknet med de andre parameterne. Reduksjon av inngangstrykket leder til den største endringen i området av massefluksen hvor strømningsustabiliteter kan oppstå. Reduksjon av inngangstrykket leder også til den største endringen av det negative stigningstallet til den karakteristiske trykkkurven.

Nomenclature

A_v	Average
c_p	Specific heat capacity [J/kgK]
D	Diameter [m]
f	Frictional factor
Fr	Froude number [-]
g	Gravitational component [m/s ²]
G	Mass flux [kg/sm ²]
H	Height difference [m]
H_{vap}	Heat of vaporization [kJ/kg]
h	Head [m]
I	Current [A]
k	Measurement
L	Pipe length [m]
m	Mass [kg]
\dot{m}	Mass flow rate [kg/s]
MFR	Mass flux range [kg/sm ²]
N	Number of measurements [-]
p	Pressure [Pa]
P	Power [W]
PR	Pressure range [Pa]
Q	Heat [W]
q	Heat flux [W/m ²]
Re	Reynolds number [-]
S	Standard deviation
T	Temperature [K]
t	Shear stress [Pa]
U	Voltage [V]
V	Velocity [m/s]
VOL	Volumetric flow rate [L/s]
w	Random function
y	Random variable
z	Length along pipe [m]
z	Random variable

Greek symbols

α	Kinetic correction factor [-]
ε	Void fraction [-]
θ	Angle with respect to the horizontal [rad]
λ	Error
μ	Dynamic viscosity [kg/ms]
ρ	Density [kg/m ³]
δ	Two-phase multiplier [-]

σ

Surface tension [N/m]

Subscripts

D

Demand

elev

Elevation

Fr

Froude number

fric

Friction

i

Inner

in

inlet

l

Liquid

mom

Momentum

out

Outer

pum

Pump

ran

Random

RMS

Root mean square

S

Supply

sat

Saturated

sys

Systematic

tot

Total

tp

Two-Phase

tur

Turbine

v

Vapor

Table of Contents

Preface	I
Abstract	III
Sammendrag	V
Nomenclature	VII
Table of Contents	IX
List of Figures	XIII
List of tables	XV
1 Introduction	1
1.1 Motivation	1
1.2 Project objectives	1
1.3 Scope.....	2
1.4 Project structure	2
2 Two-phase pressure drop	3
2.1 Modeling two-phase pressure drop	3
2.1.1 Two-phase flow definitions	3
2.1.2 Two-phase flow modeling	4
2.2 Phase flow lengths.....	6
2.2.1 Subcooled liquid throughout whole pipe.....	7
2.2.2 Two-phase liquid in the pipe.....	8
2.2.3 Superheated vapor in the pipe.....	8
3 Flow instabilities	11
3.1 Static flow instability	11
3.2 Necessary conditions the occurrence of the negative slope	14
3.3 Behavior of pressure characteristic curve	16
4 Review on error analysis	17
4.1 Fundamentals of errors in experimental work.....	17
4.2 Types of experimental errors	17
4.2.1 Systematic errors.....	18

4.2.2	Random errors.....	18
4.3	Describing errors in experimental work.....	18
4.3.1	Significant Figures	18
4.3.2	Mean value and standard deviation	18
4.4	Presenting errors	19
5	The experimental facility	21
5.1	The background of the experimental facility	21
5.2	The components of the experimental facility	21
6	Calibration and verification of instruments	29
6.1	Verification of mass flow meters.....	29
6.1.1	Pressure drop inside a horizontal pipe theory.....	29
6.1.2	Experiments on pressure drop in pipe.....	31
6.2	Heat transfer in heating section and electrical power	31
6.2.1	Theory on heat transfer and electrical power	31
6.2.2	Experiments on heat transfer and electrical power	32
7	Experimental work and discussion	33
7.1	Reference case and preliminary experiments.....	33
7.1.1	The reference case	34
7.1.2	Preliminary experiments	35
7.2	The effects of the inlet pressure.....	37
7.3	The effects of the subcooling temperature.....	40
7.4	The effects of heating power.....	44
7.5	The effects of the heating power distribution	47
7.6	Discussion of experimental work	52
8	Conclusion.....	57
References.....		59
Appendices		61
Appendix A.....		61
Appendix B.....		62
Appendix C.....		63
Appendix D.....		64

Appendix E	67
Appendix F	77
Appendix H	78

List of Figures

Figure 1: Three scenarios for how the phases can be organized in the flow inside a heated pipe with subcooled liquid at the inlet [1]	6
Figure 2: Sketch of boiling system [2]	12
Figure 3: Typical pressure characteristic curve and supply curve for boiling system [2]	12
Figure 4: Sketch of accuracy and precision in experimental measurements [13]	17
Figure 5: Sketch of an error bar	19
Figure 6: Sketch of the experimental facility	22
Figure 7: Main tank	23
Figure 8: Pump with engine	23
Figure 9: Sketch of heated test section	24
Figure 10: Heated test section	24
Figure 11: The visualization glass	25
Figure 12: Adiabatic test section	25
Figure 13: The condenser	26
Figure 14: Sketch of pressure drop measurements	29
Figure 15: Sinusoidal voltage (upper), current (middle) and power (lower) in an electric circuit element	32
Figure 16: Reference case: $p = 8.5$ bar, $T_{sub} = 30^\circ\text{C}$, $Q = 1000$ W (uniform)	34
Figure 17: Preliminary experiment for low inlet pressure. (Left: Subcooling temperature. Middle: Pressure at inlet. Right: Mass flow rate vs. Pressure drop in pipe.)	35
Figure 18: Preliminary experiment for high subcooling temperature. (Left: Subcooling temperature. Middle: Pressure at inlet. Right: Mass flow rate vs. Pressure drop in pipe.)	36
Figure 19: Low inlet pressure: $p = 6.5$ bar, $T_{sub} = 30^\circ\text{C}$, $Q = 1000$ W (uniform)	37
Figure 20: High inlet pressure: $p = 10.5$ bar, $T_{sub} = 30^\circ\text{C}$, $Q = 1000$ W (uniform)	38
Figure 21: Comparing reference case with plots of lower and higher inlet pressure	39
Figure 22: Low subcooling temperature: $p = 8.5$ bar, $T_{sub} = 20^\circ\text{C}$, $Q = 1000$ W (uniform) ..	40
Figure 23: High subcooling temperature: $p = 8.5$ bar, $T_{sub} = 40^\circ\text{C}$, $Q = 1000$ W (uniform) .	41
Figure 24: Comparing reference case with plots of lower and higher subcooling temperature	42
Figure 25: Outlet mass quality for reference case, low subcooling temperature and high subcooling temperature	43
Figure 26: Low heating power: $p = 8.5$ bar, $T_{sub} = 30^\circ\text{C}$, $Q = 500$ (uniform)	45
Figure 27: High heating power: $p = 8.5$ bar, $T_{sub} = 30^\circ\text{C}$, $Q = 1500$ W (uniform)	46
Figure 28: Comparing reference case with plots of lower and higher heating power	47
Figure 29: Step-wise increasing heating distribution	48
Figure 30: Step-wise increasing heating distribution: $p = 8.5$ bar, $T_{sub} = 30^\circ\text{C}$, $Q = 1000$ W (step-wise increasing)	49

Figure 31: Step-wise decreasing heating distribution.....	50
Figure 32: Step-wise decreasing heating power distribution: $p = 8.5$ bar, $T_{sub} = 30$ °C, $Q = 1000$ W (step-wise decreasing)	50
Figure 33: Comparing reference case with plots of step-wise increasing and decreasing heating power distributions	51
Figure 34: Typical pressure characteristic curve for two phase flow with indicated mass flux range (MFR) and pressure range (PR)	53
Figure 35: Inlet pressure effect on MFR.....	54
Figure 36: Subcooling temperature effect on MFR.....	54
Figure 37: Total heating power effect on MFR	54
Figure 38: Heating power distribution effect on MFR	55
Figure 39: Pressure-Enthalpy diagram for R-134a [18].....	61
Figure 40: Moody diagram [19].....	62
Figure 41: Diagram of complete two-phase experimental facility	63
Figure 42: Voltage calibration of Heater 1	64
Figure 43: Voltage calibration of Heater 2	64
Figure 44: Voltage calibration of Heater 3	65
Figure 45: Voltage calibration of Heater 4	65
Figure 46: Voltage calibration of Heater 5	66
Figure 47: LabVIEW screenshot.....	68
Figure 48: Contactor.....	69
Figure 49: Water sink	69
Figure 50: Locker	70
Figure 51: Heat exchangers (K6 on the left and K9 on the right).....	71
Figure 52: Heat exchanger panel	72
Figure 53: By-pass valve for pump	72
Figure 54: Instrumentation panel	73
Figure 55: Panel for heating section, right door	74
Figure 56: Inside heating locker	75
Figure 57: Panel for heating section, left door	76
Figure 58: Density as function of pressure for R-134a (values from REFPROP)	77
Figure 59: Verification of mass flow meter F1	78
Figure 60: Verification of mass flow meter F2	78

List of tables

Table 1: Parameter range of experimental facility	26
Table 2: Lower and upper limits of parameters for sensitivity analysis	37
Table 3: Summary of the effect of the pressure characteristic curve.....	52
Table 4: Mass flux ranges and pressure ranges for parameter slopes from the sensitivity analysis	53
Table 5: Sensitivity analysis for MFR	55
Table 6: Sensitivity analysis of PR.....	56
Table 7: Polynomial equations from measurements from calibration of heaters	66

1 Introduction

Forced convection boiling occurs when the saturation temperature of a flowing fluid in contact with a hot surface is exceeded. This leads to the formation of vapor bubbles in the fluid which means that the fluid contains a mixture of liquid and vapor. A flow containing both liquid and vapor is referred to as two-phase flow. Two-phase flow is common in heat exchangers in cryogenic and refrigeration processes, oil and gas pipelines and nuclear reactors. The pressure characteristic curve (also known as the S-curve, N-curve, internal curve and demand curve) of a two-phase flow system is defined as the relationship between the total pressure drop through the pipe and the mass flux [2]. Two-phase flow instabilities are undesirable phenomenon because they can lead to difficulties with the control of a system. Most two-phase flow instabilities can only occur in the region of the pressure characteristic curve that has negative gradients. The aim of this study is to experimentally investigate the pressure characteristic curve of two-phase flow in a single horizontal pipe on an existing experimental facility. The influence of the inlet pressure, subcooling temperature, applied heat and heat distribution will be analyzed. Moreover, the experimental results will be compared with the results of an existing numerical study on the pressure characteristic curve [1].

1.1 Motivation

Two-phase flow is a widely studied topic due to the importance it has in industry: In coal and gas power plants large boilers are connected to steam turbines which are used to generate electricity, nuclear reactors remove heat from the reactor core using two-phase water and pipelines transferring oil and gas might contain fluids in the two-phase region. The refrigerant R-134a is of special interest for design of refrigerator and air conditioners because it is an ozone-safe refrigerant [3]. The challenge with operating with two-phase flow is that under some circumstances flow instabilities might occur. In heat exchangers flow instabilities reduce the efficiency of heat transfer because they can cause mechanical vibrations, problems with control systems and lead to burn out of heat exchanger surfaces. Since most flow instabilities only are possible under conditions where the pressure characteristics curve has a negative slope, it is crucial to understand the behavior of the relationship between the total pressure drop and the mass flux in order to avoid them. Understanding the behavior of the pressure characteristic curve ensures the safety and the efficiency of industrial processes, which implies economic benefits.

1.2 Project objectives

The aim of this study is to experimentally analyze the behavior of the pressure characteristics curve of two-phase flow in a single, heated horizontal pipe. The effects of varying the following parameters will be analyzed: inlet pressure, subcooling temperature,

heating power and heating power distribution. The experimental results will be compared with the results an existing numerical study.

1.3 Scope

The experimental work in this study will solely be on the pressure characteristic curve of boiling two-phase flow through a single horizontal pipe with an inner radius of 5mm . The working fluid is R-134a. There will not be done any experimental work on flow instabilities in two-phase flow in this study.

1.4 Project structure

A literature review on two-phase pressure drop is given in Chapter 2. Modeling of two-phase flow and phase flow lengths are discussed in this chapter.

Two-phase flow instabilities are presented in Chapter 3. The different types of flow instabilities and the conditions for them to occur are discussed in this chapter.

Theory of error analysis is presented in Chapter 4. The types of errors and presentation of errors in experimental work is discussed in this chapter.

Chapter 5 describes the experimental facility where the experiments are done.

Chapter 6 deals with calibration and validation of instrumentation on the experimental facility.

Chapter 7 presents the experimental work done on the pressure characteristic curve of a forced boiling flow. The experimental results are explained and discussed.

Chapter 8 presents the conclusions drawn from this experimental study.

2 Two-phase pressure drop

Two-phase flow is defined as simultaneous movement of two phases through a closed channel. Even though it can be any two phases, often two-phase flow is referred to as the combination of liquid and vapor. Pressure will change along the path of two-phase flow due to changes in energy in the fluid along the path, and due to the interaction of the fluid and the surface of the channel it flows through. In this chapter a review on pressure drop in two-phase flow inside a pipe is presented [4]. Both the modeling of pressure drop and phase flow lengths will be discussed in this chapter. This review is presented to broaden the understanding of pressure drop in two-phase flow, and thereby enhance the understanding the behavior of the pressure characteristic curve.

2.1 Modeling two-phase pressure drop

Pressure drop in a two-phase flow occurs due to variations of the kinetic and potential energy of the flowing fluid, and due to friction between the fluid and the surface of the flow channel. Two models for modeling two-phase flow exist; the homogeneous flow model and the separated flow model. The main difference between the models is that in the homogeneous flow model the two phases (liquid and vapor) are assumed to have the same velocity and density, while in the separated flow model the two phases are considered to be artificially separated into two streams, each flowing in its own channel. The homogeneous model is suitable only for high mass flux values (greater than 2000 kg/m^2). The equations for the separated flow model do not depend upon the particular flow configuration. The separated flow model assumes that the velocity of each phase is constant in the given cross-section, and within the zone occupied by the phase. Only the separated flow model will be presented because it is more suitable for the experimental work of this study.

2.1.1 Two-phase flow definitions

Before taking a closer look at what needs to be considered when modeling two-phase flow, two definitions which are of importance in two-phase flow will be presented first. The first definition is the Reynolds number. The Reynolds number is a dimensionless number which gives a measure of the ratio of the internal forces to viscous forces, and thereby tells whether a flow is laminar or turbulent. The Reynolds number is defined as:

$$Re = \frac{\dot{m}D_i}{\mu} \quad \text{(Equation 1)}$$

In (Equation 1) Re is the Reynolds number, \dot{m} is the total mass flow rate of liquid and vapor, D_i is the inner diameter of the pipe and μ is the dynamic viscosity. The second important definition is the mass quality. Mass quality is the ratio of the mass of the vapor to the total mass of the two-phase mixture:

$$x = \frac{m_v}{m_v + m_l} \quad \text{(Equation 2)}$$

In (Equation 2) x is the mass quality, m_v is the mass of vapor and m_l is the mass of liquid. The mass quality tells something about the relationship between the vapor and the liquid in the two-phase flow.

2.1.2 Two-phase flow modeling

When modeling two-phase flow inside a pipe we must consider three components which cause the total pressure to change in the fluid throughout the path of the flow. The total pressure drop in a two-phase flow is the sum of the following 3 components: momentum, elevation and friction. The total pressure drop in the pipe is found by adding these three components:

$$\Delta p_{tot} = \Delta p_{mom} + \Delta p_{elev} + \Delta p_{fric} \quad \text{(Equation 3)}$$

In (Equation 3) Δp_{tot} is the total pressure drop, Δp_{mom} is the momentum component, Δp_{elev} is the elevation component and Δp_{fric} is the friction component. The influence each component has on the total pressure drop in the two-phase flow depends on the properties and conditions of the fluid, and the orientation of the pipe the fluid is flowing inside. Each of the pressure components will be discussed next.

The momentum component is associated with a change in the kinetic energy of the fluid. Since vapor tends to flow at a higher velocity than liquid, the vapor changes the momentum of the flow. Therefore the ratio between liquid and vapor in the flow will influence the momentum component. The momentum pressure component is defined as:

$$\Delta p_{mom} = \dot{m}^2 \left\{ \left[\frac{(1-x)^2}{\rho_l(1-\varepsilon)} + \frac{x^2}{\rho_v} \right]_{out} - \left[\frac{(1-x)^2}{\rho_l(1-\varepsilon)} + \frac{x^2}{\rho_v} \right]_{in} \right\} \quad \text{(Equation 4)}$$

In (Equation 4) \dot{m} is the total mass flow rate of the liquid and the vapor, ε is the void fraction, ρ_l is the density of the liquid and ρ_v is the density of the vapor. ε defines the relationship between liquid and vapor in the two-phase flow, and Steiner (1993) proposed the following expression for ε :

$$\varepsilon = \frac{x}{\rho_v} \left\{ [1 + 0.12(1-x)] \left[\frac{x}{\rho_l} + \frac{1-x}{\rho_l} \right] + \frac{1.18(1-x)[g\sigma(\rho_l - \rho_v)]^{0.25}}{\dot{m}^2 \rho_l^{0.5}} \right\}^{-1} \quad \text{(Equation 5)}$$

In (Equation 5) g is the gravitational constant (9.81 m/s^2) and σ is the surface tension.

The elevation component is associated with a change in the static pressure of the flow. It is relevant for flows where there is a change in the elevation, meaning all flows which are not strictly horizontal. The elevation pressure component is defined as:

$$\Delta p_{elev} = \rho_{tp} g H \sin(\theta) \quad \text{(Equation 6)}$$

In (Equation 6) H is the vertical height difference, θ is the angle with respect to the horizontal and ρ_{tp} is the two-phase density which is defined as:

$$\rho_{tp} = \rho_l(1 - \varepsilon) + \rho_v \varepsilon \quad \text{(Equation 7)}$$

If the channel of the two-phase flow is strictly horizontal Δp_{elev} equals 0, meaning that the elevation component does not have any influence on the pressure drop in the pipe. For a strictly vertical flow $\sin(\theta)$ equals 1. In this study Δp_{elev} will always be 0 because the orientation of the pipe in the experimental work is strictly horizontal.

The frictional component is associated with viscous effects generated due to the interaction between the fluid and the surface of the pipe the fluid flows inside. The frictional component is the most complex of the three pressure components. Grönnerud (1972) proposed a correlation for the frictional pressure component, which is developed specially for refrigerants. The correlation is based on the formula for pressure drop through a pipe containing one-phase liquid with the two-phase multiplier (δ). For one-phase liquid flow the frictional pressure drop is defined as:

$$\Delta p_l = 4f_l \left(\frac{L}{D_i} \right) \dot{m}^2 \left(\frac{1}{2} \rho_l \right) \quad \text{(Equation 8)}$$

In (Equation 8) f_l is the frictional factor for the liquid and L is the length of the pipe. Grönnerud correlated the frictional component for two-phase flow as by using the two-phase multiplier:

$$\Delta p_{fric} = \delta \Delta p_l \quad \text{(Equation 9)}$$

In (Equation 9) the two-phase multiplier δ , is defined as:

$$\delta = 1 + \left(\frac{dp}{dz} \right)_{Fr} \left[\frac{\left(\frac{\rho_l}{\rho_v} \right)}{\left(\frac{\mu_l}{\mu_v} \right)^{0.25}} - 1 \right] \quad \text{(Equation 10)}$$

In (Equation 10) $\left(\frac{dp}{dz} \right)_{Fr}$ is the frictional pressure gradient and it depends on the Froude number. The frictional pressure gradient is defined as:

$$\left(\frac{dp}{dz}\right)_{Fr} = f_{Fr} [x + 4(x^{1.8} - x^{10} f_{Fr}^{0.5})] \quad \text{(Equation 11)}$$

In (Equation 11) f_{Fr} is the Froude friction factor. The Froude number is a dimensionless number which for one-phase liquid flow is defined as:

$$Fr_l = \frac{\dot{m}^2}{gD_i\rho_l^2} \quad \text{(Equation 12)}$$

In (Equation 12) Fr_l is the liquid Froude number. The Froude friction factor depends on the value of the Froude number. If $Fr_l \geq 1$, then $f_{Fr} = 1$, or if $Fr_l < 1$, then:

$$f_{Fr} = Fr_l^{0.3} + 0.0055 \left[\ln\left(\frac{1}{Fr_l}\right) \right]^2 \quad \text{(Equation 13)}$$

It should be noted from (Equation 10) that the frictional pressure component for two-phase is always larger than for one-phase liquid. The reason for this is that δ is always larger than 1 in two-phase flow.

To further understand and study the behavior of two-phase flow it is useful to analyze the factors influencing the lengths of each phase in the pipe, and this topic will be discussed next.

2.2 Phase flow lengths

When subcooled liquid enters a heated pipe there are three possible scenarios for how the phases are organized in the pipe. The three possible phases are subcooled liquid, two-phase and superheated vapor. Figure 1 shows the three possible scenarios for how the phases can be organized when the fluid enters as subcooled liquid. The length a phase occupies in the pipe is called a phase flow length.

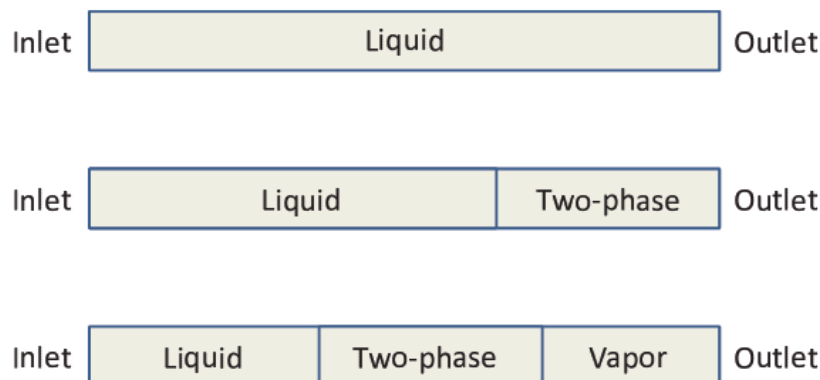


Figure 1: Three scenarios for how the phases can be organized in the flow inside a heated pipe with subcooled liquid at the inlet [1]

In the first scenario (upper sketch in Figure 1) either the heat flux is too low or the mass flux is too high for the subcooled liquid to exceed its saturation temperature and change into two-phase before the outlet of the pipe. This means that the fluid stays in the subcooled liquid phase through the whole pipe and exits as subcooled liquid. The phase flow length of the subcooled liquid equals the length of the pipe.

In the second scenario (middle sketch in Figure 1) either the heat flux is high enough or the mass flux low enough for the fluid to exceed its saturation temperature and start boiling before it reaches the outlet of the pipe. This means that there is a mixture of vapor and liquid in the pipe, with the subcooled liquid preceding the two-phase. As the heat flux is increased or the mass flux decreased, the length of the two-phase flow region will grow from the outlet towards the inlet of the pipe. The phase flow lengths of both subcooled liquid and two-phase depend on the heat flux and the mass flux.

In the third scenario (lower sketch in Figure 1) the heat flux is high enough or the mass flux low enough for the fluid to boil completely and turn into superheated vapor before the outlet of the pipe. The phase flow length of the subcooled liquid, two-phase and superheated vapor will depend on the amount of heat added and the mass flux.

To understand the factors affecting the phase lengths it is necessary to set energy balances for each scenario, and this will be done next.

2.2.1 Subcooled liquid throughout whole pipe

In the first scenario the fluid remains as subcooled liquid throughout the whole pipe. The following energy balance for the first scenario can be set by analyzing the one-phase liquid region [5]:

$$Q = \dot{m}c_p(T_{sat} - T_{in}) \quad \text{(Equation 14)}$$

In (Equation 14) Q is the heat added to the flow, c_p is the specific heat capacity of the liquid, T_{sat} is the saturation temperature of the fluid at the pressure of the flow and T_{in} is the inlet temperature of the subcooled liquid. We can introduce mass flux, which is defined as the ratio of the mass flow to the cross sectional area of the pipe. The mass flux in a circular pipe is defined as:

$$G = \frac{\dot{m}}{(\pi D_i^2/4)} \quad \text{(Equation 15)}$$

In (Equation 15) G is the mass flux. We can also introduce the heat flux which is the ratio of the heat to the outer area of the pipe:

$$q = \frac{Q}{\pi L D_o} \quad \text{(Equation 16)}$$

In (Equation 16) q is the heat flux and D_o is the outer diameter of the pipe. An expression for the phase flow length required for boiling to occur is found when we combine (Equation 15) and (Equation 16). This expression is then inserted into (Equation 14) and solved for L :

$$L_l = \frac{G}{q_w} \frac{D_i^2}{4D_o} c_p (T_{sat} - T_{in}) \quad \text{(Equation 17)}$$

In (Equation 17) the term $(T_{sat} - T_{in})$ is often referred to as the subcooling temperature. L_l is the required length for experiencing boiling at the outlet of the pipe. If L_l is larger than the length of the pipe, the liquid will remain as subcooled liquid. If L_l is equal to the length of the pipe, boiling will occur at the outlet of the pipe where the fluid will be saturated liquid. If L_l is smaller than the length of the pipe, the fluid will enter the two-phase region at L_l and the fluid might even be superheated vapor at the outlet.

2.2.2 Two-phase liquid in the pipe

In the second scenario there is both subcooled liquid and two-phase fluid in the pipe. The following energy balance can be set for the two-phase flow length:

$$Q = \dot{m} H_{vap} \quad \text{(Equation 18)}$$

In (Equation 18) H_{vap} is the heat of vaporization. The heat of vaporization is the required energy to transform an amount of liquid into vapor. When introducing the mass flux and the heat flux into (Equation 18), and solve for the length of needed for evaporating the whole fluid we get:

$$L_{tp} = \frac{G}{q_w} \frac{D_i^2}{4D_o} H_{vap} \quad \text{(Equation 19)}$$

In (Equation 19) L_{tp} is the length needed to evaporate the whole refrigerant, meaning that it is in the condition of saturated vapor at the outlet.

2.2.3 Superheated vapor in the pipe

In the third scenario there is subcooled liquid, two-phase fluid and superheated vapor in the channel. The flow length of the superheated vapor is defined as the total length of the pipe minus the lengths occupied by the subcooled liquid and the two-phase floe. The length of the superheated vapor phase is defined as:

$$L_{sv} = L - L_l - L_{tp} \quad (\text{Equation 20})$$

In (Equation 20) L_{sv} is the length of the superheated vapor phase and L is the total length of the pipe. In this study the phase flow length of superheated vapor is not of interest because the focus is two-phase flow.

3 Flow instabilities

As mentioned in the Chapter 1.3 no experiments on flow instabilities will be performed during this study. However, a review on flow instabilities is presented in this chapter for the purpose of obtaining a broader understanding on the topic of two-phase flow where flow instabilities play an important role. This review on two-phase flow instabilities is based on references [1, 6, 7]. Information and figures obtained from other sources are indicated in the text. Also, the necessary conditions for flow instabilities to occur and the behavior of the pressure characteristic curve are discussed here.

Flow instabilities are an undesired and problematic phenomenon in all systems involving two-phase flow such as cryogenic and refrigeration processes and nuclear reactors. Flow instabilities can cause mechanical vibrations, problems of system control and lead to burn out and breakage of equipment. All this leads to a reduced efficiency of industrial processes and therefore economic losses. A flow is defined as stable if after small perturbations, its new operating conditions tend asymptotically towards the initial ones. If this is not the case, the flow is defined as unstable, meaning that it is exposed to flow instabilities. Flow instabilities can be divided into two main groups: static and dynamic flow instabilities. Only static flow instabilities will be discussed here.

3.1 Static flow instability

A flow is subject to static instability if a small change from its equilibrium point results in the flow not having a steady-state condition nearby the original state, causing the system to move to a different steady-state condition. The most important static flow instability is the Ledinegg instability, which is also called flow excursion instability. The Ledinegg instability involves a sudden change in the mass flow rate, and it can be explained by considering the sketch of a boiling system in Figure 2.

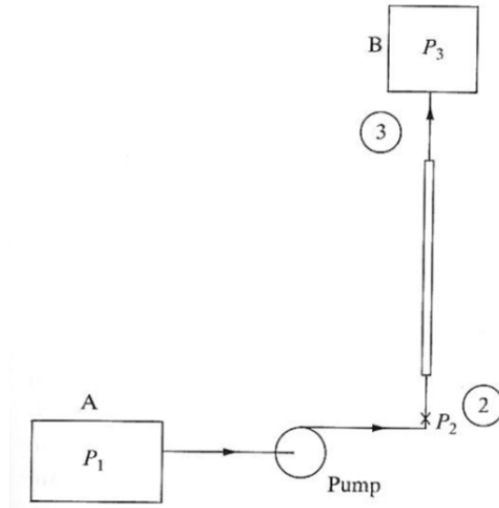


Figure 2: Sketch of boiling system [2]

Figure 2 shows a boiling system where a subcooled liquid is being pumped from reservoir A at pressure P_1 , to a higher pressure P_2 at point 2. Between points 2 and 3 the fluid is heated in a pipe at a constant heat flux. When exiting the heated pipe, and entering reservoir B, the pressure of the fluid is P_3 . Figure 3 shows a possible relationship between the total pressure drop and the mass flow in the heated pipe. In Figure 3 x-axis gives the mass flow rate and the y-axis gives the total pressure drop.

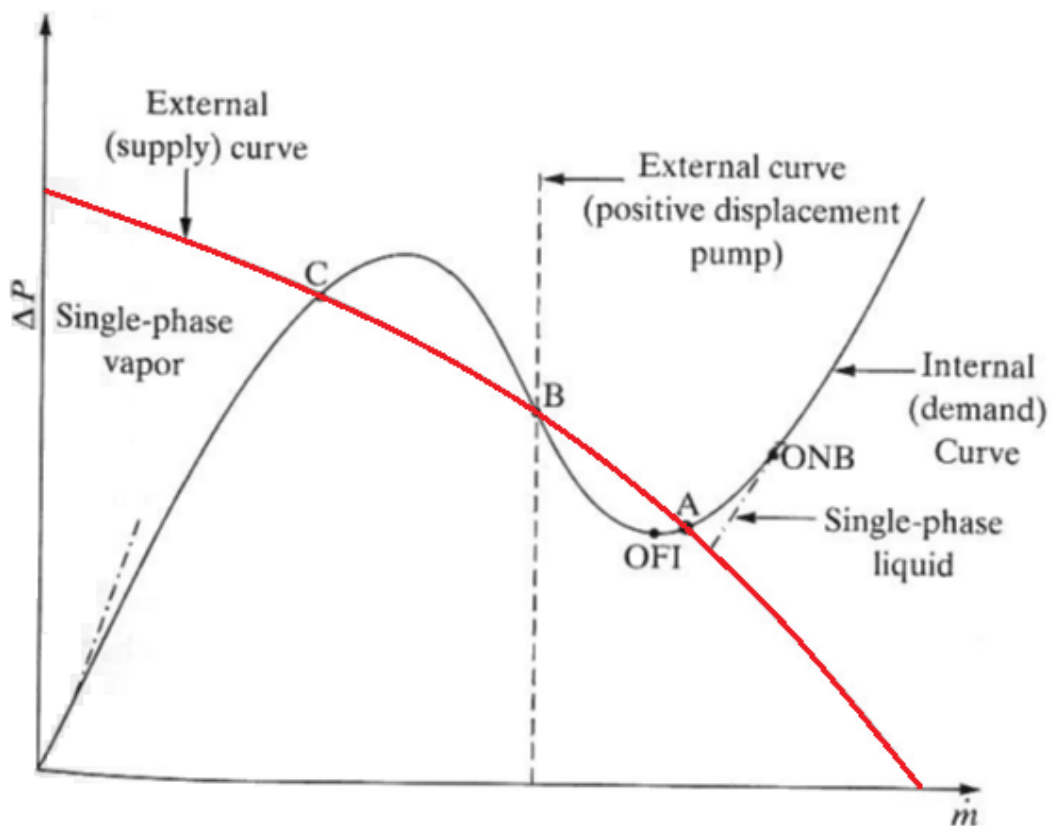


Figure 3: Typical pressure characteristic curve and supply curve for boiling system [2]

It should be noted that the shape of the heated pipe pressure drop depends on many factors. The black curve is the total pressure drop ($P_2 - P_3$) in the heated pipe plotted as a function of the mass flow rate (\dot{m}). Under given conditions the pressure drop in the heated channel sometimes has an N-shape look (also referred to as an S-shape). This N-shaped curve is called the pressure characteristic curve (or demand curve), and it gives the needed pressure difference ($P_2 - P_3$) to drive the flow through the heated pipe. In this study the relationship between the total pressure drop through the pipe and the mass flow will always be called the pressure characteristic curve.

The red curve in Figure 3 is called the supply curve and it is a typical $\Delta P - \dot{m}$ characteristic behavior of a pump which drives the flow. When considering the right side of the pressure characteristic curve in Figure 3 it can be seen that at very high mass flow rates the fluid stays in the subcooled liquid state throughout the whole heated pipe. When decreasing the mass flow, eventually the *onset of nucleate boiling* (ONB) point will be reached. Reaching the ONB point means that the saturation temperature of the fluid is exceeded, and the fluid starts to boil. Boiling will occur at the outlet of the heated channel represented with a two-phase flow region. By reducing the mass flow rate further the two-phase phase length will grow from the outlet of the pipe and towards the inlet. The lowest point of the pressure characteristic curve is called the *onset of flow instability* (OFI) point. A reduction of mass flow beyond the OFI point can lead to an increase in ($P_2 - P_3$). This increase in pressure drop with decreasing mass flow rate occurs because the frictional and momentum components of the pressure drop are larger for two-phase flow than for subcooled liquid. At very low mass flow rates, on the left side of Figure 3, ($P_2 - P_3$) is again reduced. Steady state operation implies that that the $\Delta P -$ values for the supply and demand curve are the same, and these values are seen in Figure 3 as the points where the black and red curve intersect (points A, B and C). The system is unstable if the slope of the demand curve is more negative than the slope of the supply curve. This occurs because the pump cannot counteract even a small perturbation in the mass flow from the steady-state. A mathematical expression for this flow instability criterion is:

$$\frac{\partial \Delta p_S}{\partial \dot{m}} \leq \frac{\partial \Delta p_D}{\partial \dot{m}} \quad \text{(Equation 21)}$$

In (Equation 21) Δp_S is the supply pressure difference and Δp_D is the demand pressure difference. In Figure 3 the intersection points A and C lie where the slope of the supply curve is more negative than the slope of the demand curve. This means that a perturbation in \dot{m} in those points causes an imbalance in the supply and demand values of ΔP that brings the system back to its original steady-state. However, intersection point B lies where the slope of the supply curve is less negative than the slope of the demand curve, and it is therefore unstable. A small positive perturbation of \dot{m} will cause the system to move to the steady state point A, while a small negative perturbation in \dot{m} will cause the system to move to the steady-state point C.

A sudden change in mass flow rate can reduce the efficiency of a heat transferring process since it may lead to burnout of the surface. Theoretically a flow could remain stable in an unstable area as defined in (Equation 21) if the flow was not subjected to any perturbations. However, in reality a flow will always experience small perturbations due to turbulence, nucleation or slug flow.

3.2 Necessary conditions for the occurrence of the negative slope

Next we will take a closer look at the condition which is necessary for the occurrence of a negative slope in the pressure characteristic curve, which is the criterion for flow instabilities to occur. All the derived equations in this section are from [1]. A negative slope in the pressure characteristic curve is mathematically defined as:

$$\frac{d\Delta P}{dG} < 0 \quad \text{(Equation 22)}$$

In (Equation 22) ΔP is the total pressure difference in the pipe and G is the mass flux. It is possible to state that the total pressure difference along the pipe is a function of the mass flux and the outlet mass quality:

$$\Delta P = \Delta P[G, x_{out}(G)] \quad \text{(Equation 23)}$$

In (Equation 23) x_{out} is the outlet mass quality of the flow. The outlet quality is itself a function of the mass flux. To further analyze this condition, we use the total derivative. For a function $w(y, z)$, the total derivative of the function is defined as [8]:

$$\frac{dw}{dy} = \frac{\partial w}{\partial y} + \frac{\partial w}{\partial z} \frac{dz}{dy} \quad \text{(Equation 24)}$$

When inserting (Equation 23) into (Equation 24), we can define the condition for the negative slope as:

$$\frac{d\Delta P}{dG} = \frac{\partial \Delta P}{\partial G} + \frac{\partial \Delta P}{\partial x_{out}} \frac{dx_{out}}{dG} \quad \text{(Equation 25)}$$

For a negative slope to occur in the pressure characteristic curve there has to be two-phase flow at the outlet of the pipe, meaning that $0 \leq x_{out} \leq 1$. It is possible to divide the total pressure drop in the pipe into two terms: the pressure drop in the subcooled liquid flow region and the pressure drop in the two-phase flow region:

$$\Delta P[G, x_{out}(G)] = \Delta P_l[G, x_{out}(G)] + \Delta P_{tp}[G, x_{out}(G)] \quad \text{(Equation 26)}$$

In (Equation 26) ΔP_l is the pressure drop in the subcooled liquid and ΔP_{tp} is the pressure in the two-phase flow. When combining (Equation 22), (Equation 25) and (Equation 26), and introducing phase flow lengths we get:

$$\frac{\partial \Delta P_l}{\partial G} + \frac{\partial \Delta P_{tp}}{\partial G} < \left(\frac{\partial \Delta P_l}{\partial L_l} - \frac{\partial \Delta P_{tp}}{\partial L_{tp}} \right) \frac{\partial L_{tp}}{\partial x_{out}} \frac{dx_{out}}{dG} \quad \text{(Equation 27)}$$

In (Equation 27) we will always have the following 5 conditions:

$$\frac{\partial \Delta P_l}{\partial G} > 0 \quad \text{(Equation 28)}$$

$$\frac{\partial \Delta P_{tp}}{\partial G} > 0 \quad \text{(Equation 29)}$$

$\frac{\partial \Delta P_l}{\partial G}$ and $\frac{\partial \Delta P_{tp}}{\partial G}$ in (Equation 28) and (Equation 29) will always be larger than 0 because if the outlet mass quality is kept constant, an increase in the mass flux will result in an increase in the pressure drop for both one-phase liquid and two-phase.

$$\left(\frac{\partial \Delta P_l}{\partial L_l} - \frac{\partial \Delta P_{tp}}{\partial L_{tp}} \right) \leq 0 \quad \text{(Equation 30)}$$

From (Equation 30) it can be seen that the pressure drop related to two-phase flow as a function of only the phase flow length of the two-phase will always be larger than the pressure drop of the one-phase liquid related only to the phase flow length of the liquid. (Equation 30) is related to the inlet pressure of the fluid.

$$\frac{\partial L_{tp}}{\partial x_{out}} \geq 0 \quad \text{(Equation 31)}$$

From (Equation 31) it can be seen that as x_{out} increases, the length of phase flow length of the two-phase flow will increase until $x_{out} = 1$. When x_{out} decreases, the phase flow length of the two-phase will decrease until $x_{out} = 0$. At $x_{out} = 0$ the phase flow length of the two-phase will vanish and there will only be liquid one-phase fluid in the pipe, when neglecting subcooled boiling. (Equation 31) is related to the heating power distribution.

$$\frac{dx_{out}}{dG} \leq 0 \quad \text{(Equation 32)}$$

From (Equation 32) it can be observed that the mass quality at the outlet will decrease with increasing mass flux. (Equation 32) is related to the subcooling temperature of the fluid.

Next the behavior of the pressure characteristic curve with the influence of different parameters will be discussed.

3.3 Behavior of pressure characteristic curve

This section reviews the available literature on how different parameters relevant for this study affect the behavior of the pressure characteristics curve. The literature review is based on experimental work done by others on boiling two-phase flow.

The inlet pressure plays an important role in the pressure characteristic curve. Increasing inlet pressure results in a flatter shape of the pressure characteristic curve, while a lower inlet pressure results in a steeper negative pressure gradient in the pressure characteristic curve [9].

The subcooling temperature is also of relevance in two-phase flow. When the subcooling temperature is increased, the negative slope of the pressure characteristic curve becomes steeper. A decrease in the subcooling temperature results in it becoming flatter. This is the case for both horizontal flow [10] and vertical flow [11].

The heating power applied to the surface of the flow has a relative effect on the pressure characteristic curve for horizontal flow [12]. This means that the shape of the pressure characteristic curve remains the same, but the pressure drop increases with increasing heating power. However, for vertical flow higher heating power makes the negative slope of pressure characteristic slightly steeper, while a lower heating power make it slightly flatter [11].

There was not found any literature on the effects the heating distribution has on the pressure characteristic curve. Neither was there found an experimental study where the effects of inlet pressure, subcooling temperature, heating power and heating distribution were all analyzed in one single study.

4 Review on error analysis

In experimental work no physical quantity can be measured with perfect certainty. There are errors and uncertainties in all experimental measurements. It is important to know how large the uncertainties are in order to know how reliable the results of the experiments are. Since the main focus of this project is experimental work a review on error analysis is presented in this chapter [13, 14].

4.1 Fundamentals of errors in experimental work

Experimental error is defined as the difference between a measurement of a physical quantity and the true value of the physical quantity. The experimental error itself is a measure of its accuracy and precision. Accuracy measures how close the measured value is the true value. However, since the “true” value of physical quantity is not often known, it may not be possible to truly determine the accuracy and it must be estimated. Precision measures how closely two or more measurement agree with each other. Precision is also called “repeatability” or “reproducibility”. Measurements which have high precision tend to give values which are close to each other. Figure 4 is an illustration of the difference between accuracy and precision in four simple sketches.

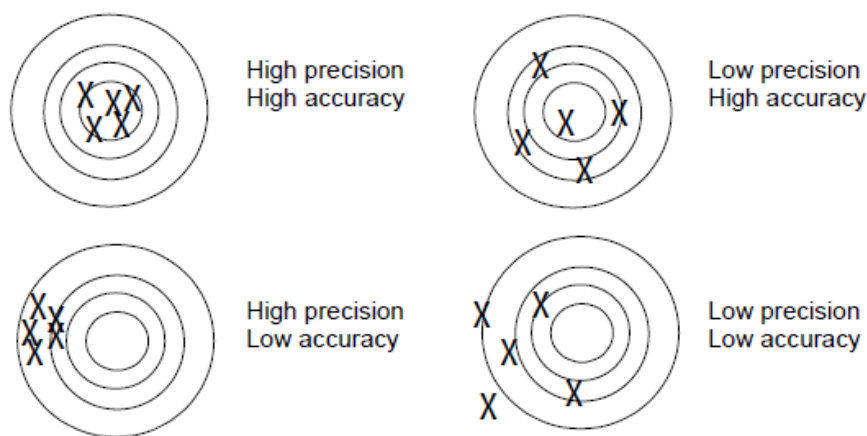


Figure 4: Sketch of accuracy and precision in experimental measurements [13]

It can be seen from Figure 4 in the sketch in the upper left corner that the best measurements have both high precision and accuracy.

4.2 Types of experimental errors

Experimental errors are divided into two categories: systematic errors and random errors. Both error categories will be discussed next.

4.2.1 Systematic errors

The first type of experimental errors is called systematic errors. Systematic errors affect the accuracy of the measurements. It is not possible to increase the accuracy of the measurements by repeating the experiments because the sources to systematic errors lie within the measuring instrumentation. Therefore there will always be some systematic errors since no instrument is perfectly calibrated and maintained. There will also be errors in the readings from the instruments. Often the manufacturer of the instruments specifies the systematic error.

4.2.2 Random errors

The second type of experimental errors is called random errors. Random errors are errors that affect the precision of the measurements. Random errors arise from statistical fluctuations, variations in the quality measured and resolutions effects. Sometimes random errors are due to the experimental technique. The random uncertainties produce scatter in observed values. Unlike with systematic errors, the precision of the measurements subjected to random errors can be improved by repeating the measurements. Random errors are easily analyzed by statistical analysis. A common source of random error is the inability to read an instrument because the readings fluctuate during the measurements.

4.3 Describing errors in experimental work

All scientific results from experiments must be describes with the accuracy of the measurements. Two different ways of describing the accuracy and precision of experimental measurements will be discussed next.

4.3.1 Significant Figures

One way of describing accuracy and precision is through significant digits. The least significant digit in a measurement depends on the smallest unit which can be measured using the measuring instrument. The precision of a measurement can then be estimated by the number of significant digits with which the measurement is reported. Usually any measurement is reported to a precision equal to 1/10 of the smallest graduation on the instrument, and the precision is said to be 1/10 of the smallest graduation. For example, an experimental measurement using a ruler with 1 mm graduations will have a precision of ± 0.1 mm. Other rules apply for digital instruments. Like mentioned before, often the error is specified by the manufacturer of the instrument. However, if the error is not specified by the manufacturer, the precision is ± 0.5 of the smallest unit on the instrument. For example, a digital voltmeter that reads 1.493 V will have a precision of ± 0.5 of 0.001, which is ± 0.0005 V.

4.3.2 Mean value and standard deviation

The other way of describing accuracy and precision is by using the mean value and the standard deviation. When a measurement is repeated under the same conditions many times, the measured values are grouped around a central value. For a set of data with N measurements (k_1, k_2, \dots, k_N) the average or mean value of that set of data is defined as:

$$Av = \frac{1}{N} \sum_{i=1}^N k_i \quad \text{(Equation 33)}$$

In (Equation 33) Av is the mean (also called average) value.

The standard deviation, also called the mean square deviation, shows how much variation there is in the set of measurements from the average. Standard deviation is defined as:

$$S = \sqrt{\sum_{i=1}^N \frac{1}{N} (k_i - Av)^2} \quad \text{(Equation 34)}$$

In (Equation 34) S is the standard deviation. The larger S is, the larger the variation in the values of the data set is. This means that a set of measurements having similar values will have a smaller S , while a set of measurements having different values will have a larger S .

4.4 Presenting errors

When presenting errors in experiments, both the random and systematic errors need to be accounted for. One way of combining the error is to add them in quadrature. If λ_{ran} is the random error and λ_{sys} is the systematic error, the total error is found by applying [15]:

$$\lambda_{tot} = \sqrt{\lambda_{ran}^2 + \lambda_{sys}^2} \quad \text{(Equation 35)}$$

In (Equation 35) δ_{tot} is the total error. δ_{tot} can be presented in experimental results by using error bars. Error bars graphically represent the total error in a set of data, and the length of each error bar is δ_{tot} . Figure 5 shows an example of error bars with the mean value in the middle indicated by the red dot, and the length error bars represented with the double head arrows.

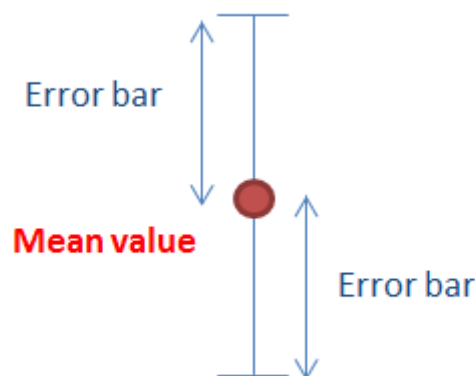


Figure 5: Sketch of an error bar

5 The experimental facility

This chapter deals with the two-phase experimental facility the experimental work is performed on. This chapter provides information about the background and components of the experimental facility.

5.1 The background of the experimental facility

The experimental facility is a closed loop which circulates refrigerant R-134a (1,1,1,2-Tetrafluorethane). It has been designed and developed by Ezequiel M. Chiapero and Leonard C. Ruspini with assistance of Carlos A. Dorao, Maria Fernandino, Håvard Rekstad, Reidar Tellebon and Marius Østnor Døllner at the department of Energy and Process Engineering at NTNU in Trondheim (Norway) in the period 2008 – 2012. The experimental facility is a part of the Two-Phase Instability project, which is financially supported by Statoil ASA and the Department of Energy and Process Engineering (NTNU). The experimental facility has been used for measurements of heat transfer coefficients and pressure drop in two-phase flow. Also, it has been used for analyzing two-phase flow instabilities. A diagram of the complete experimental facility can be seen in Figure 41 in Appendix C.

5.2 The components of the experimental facility

The complete experimental facility (Figure 41) contains some components which are not relevant for this study. The components which are not relevant briefly be mentioned at the ends of the chapter. The components of the experimental facility which are relevant for this study will be presented next, and each of the components will be presented with a picture. The components which are relevant for this project are the following:

- Main tank
- Pump
- Pre-heater/Conditioner
- Heat test section
- Visualization glass with high speed camera
- Adiabatic test section
- Condenser

From this point the experimental facility is referred to as the part of the complete experimental facility that contains the above listed components. A schematic representation of the experimental facility can be seen in Figure 6. The circles, except the pump, in Figure 6 indicate instruments for measuring temperature and pressure.

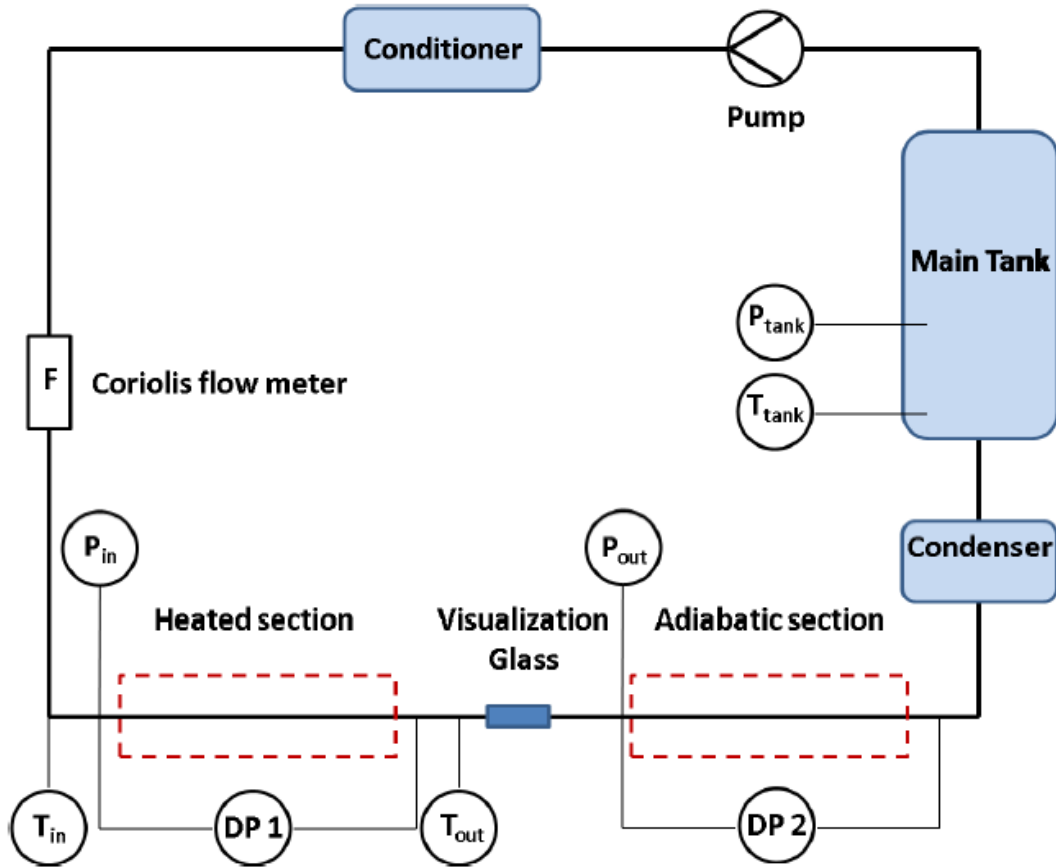


Figure 6: Sketch of the experimental facility

Initially the fluid pressure is set by controlling the temperature in the main tank where R-134a is at saturation conditions. Figure 7 is a picture of the main tank. The saturation pressure corresponding to a given saturation temperature can be obtained from the pressure-enthalpy diagram for R-134a in Figure 39 found in Appendix A.



Figure 7: Main tank

Figure 8 is a picture of the pump with the engine which drives it. The pump is a magnetically couple gear pump from Liquiflo, and it is used for driving the fluid around the closed loop. The advantage of a gear pump is the low pressure noise and absence of lubricant oil. The pump allows pressure drops in the range 4-10 bar. In parallel to the pump there is a by-pass branch with a valve used to change the flow rate in the circuit. The pump itself is located to the right of the engine and it cannot be seen directly because it is covered with black isolation.



Figure 8: Pump with engine

After the pump there is a pre-heater/conditioner which is a shell and tube heat exchanger with glycol flowing in the shell side used for adjusting the temperature of the refrigerant. The pre-heater/conditioner will later be referred to as the K6-heat exchanger.

Next, the refrigerant flows through a coriolis mass flow meter before entering the heated stainless steel test section where heat is applied to the refrigerant. Figure 9 is a sketch of the heated test section.

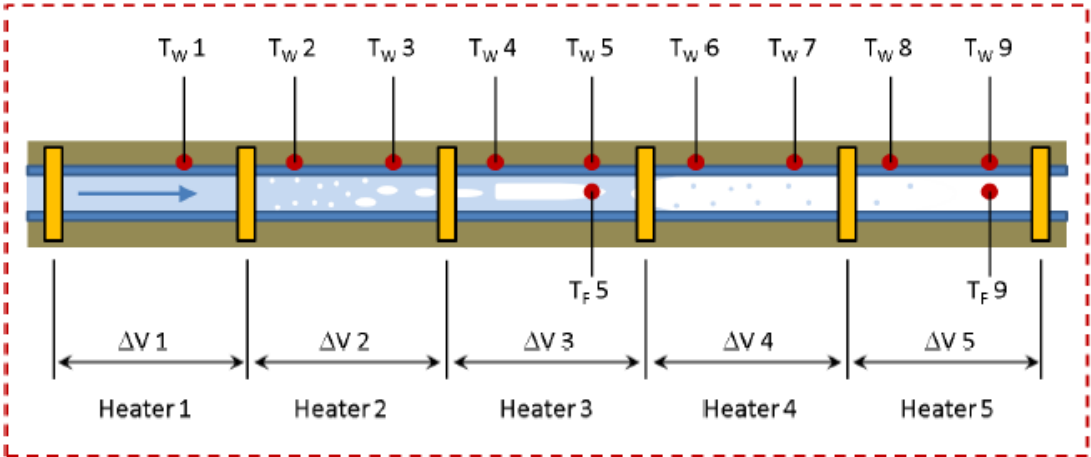


Figure 9: Sketch of heated test section

The heated test section consists of 5 segments, each containing a heater where the applied heating power can be specified individually. The maximal power that can be applied in each heater is 500 W. Each segment is 0.4 m long, having an inner diameter of 5 mm and an outer diameter of 8 mm. 9 thermocouples ($T_{w1} - T_{w9}$) are distributed along the wall surface of the heated test section for measuring the wall temperature, and two thermocouples (T_{f5} and T_{f9}) are located inside the pipe for measuring the fluid temperature. The thermocouples are type T thermocouples with 0.5 mm diameter. Figure 10 is a picture of the heat test section.



Figure 10: Heated test section

Figure 11 is a picture of the visualization glass which is a transparent pipe used for observing and filming the flow. It is also possible to record the flow inside the visualization pipe using a high speed camera as can be seen on the right side of Figure 10.



Figure 11: The visualization glass

After the visualization glass the flow enters the adiabatic test section which is a 1 m long steel tube used for measuring the pressure drop of the two-phase flow. Figure 12 is a picture of the adiabatic test section. The pressure drop measurement is done with a differential pressure transducer, also called a DP cell. The inner and outer diameter of the tube in the adiabatic test section is the same as for the heated test section.



Figure 12: Adiabatic test section

Next, there is a condenser that has a capacity of 8 L which is located above the main tank. Figure 13 is a picture of the condenser. The condenser is a shell and tube heat exchanger with glycol on the tube side. Later the condenser will be referred to as the K9-heat exchanger. The supplier of the condenser is Moderne Kjøling and it has a power input condenser of 1.8 kW.

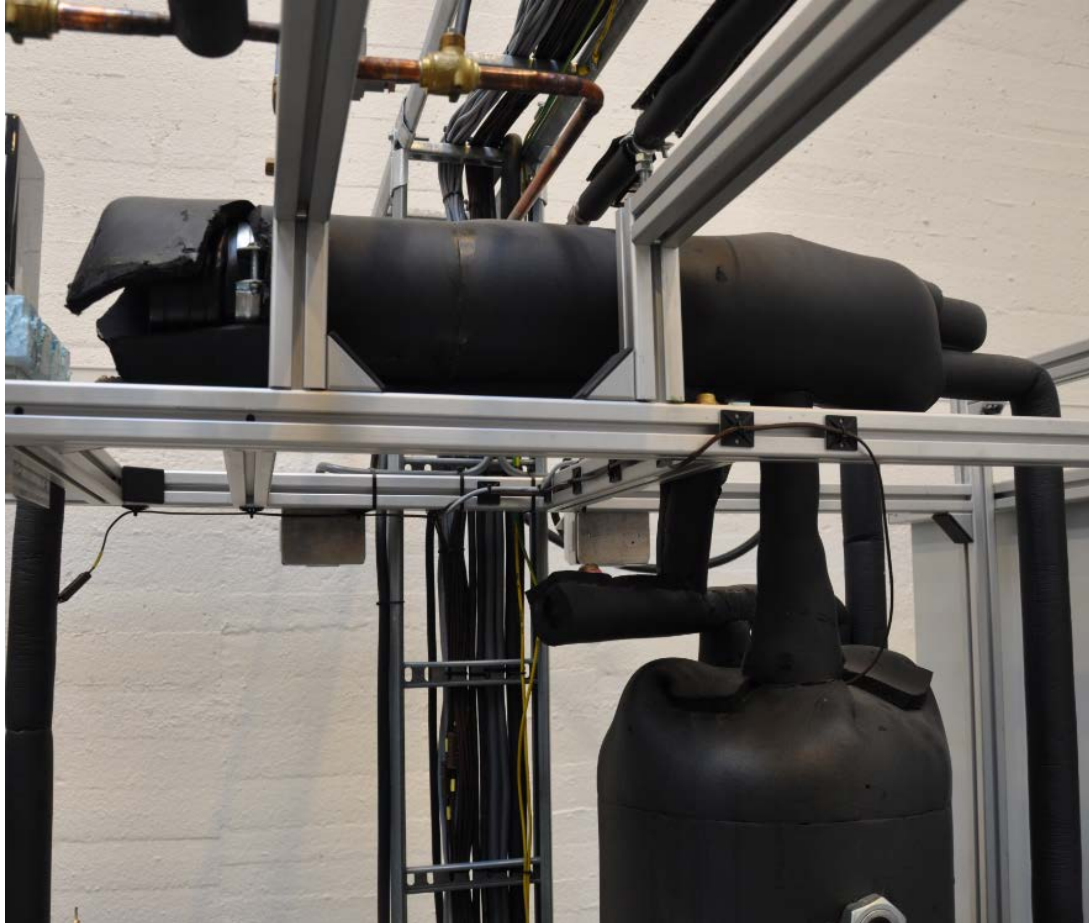


Figure 13: The condenser

After the condenser the refrigerant enters the main tank where it initially started and the loop is completed.

Table 1 provides an overview of the physical ranges the experimental facility can handle, where the minimal and maximal values of four parameters can be seen.

Table 1: Parameter range of experimental facility

Parameter	Minimal value	Maximal value
System pressure	4 bar	12 bar
Inlet temperature	-20 °C	40 °C
Subcooling	0 °C	60 °C
Max heating combined heating power	0 W	2.5 kW

As mentioned earlier the experimental facility also contains components which are not relevant for this study because they are not be used in the experimental work. The first component is a multi-pipe tests section. The experiments relevant for this study are single pipe experiments, and therefore the multi-pipe test section will not be presented. The second component is a surge tank which is used for performing flow instability experiments, and therefore it will not be presented.

A user manual for the experimental facility can be found in Appendix E. The user manual contains information on how to get access to the experimental facility and how to start it up.

6 Calibration and verification of instruments

This chapter deals with calibration and verification of instruments at the experimental facility. When performing experimental work it is important to ensure that the instruments at the experimental facility operate in an optimal manner. One way of ensuring reliable operation is by calibration and verification of the instruments. First the verification of mass flow meters is presented, and then the calibration of the heaters is presented.

6.1 Verification of mass flow meters

Verification of the mass flow meters is done through pressure drop measurements for single phase flow through the adiabatic test section. Figure 14 is a sketch of the pressure drop measurements in the adiabatic test section that can be seen in Figure 12. A DP cell was used for measuring how much the pressure changes from the inlet to the outlet of the 1 m pipe in the adiabatic test section.

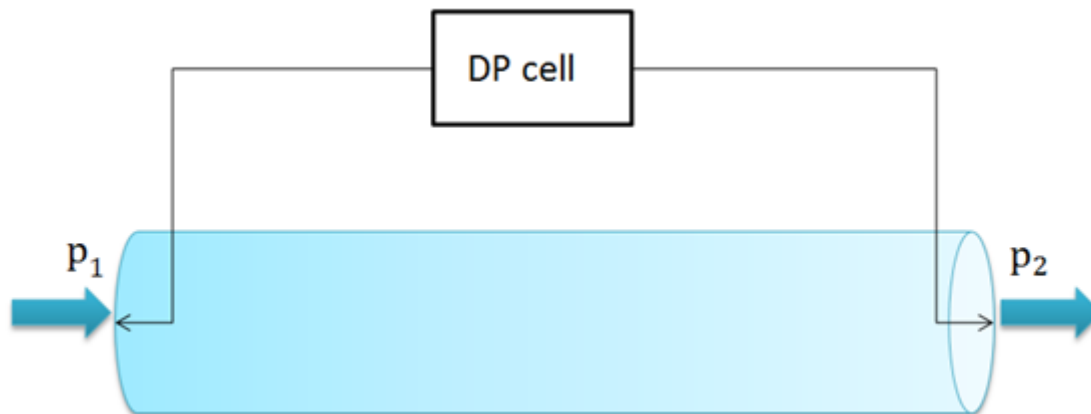


Figure 14: Sketch of pressure drop measurements

6.1.1 Pressure drop inside a horizontal pipe theory

The theory presented here for the total pressure drop in a horizontal pipe is based on [16]. Like explained in Chapter 2, for flow inside a pipe the pressure will decrease due to the effects of friction, elevation and viscosity. The energy equation for steady, incompressible flow through a pipe of constant area is:

$$\left(\frac{p}{\rho g} + \frac{\alpha}{2g} V^2 + H\right)_1 = \left(\frac{p}{\rho g} + \frac{\alpha}{2g} V^2 + H\right)_2 + h_{tur} - h_{pum} + h_{fri} \quad \text{(Equation 36)}$$

In (Equation 36) p is the pressure, α is the kinetic correction factor, ρ is the density and V is the velocity of the fluid. H is the difference in height and h are the head terms for the turbine, the pump and friction. The terms in the parentheses are marked as 1 and 2, where 1 indicated the state of the fluid upstream and 2 the state of the fluid downstream. In the

experimental facility there is no change in elevation, meaning that $H = 0$. The flow is assumed to be fully developed, meaning that the velocity profile is not changing, which implies that $\alpha_1 = \alpha_2$ and $V_1 = V_2$. When eliminating the terms which equalize, the following expression is obtained:

$$h_{friction} = \frac{(p_1 - p_2)}{\rho g} \quad \text{(Equation 37)}$$

It is also possible to express the head loss in terms of the wall shear stress:

$$h_{friction} = \frac{4t L}{\rho g D_i} \quad \text{(Equation 38)}$$

In (Equation 38) t is the shear stress, L is the length of the pipe and D_i is the pipe diameter. For turbulent flow $h_{friction}$ is proportional to V^2 , and a correlation for the head loss is:

$$h_{friction} = f_{Re} \frac{L V^2}{d 2g} \quad \text{(Equation 39)}$$

In (Equation 39) f_{Re} is a dimensionless parameter called the Darcy friction factor and it depends upon the Reynolds number, the wall roughness height and the geometry of the pipe. The Darcy friction factor can be obtained from a Moody chart which can be found in Figure 40 in Appendix B. When combining (Equation 37) and (Equation 39) an expression for the pressure drop in the pipe is obtained:

$$p_1 - p_2 = f_{Re} \frac{L}{2d} \rho V^2 \quad \text{(Equation 40)}$$

In order to compare the experimental data with the theory we can compare the value of the Darcy fractional factor based on experimental data with the theoretical value. For turbulent flow ($Re \geq 4,000$) Blasius proposed the following correlation for f_{Re} :

$$f_{Re} = 0.316 Re^{-0.25} \quad \text{(Equation 41)}$$

Combining the expression for the pressure drop in a pipe (Equation 40) with the definition of the Reynolds number, we get an expression of the frictional factor based on experimental data:

$$f_{Re} = \frac{(p_1 - p_2) \pi D^4}{2 Re \mu L} \frac{1}{VOL} \quad \text{(Equation 42)}$$

In (Equation 42) VOL is the volumetric flow in the pipe. When (Equation 41) and (Equation 42) are equated an expression for the volumetric flow rate as a function of pressure difference is obtained:

$$VOL = \left[\frac{(\pi^7 D^{19})^{\frac{1}{4}}}{0.632(4^{\frac{3}{4}})L(\mu\rho^3)^{\frac{1}{4}}} \Delta P \right]^{\frac{4}{7}} \quad \text{(Equation 43)}$$

6.1.2 Experiments on pressure drop in pipe

The measurements of the pressure drop were done for 7 different flow rate values. The flow rate values were set to 1.4, 1.2, 1.0, 0.8, 0.6, 0.4 and 0.2 *L/min*. The results can be found in Appendix G. From Figure 59 and Figure 60 in Appendix G it can be seen that the experimental results fit well with the theoretical.

6.2 Heat transfer in heating section and electrical power

The calibration of the heaters was done by comparing the inserted value of the heating power to the heat actually provided to the fluid. Heat that is applied by the heaters in the heat section (Figure 9) is controlled in LabVIEW. There is a difference between the value of the heat that is inserted in LabVIEW and the heat that the heaters actually transfer to the fluid. A correlation between the values inserted in LabVIEW and the actual heating power provided by the heaters was found.

6.2.1 Theory on heat transfer and electrical power

This subchapter provides the theory relevant for the calibration of the heaters. First the theory on heat transfer will be presented, and then theory on electrical power will be presented. The energy balance for a heated one-phase liquid flow through a channel the is defined as [5]:

$$Q = \dot{m}c_p(T_{in} - T_{out}) \quad \text{(Equation 44)}$$

In (Equation 44) Q is the heat transferred to the fluid, \dot{m} is the mass flow, c_p is the specific heat capacity of the fluid and $(T_{in} - T_{out})$ is the temperature difference between inlet and outlet of the channel the fluid is flowing in.

The power provided in an electrical circuit element is defined as the product of the voltage and the current [17]:

$$P = UI \quad \text{(Equation 45)}$$

In (Equation 45) P is the power provided in the element, U is the voltage drop across the element and I is the current in the element. Most voltage and current sources do not produce constant current and voltages. This means that the values of the voltage, current and power are functions of time. Figure 15 shows typical voltage, current and power distributions which are sinusoidal (note that the voltage is defined as V in Figure 15).

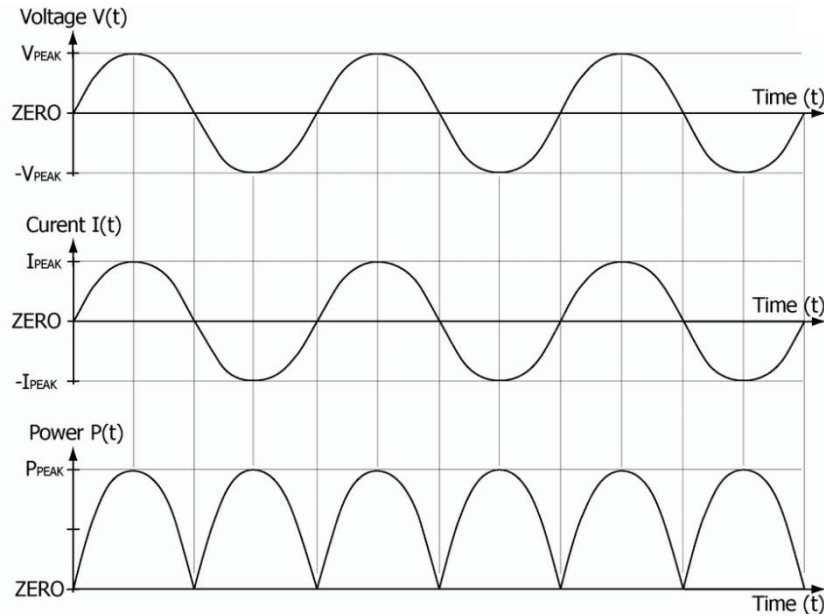


Figure 15: Sinusoidal voltage (upper), current (middle) and power (lower) in an electric circuit element

For time varying voltages and currents the power is usually defined by using the root mean square. The root mean square is defined as:

$$RMS = \sqrt{\frac{1}{N} (k_1^2 + k_2^2 + \dots + k_N^2)} \quad \text{(Equation 46)}$$

In (Equation 46) RMS is the root mean square. k can represent the current, voltage and power. The average power is then defined as:

$$P_{avg} = V_{RMS} I_{RMS} \quad \text{(Equation 47)}$$

6.2.2 Experiments on heat transfer and electrical power

In the calibration of the heaters an oscilloscope was used for measuring the electrical power provided to the heated test section. For each heater the current and voltage drop was measured, from which the power was obtained using (Equation 47). The root mean square value of the voltage measured with the oscilloscope was fitted with the root mean square value of the voltage obtained from LabVIEW. The results of the calibration for all the 5 heaters can be found in Appendix D.

7 Experimental work and discussion

This chapter presents, explains and discusses the experimental work that has been done on the experimental facility presented in Chapter 5. The aim of the experimental work is to investigate the behavior of the pressure characteristic curve in two-phase flow through a sensitivity analysis. The sensitivity analysis was done by comparing a reference case with experiments where one parameter is changed, while all the other parameters are kept at the same values as for the reference case. The parameters analyzed during the sensitivity analysis were the inlet pressure, subcooling temperature, total heating power and heating power distribution. The total pressure drop in the pipe was measured using a differential pressure transducer (also called a DP cell). For all experiments the conditions will be held at a constant value, while only the value of the mass flux is changed.

First the reference case and preliminary experiments are presented. Then a sensitivity analysis on the inlet pressure, subcooling temperature, applied heating power and heat distribution is presented. The experimental work is also compared with the result from an existing numerical study. Extraction and processing of data from the experimental measurements was done using REFPROP (Reference Fluid Thermodynamic and Transport Properties Database) and MATLAB (Matrix Laboratory). REFPROP is a database for fluid thermodynamic and transport properties, and it was used for obtaining values of properties of R-134a at experimentally measured temperatures and pressures. MATLAB is a programming language which was used for processing the data obtained from REFPROP.

For all the presented results, except for the preliminary experiments, an error analysis was done. The error analysis is based on theory from Chapter 4 and it is presented using error bars. The systematic error in the measurements comes from the DP cell, where the manufacturer of the DP cell claims that the differential pressure accuracy is 0.075 % of the full-scale. For every experimental measurement reported 120 data points were required, but the number of experiments measurements differs for each case in the sensitivity analysis. The number of experimental measurements depends on the shape of the pressure characteristic curve, and for each case enough measurements were taken for the full shape of the curve to be seen properly.

7.1 Reference case and preliminary experiments

A reference case was set for the purpose of comparing and analyzing the results of the sensitivity analysis. Two preliminary experiments were done before the sensitivity analysis to explore the design conditions of the experimental facility, and also to set the boundary conditions for the sensitivity analysis. Another motivation for doing the preliminary experiments is to ensure that the experimental facility performs well at the boundary conditions.

7.1.1 The reference case

In the reference case the conditions were set to 8.5 bar inlet pressure, subcooling temperature of 30 °C and total uniform heating power of 1000 W. Uniform heating power of 1000 W means that the heating power is set to 200 W in each of the five heaters. Figure 16 shows a graph of the pressure characteristic curve for the reference case. In Figure 16 the x-axis gives the mass flux and the y-axis gives the total pressure difference over the pipe.

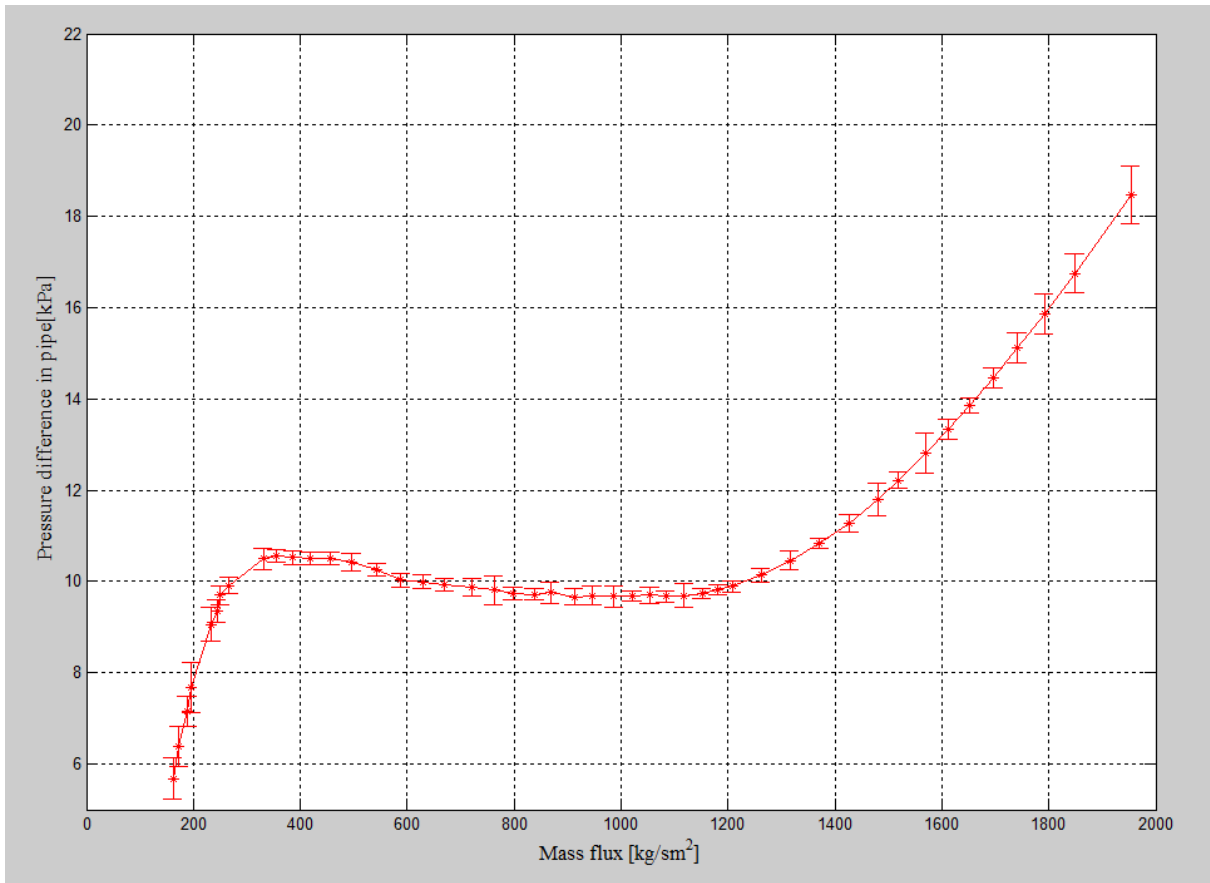


Figure 16: Reference case: $p = 8.5$ bar, $T_{sub} = 30^\circ\text{C}$, $Q = 1000$ W (uniform)

In Figure 16 it can be seen the plot has an N-shape. This N-shape is characterized by the negative slope in the pressure difference in the region where the mass flux ranges from ca. 300 kg/sm^2 to ca. 1050 kg/sm^2 . In the point where the onset of boiling is reached a two-phase region starts to grow from the outlet of the pipe and towards the inlet. A two-phase region at the outlet brings about two counteracting effects occur: The first effect is a decrease in pressure drop with a reduction in the mass flux, because less force (pressure) is required to push the flow through the pipe. The second effect is an increase in pressure drop because the frictional component for two-phase flow is much higher than for one-phase liquid flow. Also, since two-phase flow has a lower density than one-phase liquid the momentum component will increase for two-phase flow, as can be seen from (Equation 4) and (Equation 5). The reason why the frictional factor is larger for two-phase flow than for one-phase liquid can be seen by analyzing (Equation 9) and (Equation 10). The influence each of the counteracting effects decides the shape of the characteristic pressure curve. In the reference case shown in Figure 16 the second effect is larger than the first and the net

result is an increasing pressure with decreasing mass flux in one part of the pressure characteristic curve, resulting in an N-shape [1].

7.1.2 Preliminary experiments

Preliminary experiments were done before the experiments of the sensitivity analysis for two reasons: to set the boundaries of the sensitivity analysis, and to ensure that the performance of the experimental facility is satisfying. The larger the range of the sensitivity analysis is, the easier it is to observe the effects the parameters have on the pressure characteristics curve.

The first preliminary experiment was done for determining the boundaries of the sensitivity analysis for the inlet pressure. The lower value the inlet pressure can have in the sensitivity analysis depends on the heat exchanging ability of the K6-heat exchanger (the K6-heat exchanger be seen in on the on the left side in Figure 51 in Appendix E). For the lower value of the inlet pressure a to be determined, a subcooling temperature of 30°C (same as reference case) needs to be maintained while the inlet pressure is set as low as possible. Initially the inlet pressure was set to 5 bar, and then it was tested if it is possible to get the subcooling temperature the same as for the reference case. Figure 17 shows the graphs for the subcooling temperature, the inlet pressure and the pressure difference as functions of the mass flux.

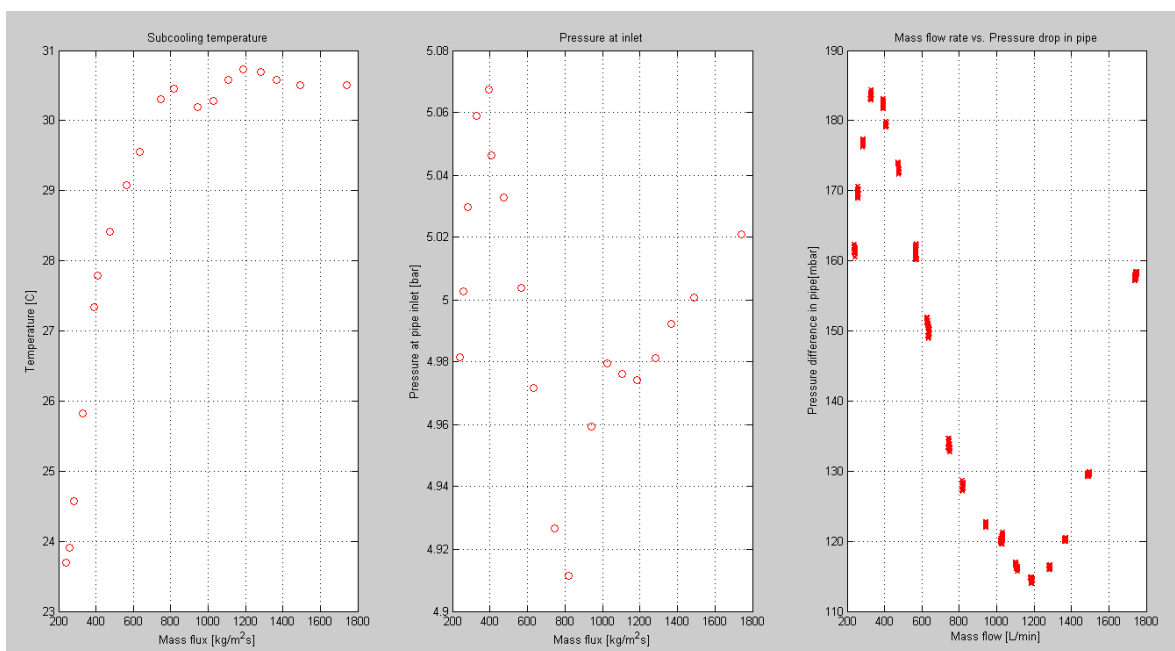


Figure 17: Preliminary experiment for low inlet pressure. (Left: Subcooling temperature. Middle: Pressure at inlet. Right: Mass flow rate vs. Pressure drop in pipe.)

From the graph for the subcooling temperature, on the left in Figure 17, it can be seen that it is not possible for inlet pressure of 5 bar to achieve a subcooling temperature of 30 °C for mass flux values lower than ca. 700 kg/sm². When the inlet pressure was increased it was possible to get subcooling temperatures which approached 30°C for all mass fluxes value.

The limit for how low the inlet pressure can be when the subcooling temperature is 30°C is 6.5 *bar*. Therefore 6.5 *bar* is set as the lower value and 10.5 *bar* is set as the upper value for the inlet pressure in the sensitivity analysis

The second preliminary experiment was done for determining the upper limit for the subcooling temperature in the sensitivity analysis. This value was investigated by setting the K6- heat exchanger to cool the flow as much as possible, while keeping all other conditions equal to the reference case. Initially it was tested if it is possible to get a subcooling temperature of 50 °C, while the other conditions are the same as for the reference case. Figure 18 shows the graphs for the subcooling temperature, the inlet pressure and the pressure difference across the pipe in the test section as functions on the mass flux when we tried to set the subcooling temperature to 50°C.

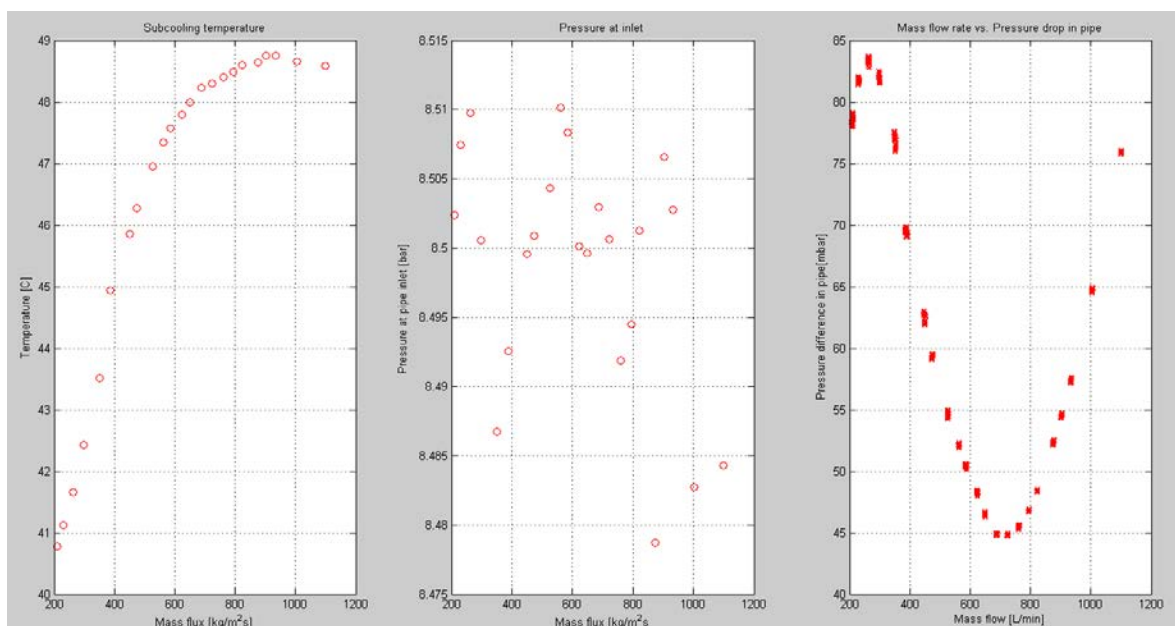


Figure 18: Preliminary experiment for high subcooling temperature. (Left: Subcooling temperature. Middle: Pressure at inlet. Right: Mass flow rate vs. Pressure drop in pipe.)

It can be seen from the graph on the left in Figure 18 that a subcooling temperature of 50 °C for mass flux values lower than ca. 900 kg/sm^2 is not possible. When the subcooling temperature was reduced it was concluded that the highest value for the subcooling temperature for inlet pressure of 8.5 *bar* is 40 °C. Therefore 40 °C was set as the upper value and 20 °C the lower value for the subcooling temperature in the sensitivity analysis.

There was no need to do a preliminary experiment for the total heating power because the upper limit was known from previous experiments done by the co-supervisor of this project. Due to the danger of overheating one of the heaters, it was determined that the upper limit of total heating power should be 1500 W (300 W in each heater), and therefore the lower limit was set to 500 W (100 W in each heater). Table 2 provides an overview of the lower and upper limits for the sensitivity analysis for inlet pressure, subcooling temperature and heating power.

Table 2: Lower and upper limits of parameters for sensitivity analysis

Parameter	Lower limit	Reference case	Upper limit
Inlet Pressure [bar]	6.5	8	10.5
Subcooling temperature [°C]	20	30	40
Total heating power [W]	500	1000	1500

7.2 The effects of the inlet pressure

The effects of varying the inlet pressure on the pressure characteristic curve have been examined in the sensitivity analysis. From the preliminary experiments it was concluded that the lower and upper limits for the inlet pressure are respectively 6.5 *bar* and 10.5 *bar*.

The effects of low inlet pressure were examined by setting the inlet pressure of the fluid to 6.5 *bar*. Figure 19 shows a graph of the pressure characteristic curve for inlet pressure of 6.5 *bar*. In Figure 19 the x-axis gives the mass flux and the y-axis gives the total pressure difference over the pipe.

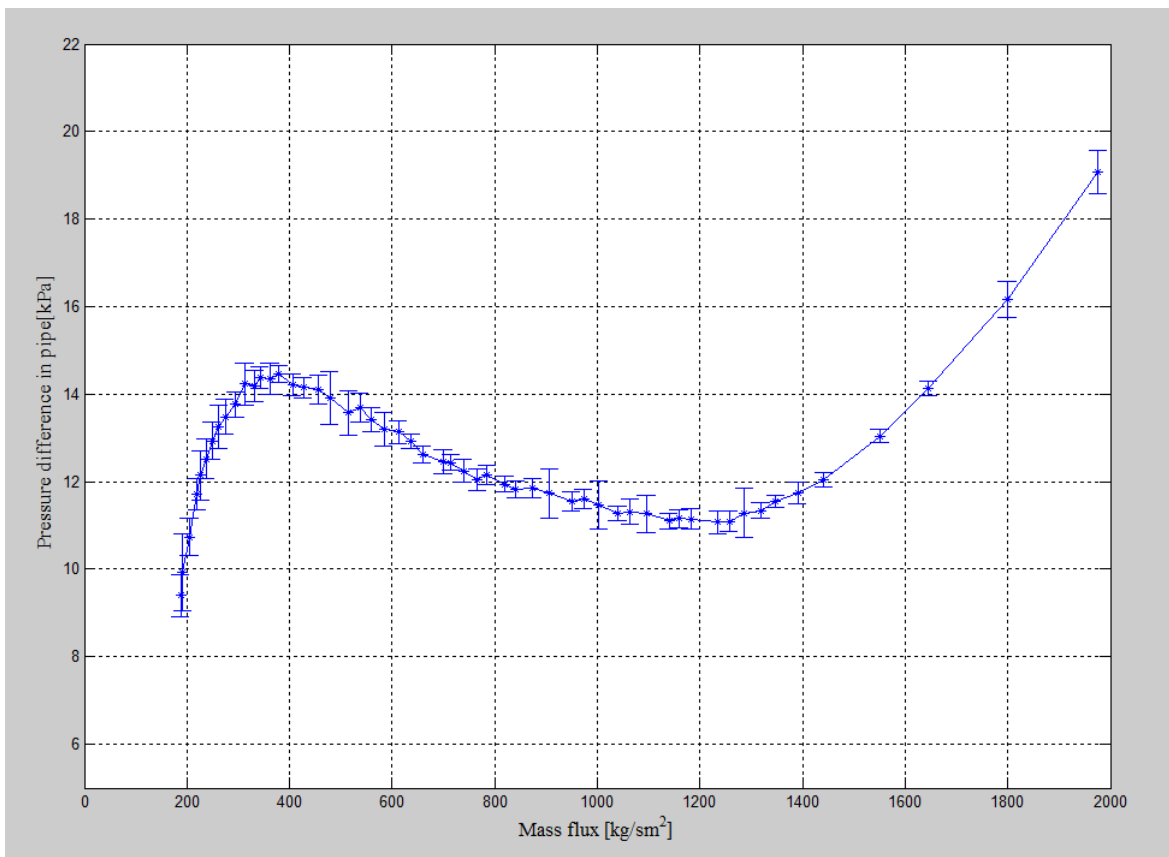


Figure 19: Low inlet pressure: $p = 6.5$ bar, $T_{\text{sub}} = 30$ °C, $Q = 1000$ W (uniform)

It can be seen in Figure 19 that there is a negative slope in the pressure characteristics curve for mass flux values from ca. 380 kg/sm^2 to ca. 1235 kg/sm^2 .

The effects of high inlet pressure were examined by setting the inlet pressure of the fluid to 10.5 bar. Figure 20 shows a graph of the pressure characteristic curve for inlet pressure of 10.5 bar. In Figure 20 the x-axis gives the mass flux and the y-axis gives the total pressure difference over the pipe.

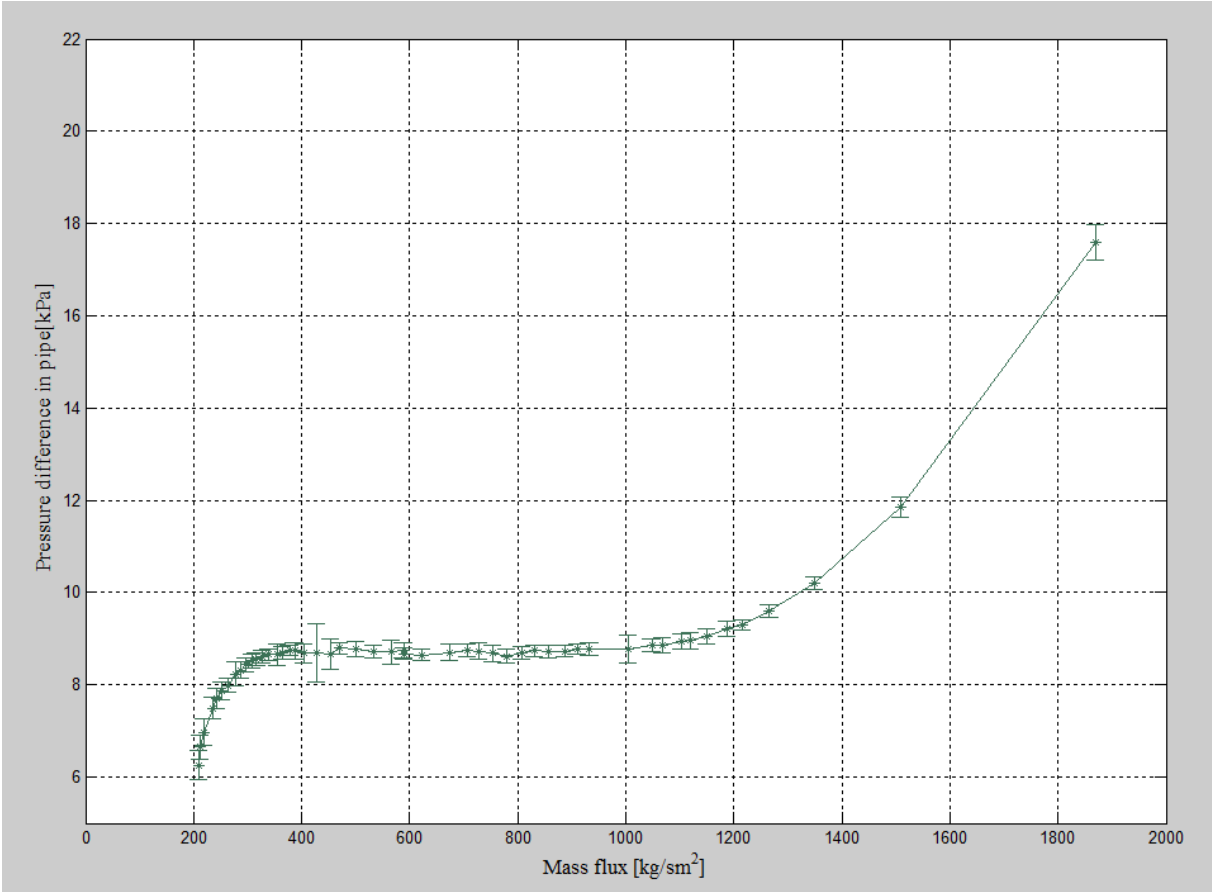


Figure 20: High inlet pressure: $p = 10.5 \text{ bar}$, $T_{\text{sub}} = 30 \text{ }^\circ\text{C}$, $Q = 1000 \text{ W}$ (uniform)

There is no negative slope in the pressure characteristic curve in Figure 20.

Figure 21 shows the graphs for the pressure characteristic curves for the low and high inlet pressure together with the reference case. In Figure 21 the x-axis gives the mass flux and the y-axis gives the total pressure difference over the pipe.

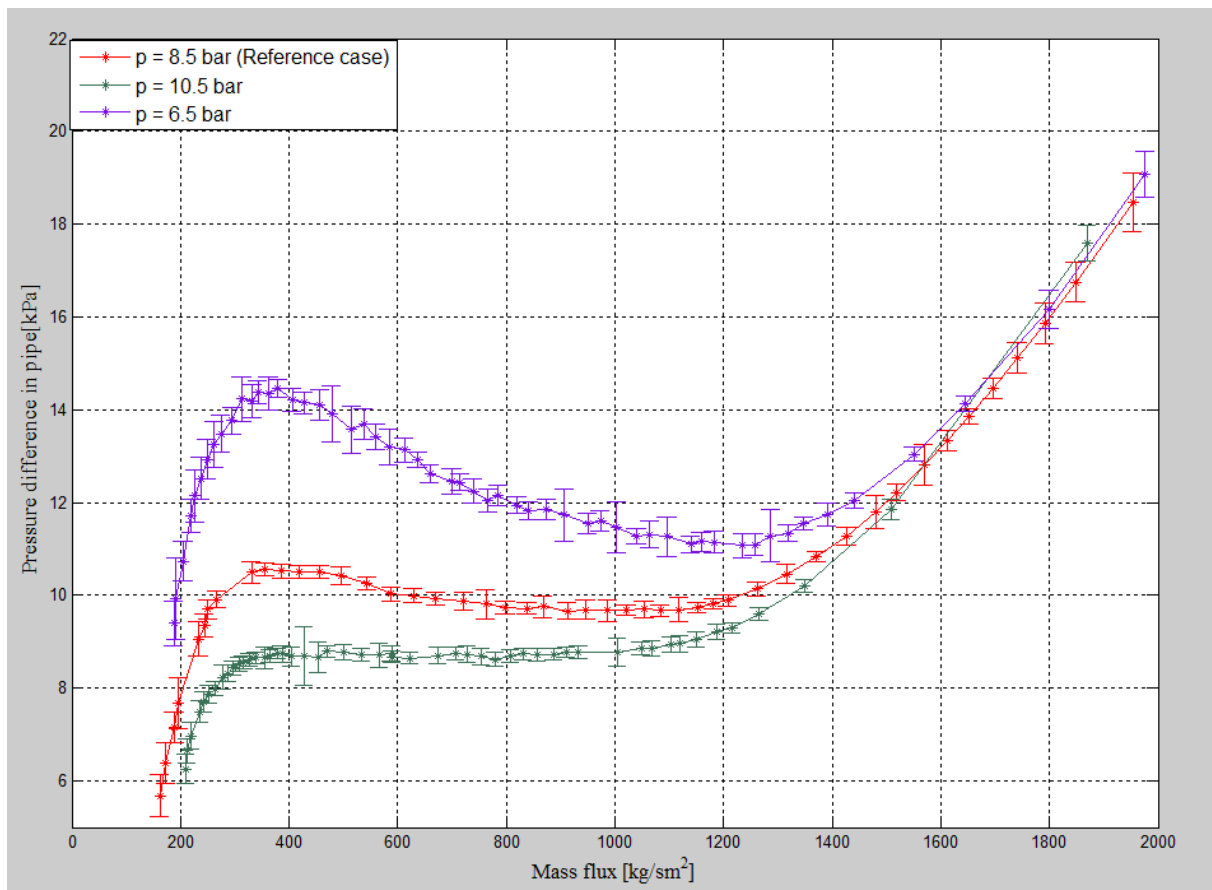


Figure 21: Comparing reference case with plots of lower and higher inlet pressure

Figure 21 shows that the inlet pressure has a large influence on the shape of the pressure characteristic curve. A lower inlet pressure make the N-shape of the pressure characteristic curve steeper, while a higher inlet pressure makes it flatter.

The explanation for this behavior of the pressure characteristic curve is found by analyzing the properties of the phases. As the pressure is increased the values for the densities for the liquid and vapor phase of the refrigerant approach each other until the critical pressure where the values become equal. A graph of the density for liquid and vapor as a function of pressure can be seen in Figure 58 in Appendix F. The viscosities of the phases will also approach each other as the pressure increases [1]. Higher pressure means that the effect of the two-phase flow region in the pipe gets smaller due to the decrease in the momentum component of the pressure drop. By analyzing (Equation 4) and (Equation 5) it can be seen that higher pressure makes Δp_{mom} decrease. From (Equation 10) in can be seen that the two-phase multiplier will decrease with higher inlet pressure and increase with lower inlet pressure. This affects the frictional component in the total pressure drop, making it decrease for higher pressure and increase for lower pressure, as can be seen from (Equation 9). The effects of the inlet pressure can also be seen by analyzing (Equation 30). The experimental result for the inlet pressure fit well with the results from the numerical study [1].

7.3 The effects of the subcooling temperature

The effects the subcooling temperatures have on the pressure characteristic curve were examined at values of 20 °C and 40 °C. The subcooling temperature is defined as the difference in temperature at the inlet of the pipe and the saturation temperature at the inlet pressure.

The effects of low subcooling temperature were examined by setting the subcooling temperature to 20 °C. Figure 22 shows the pressure characteristic curve for subcooling temperature of 20 °C. In Figure 22 the x-axis gives the mass flux and the y-axis gives the total pressure difference over the pipe.

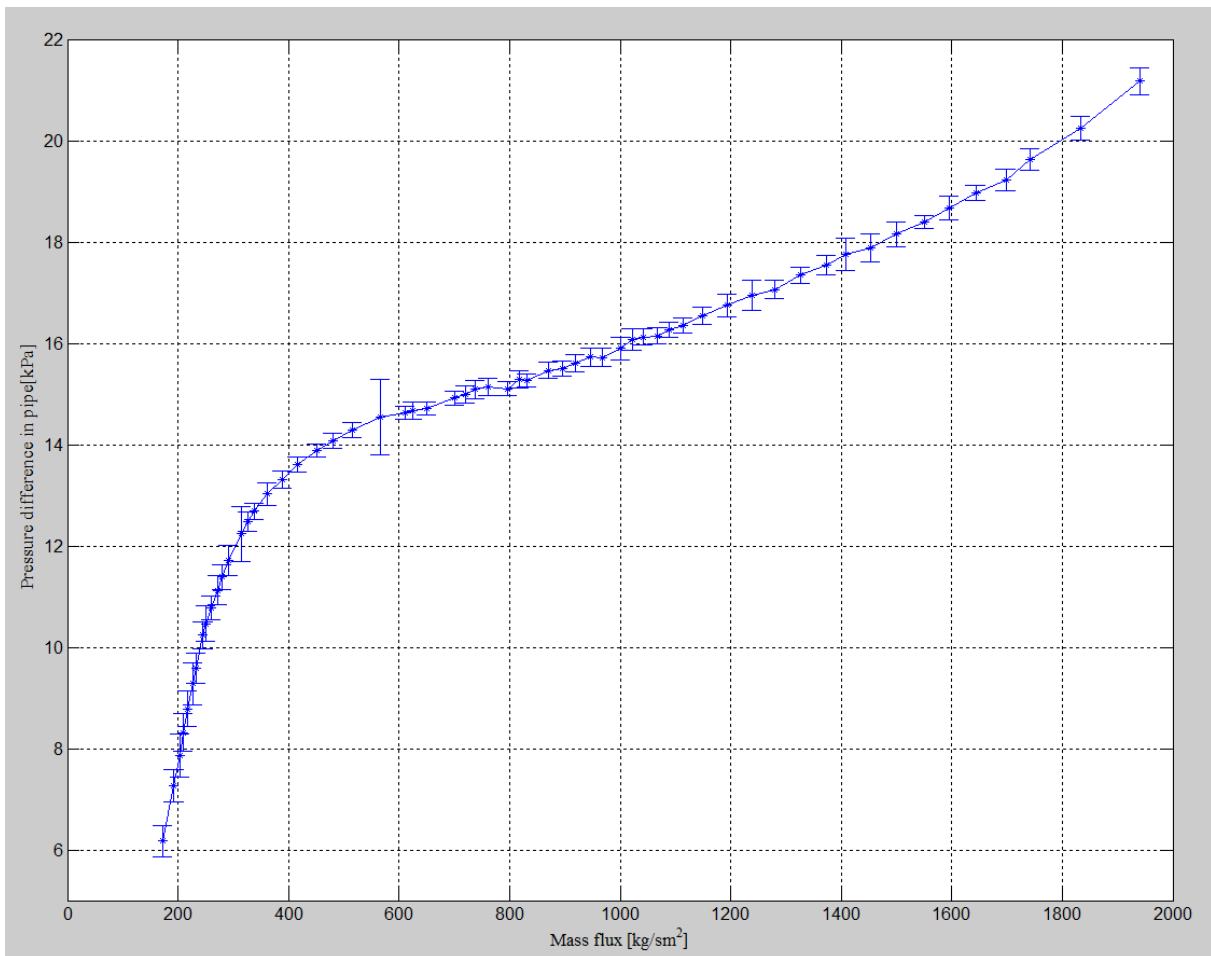


Figure 22: Low subcooling temperature: $p = 8.5 \text{ bar}$, $T_{\text{sub}} = 20 \text{ °C}$, $Q = 1000 \text{ W (uniform)}$

From Figure 22 it can be seen than there is no negative slope in the plot of the pressure characteristic curve.

The effects of high subcooling temperature were examined by setting the subcooling temperature to 40 °C. Figure 23 shows the pressure characteristic curve for subcooling temperature of 40 °C. In Figure 23 the x-axis gives the mass flux and the y-axis gives the total pressure difference over the pipe.

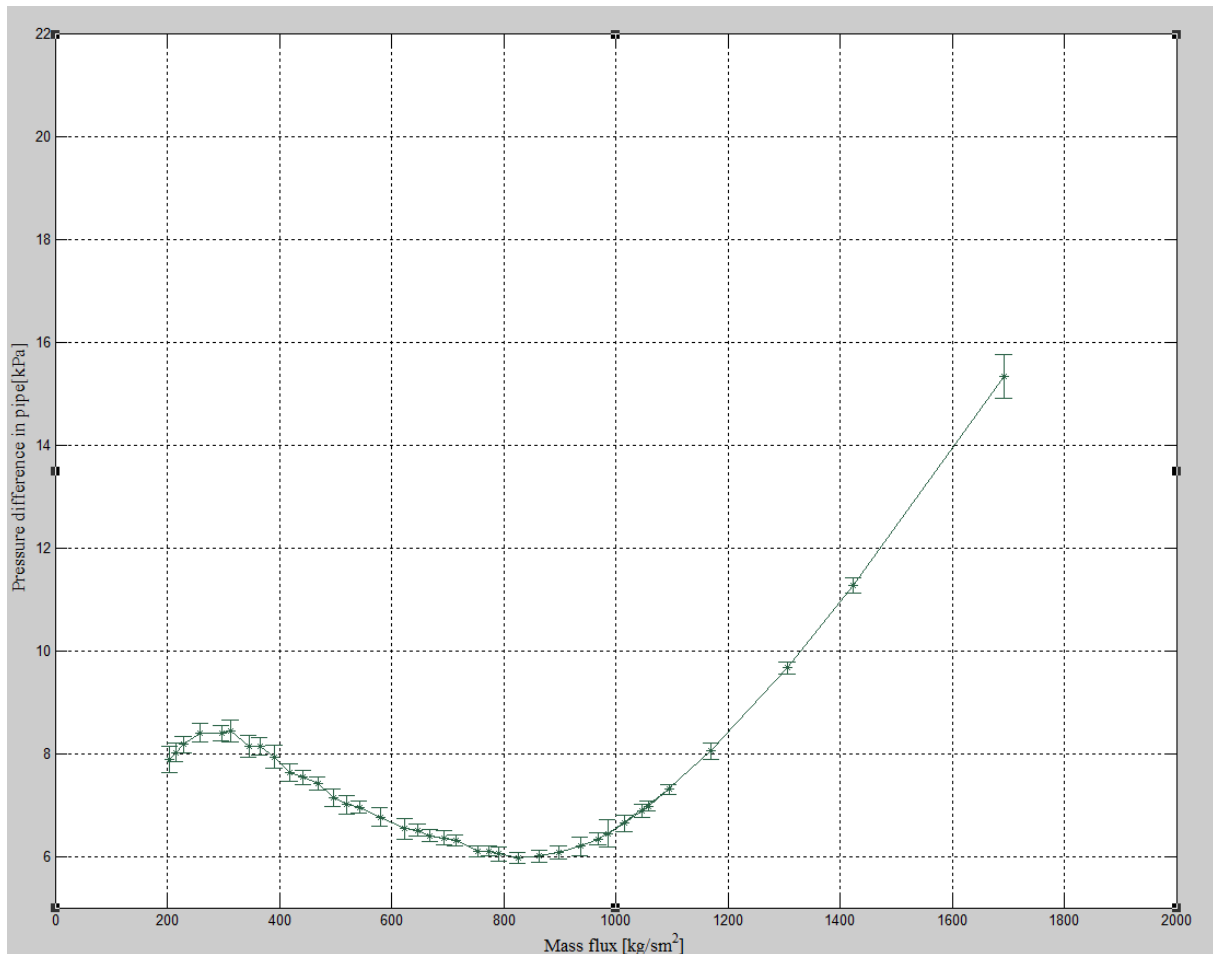


Figure 23: High subcooling temperature: $p = 8.5 \text{ bar}$, $T_{\text{sub}} = 40 \text{ °C}$, $Q = 1000 \text{ W}$ (uniform)

From Figure 23 it can be seen that there is a negative slope in the plot at mass flux values from ca. $295 \frac{\text{kg}}{\text{sm}^2}$ to ca. $825 \frac{\text{kg}}{\text{sm}^2}$.

In Figure 24 the graphs of the pressure characteristic curves for low and high subcooling temperature are plotted with the reference case. In Figure 24 the x-axis gives the mass flux and the y-axis gives the total pressure difference over the pipe.

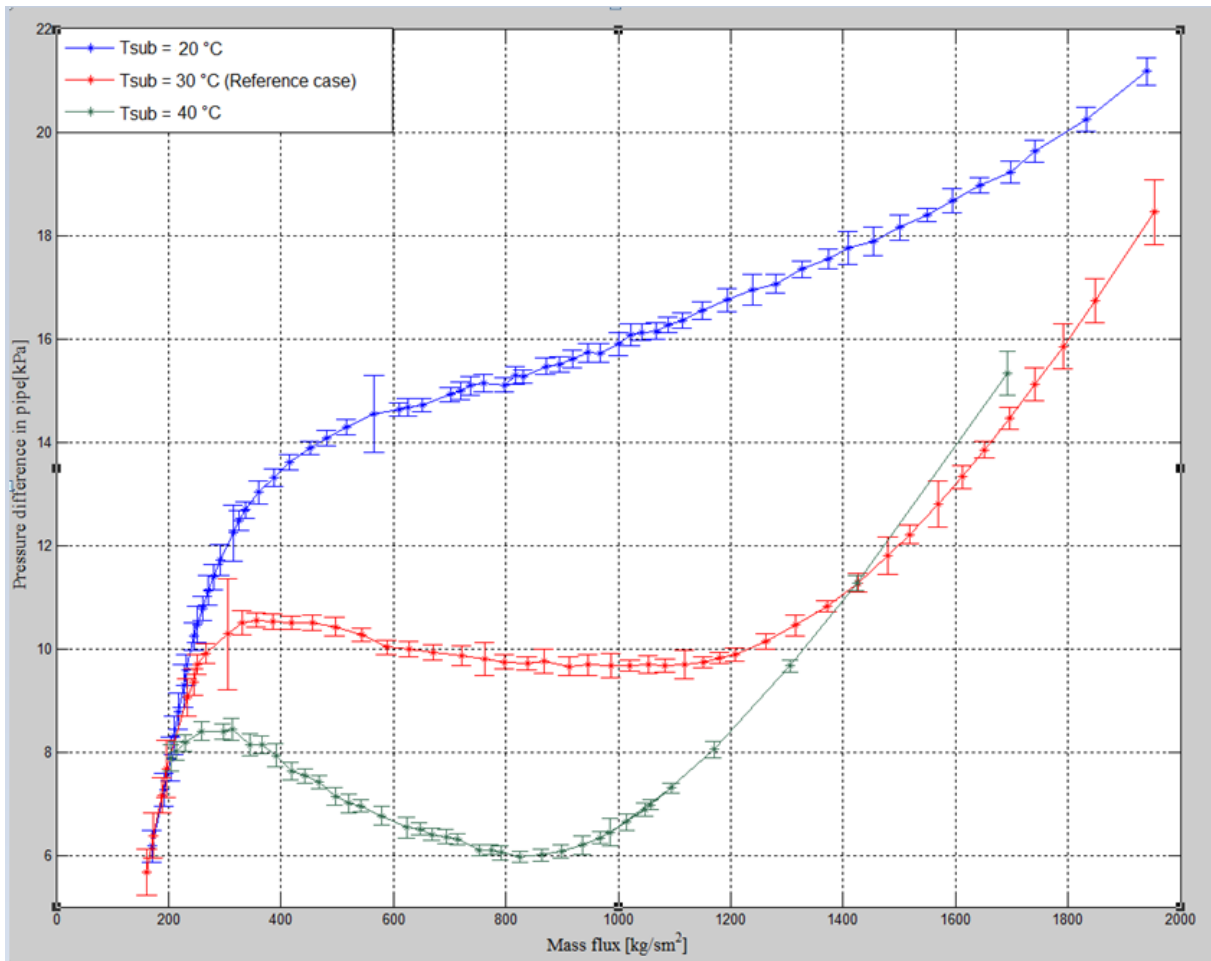


Figure 24: Comparing reference case with plots of low and high subcooling temperature

It can be seen from Figure 24 that the subcooling temperature has a large effect on the presence of the negative slope in the pressure characteristic curve. A lower subcooling temperature makes the N-shape of the pressure characteristic curve flatter, while a high subcooling temperature makes it steeper. It should be noted from Figure 24 that the plot for the 40 °C does not fit with the plot for the reference case for high mass flux values (one phase liquid region). This is due to the difficulty of maintaining an inlet pressure of 8.5 bar for high mass flux values.

As explained earlier the reason for the negative slope in the pressure characteristic curve is the occurrence of the two-phase region that grows from the outlet of the pipe. The influence of the inlet temperature can be examined by looking at the phase flow lengths defined in (Equation 17) and (Equation 19). Let us analyze the case for the mass flux which results in saturated vapor at the outlet of the pipe, meaning that the mass quality at the outlet equals 1 ($x_{out} = 1$). For this case the sum of the phase length for the liquid and the two-phase will equal the length of the tube, which can be seen as the second scenario in Figure 1. When solving (Equation 17) and (Equation 19) for that mass fluxes for saturated vapor at the outlet, and equating the answers we get expressions for the phase flow lengths. For the two-phase flow length we get:

$$L_{tp} = L \frac{H_{vap}}{c_p T_{sub} + H_{vap}} \quad (\text{Equation 48})$$

And for the liquid flow length we get:

$$L_l = L \frac{c_p T_{sub}}{c_p T_{sub} + H_{vap}} = L \frac{1}{1 + (H_{vap}/c_p T_{sub})} \quad (\text{Equation 49})$$

From (Equation 48) and (Equation 49) it can be seen that a higher subcooling temperature gives a higher value for L_l and a lower value for L_{tp} . Based on the sensitivity analysis for the inlet pressure, this would lead to assume that higher subcooling temperature results in a flatter N-shape of the pressure characteristic curve. However, as can be seen from Figure 24 the opposite is the case. A higher subcooling temperature leads to a deeper N-shape of the pressure characteristic curve. In order to explain this behavior of the pressure characteristic curve we must analyze the outlet quality of the flow as a function of the mass flux [1]. Figure 25 shows the outlet quality as a function of the mass flux for the reference case and the sensitivity analysis. The x-axis gives the mass flux and the y-axis gives the outlet quality.

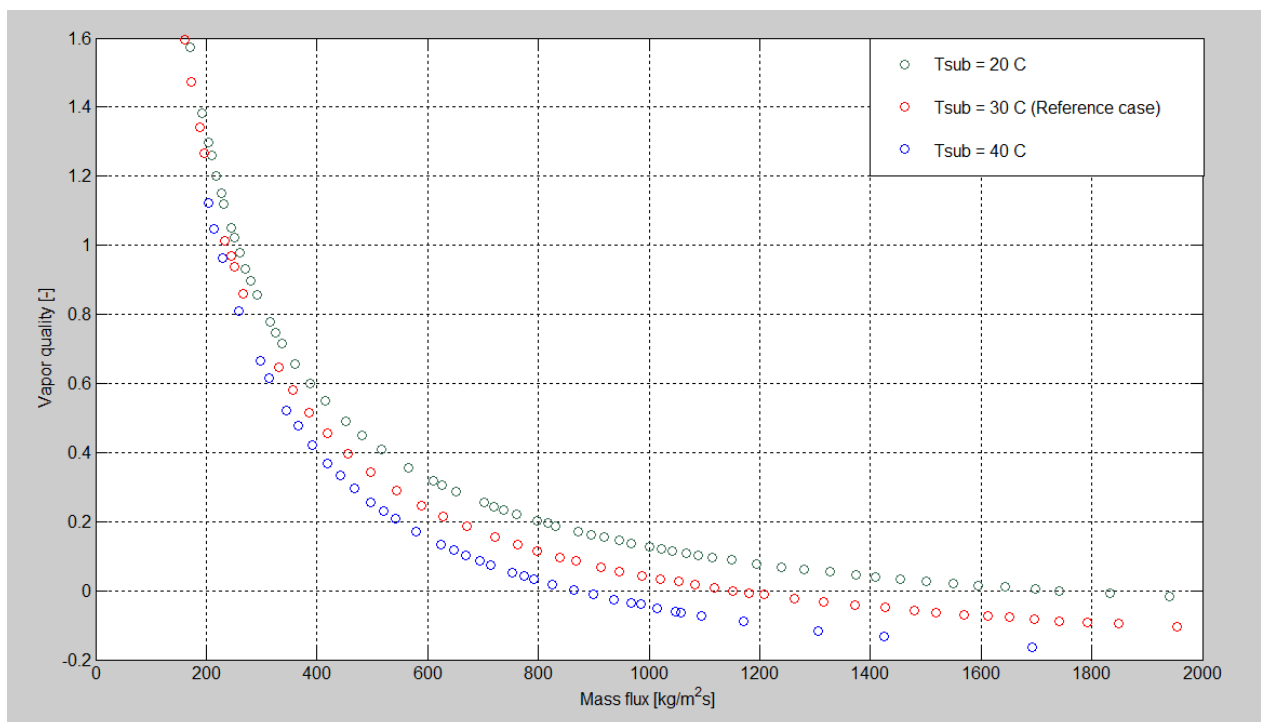


Figure 25: Outlet mass quality for reference case, low subcooling temperature and high subcooling temperature

The rate of change of the outlet mass quality with the mass flux in the condition of saturated liquid ($x_{out} = 0$) is strongly related to the subcooling temperature, as can be seen from Figure 25. The plot for subcooling temperature of 40 °C reaches the conditions of saturated liquid at a lower mass flux value than both the plot for the reference case and the subcooling temperature of 20 °C.

The important aspect to consider is the slope of the outlet mass quality as a function of the mass flux when the outlet mass quality approaches 0. This is important because it gives an idea of the amount of change in the outlet mass quality for a change in the mass flux, which is related to the length of the two-phase flow length. For an outlet mass quality equal to 0, the two-phase flow length is 0. While for an outlet mass quality of 1, the two-phase flow length is at its maximum length. Therefore the slope at outlet quality shows the rate of growth of the two-phase flow length as a function of the decrease in the mass flux. The outlet quality expressed as function of mass flux can be obtained by setting an energy balance for the flow inside the pipe:

$$Q = \dot{m}(c_p T_{sub} + H_{vap} x_{out}) \quad (\text{Equation 50})$$

In (Equation 50) the first term inside the brackets is related to one-phase liquid, while the second term is related to two-phase flow. When introducing mass flux and heat flux, we get an expression for the outlet mass quality:

$$x_{out} = \frac{q_w \pi D_o L}{GAH_{vap}} - \frac{c_p T_{sub}}{H_{vap}} \quad (\text{Equation 51})$$

From (Equation 51) it can be observed that as the mass flux G increases towards infinity, x_{out} will go towards $-c_p T_{sub}/H_{vap}$. For small subcooling temperatures near 0, the outlet quality reaches 0 for mass fluxes which are very larges. This can also be seen from Figure 25 because the subcooling temperature of 20 °C reaches outlet mass quality of 0 at a much higher value than the subcooling temperature of 40°C. For the case of subcooling temperatures close to 0, x_{out} reaches 0 for very large mass flux values.

When we analyze the partial derivative of the outlet quality with respect to the mass flux at the point where $x_{out} = 0$:

$$\frac{\partial x_{out}}{\partial G} (x_{out} = 0) = -\frac{(c_p T_{sub})^2}{q_w H_{vap}} \frac{A}{L \pi D_o} \quad (\text{Equation 52})$$

Even though a smaller subcooling temperature leads to longer liquid phase lengths, and therefore should lead to a steeper N-shape of the pressure characteristic curve, the effect can be overcome by the rate of growth of the outlet quality with changes in the mass flux. The rate of growth of the outlet quality results in a sudden increase in the pressure drop with a decrease in the mass flux for outlet mass qualities close to 0. This is the case for the sensitivity analysis. The experimental results for the subcooling temperature fit well with the numerical results for the numerical study [1].

7.4 The effects of heating power

The effects of varying of the total heating power were examined. The sensitivity analysis was done at uniform total heating power of 500 W and 1 500 W.

The effects of low total heating power have on the pressure characteristic curve were examined by setting the total heating power of all five heaters to 500 W. This means that the heating power in each of the five heaters was set to 100 W. Figure 26 shows the pressure characteristic curve for total heating power of 500 W. In Figure 26 the x-axis gives the mass flux and the y-axis gives the total pressure difference over the pipe.

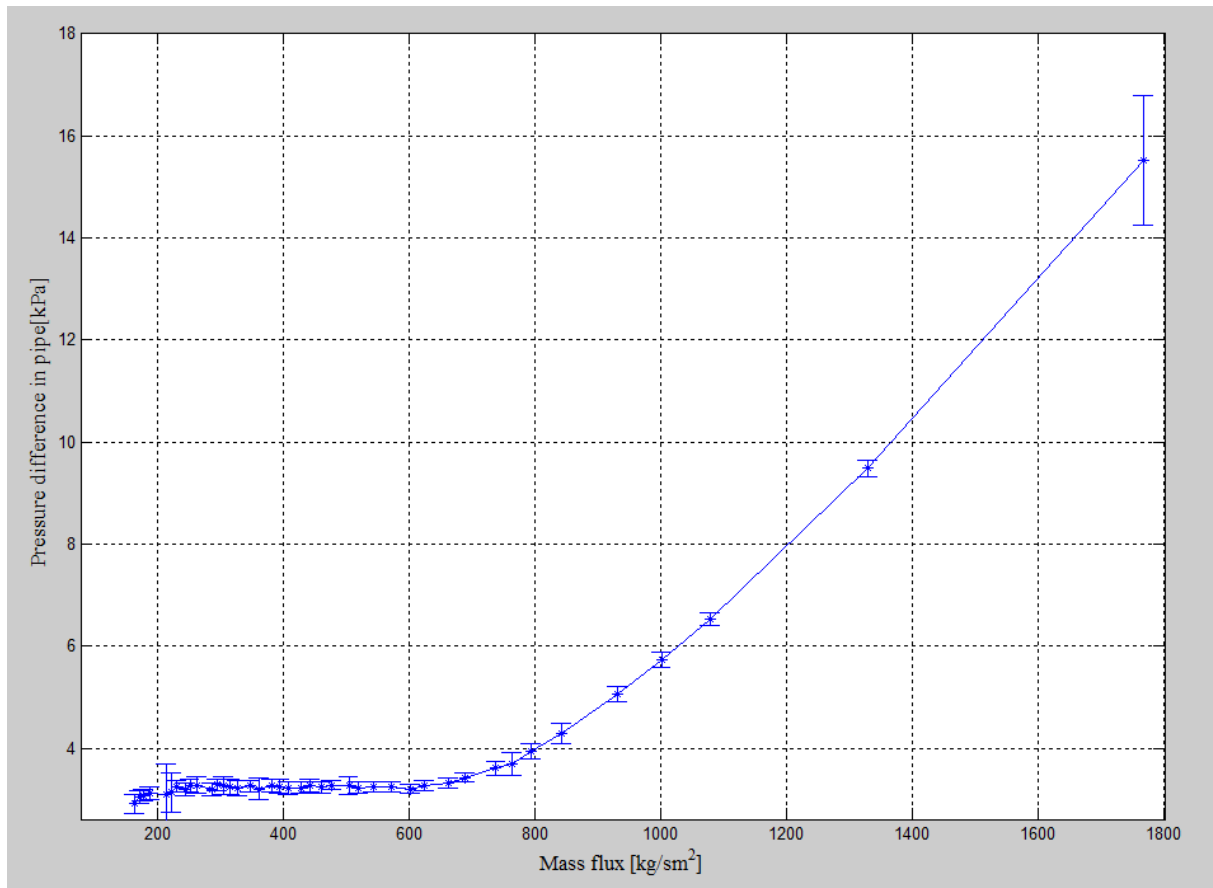


Figure 26: Low heating power: $p = 8.5$ bar, $T_{\text{sub}} = 30$ °C, $Q = 500$ (uniform)

From Figure 26 it can be seen that there is no negative slope in the plot of the pressure characteristic curve.

The effects of high total heating power have on the pressure characteristic curve were examined by setting the total heating power to 1500 W. This means that the heating power in each of the five heaters was 200 W. Figure 27 shows the pressure characteristic curve for a power heating of 1500 W. In Figure 27 the x-axis gives the mass flux and the y-axis gives the total pressure difference over the pipe.

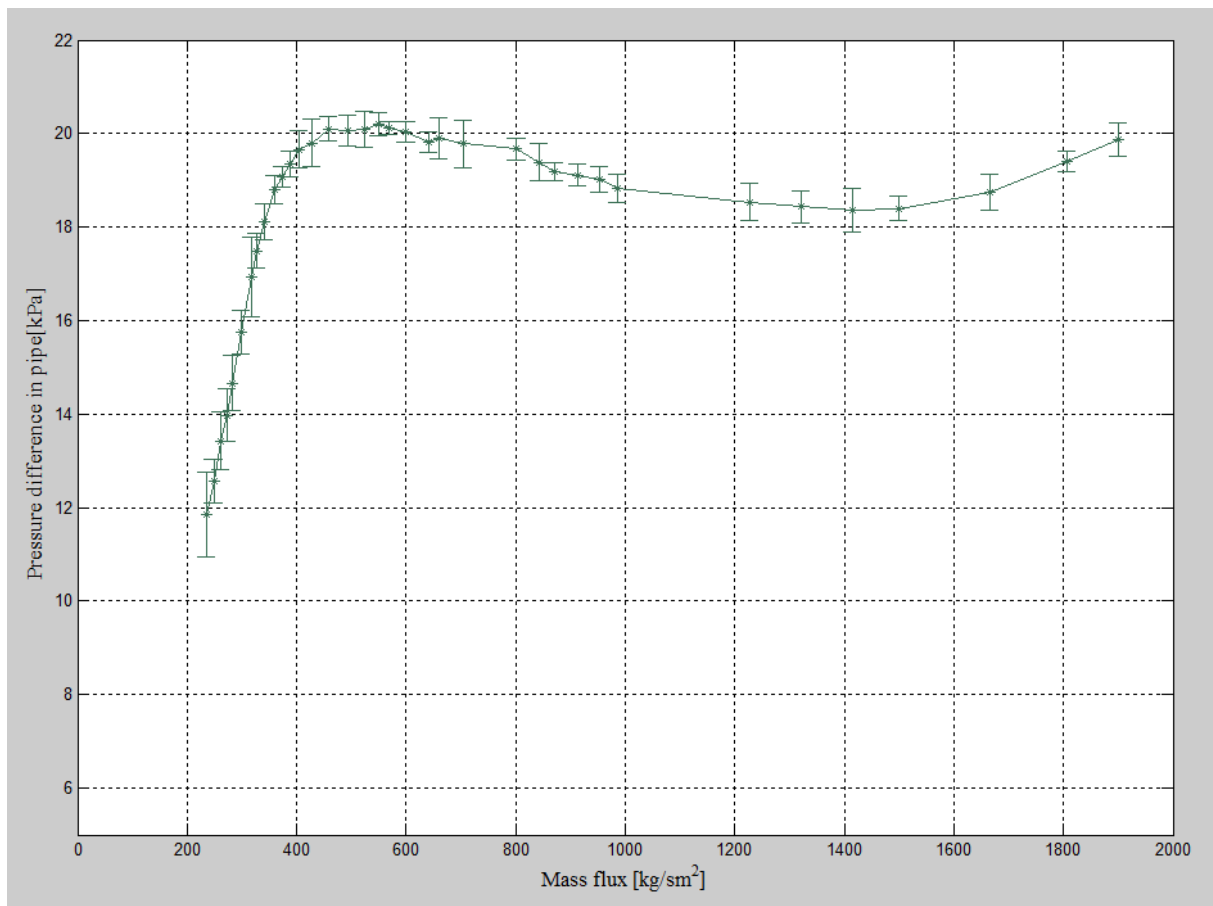


Figure 27: High heating power: $p = 8.5 \text{ bar}$, $T_{\text{sub}} = 30 \text{ }^\circ\text{C}$, $Q = 1500 \text{ W}$ (uniform)

From Figure 27 it can be seen that there is a negative slope in the pressure characteristic curve in for the mass flux values from ca. $645 \frac{\text{kg}}{\text{sm}^2}$ to ca. $1500 \frac{\text{kg}}{\text{sm}^2}$.

In Figure 28 the plots for the pressure characteristic curves for the high and low total heating powers of respectively 500 W and 1500 W are compared with the reference case. In Figure 28 the x-axis gives the mass flux and the y-axis gives the total pressure difference over the pipe.

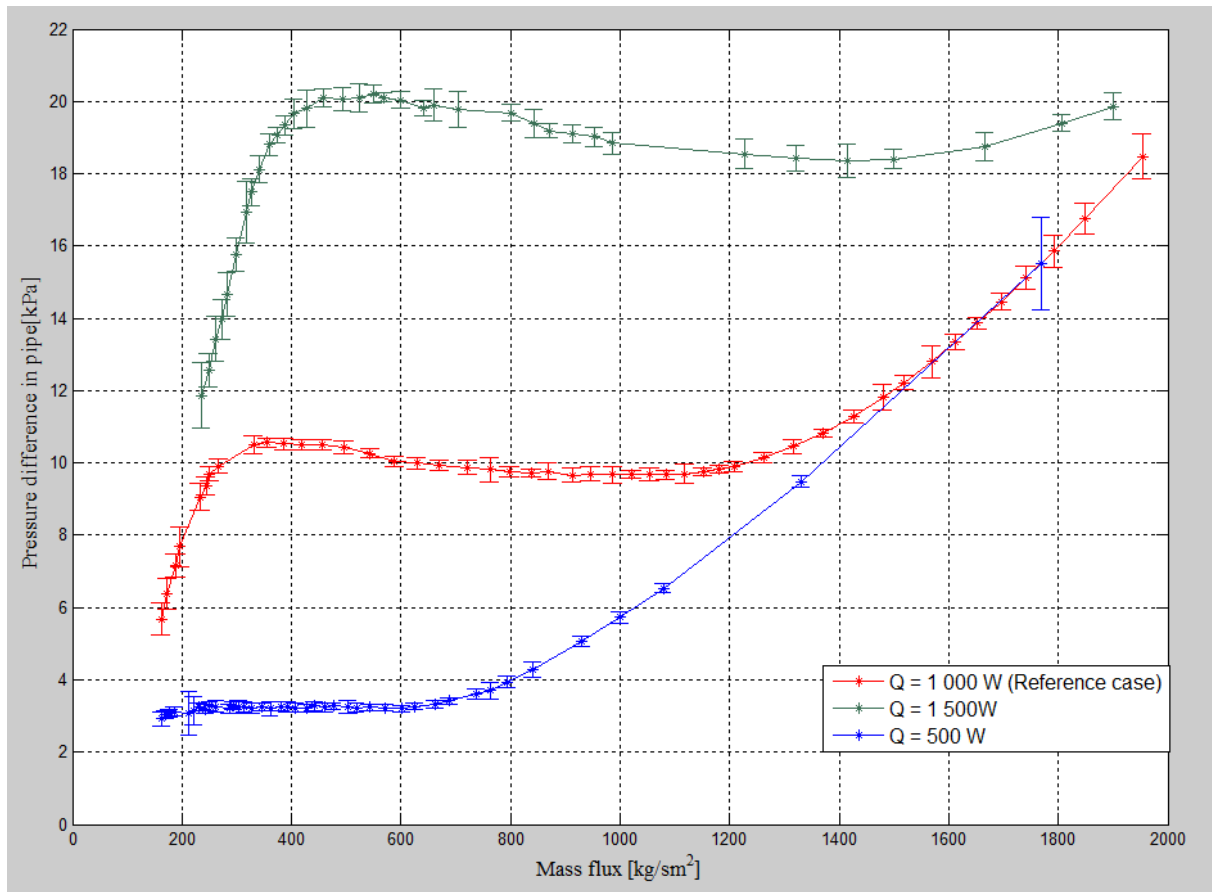


Figure 28: Comparing reference case with plots of lower and higher heating power

It can be seen from Figure 28 that the heating power has an influence on the pressure characteristic curve. For a higher total heating power the negative slope is steeper, while it does not exist for a lower total heating power.

When the total heating power is increased for the same mass flux the enthalpy at the outlet is higher. The experimental results for the heating power do not fit completely with the numerical results from the numerical study [1]. In the numerical study the shape of the pressure characteristic curve did not change for increased or decreased heating power.

7.5 The effects of the heating power distribution

The effects of varying the heating power distribution were examined. A distribution of the heating power is important to investigate because in many heat exchange applications the heat flux exchanged is not uniform, but rather a function of the temperature difference between the fluids. This is typical for heat exchangers. The sensitivity analysis was done for a step-wise increasing and a step-wise decreasing heating power distribution. The mean value of the heating power distributions in the sensitivity analysis is the same. Only linearly step-wise (not quadratic and cubic) increasing and decreasing heating distributions are investigated in the sensitivity analysis due to danger of overheating the heaters.

The effects of a step-wise increasing heating power distribution were analyzed using the heat distribution shown in Figure 29. In Figure 29 the horizontal axis gives the number of the heater and the vertical axis gives the heating power in W . Heater 1 was set to a heating power of $100\ W$. The rest of the heaters were set to a heating power that is $50\ W$ higher than the heater to their left, meaning that heater 5 had a heating power of $300\ W$.

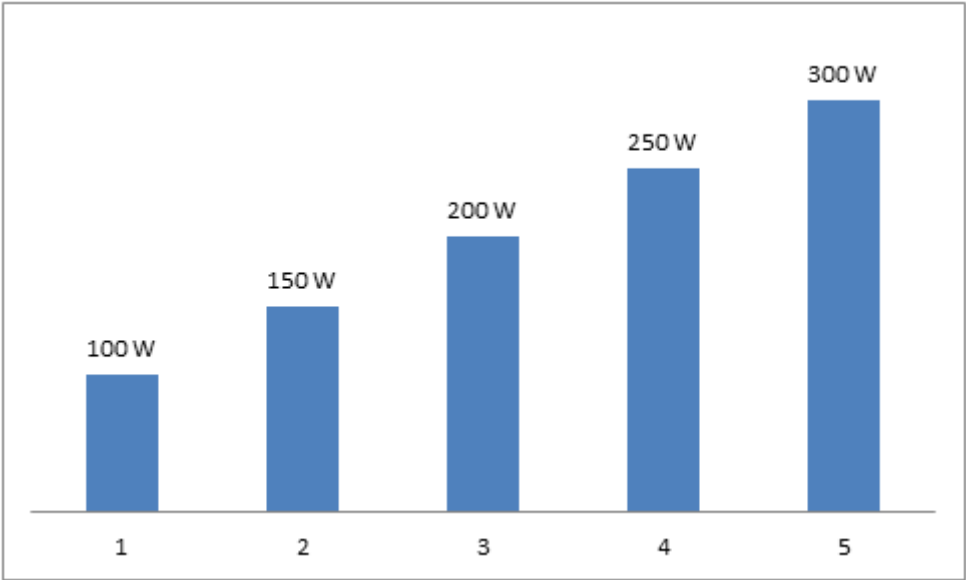


Figure 29: Step-wise increasing heating distribution

Figure 30 shows the pressure characteristic curve for the step-wise increasing heating power distribution. In Figure 30 the x-axis gives the mass flux and the y-axis gives the total pressure difference over the pipe.

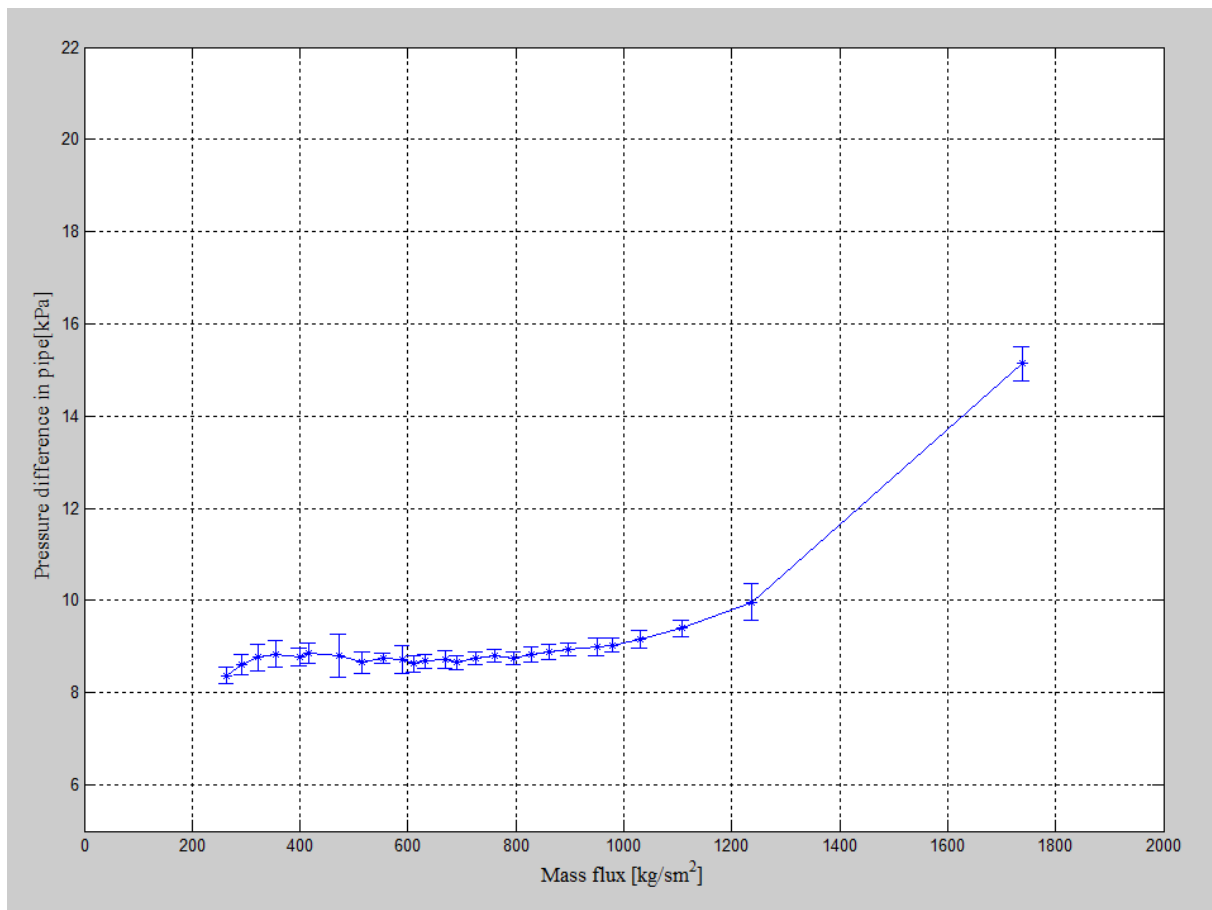


Figure 30: Step-wise increasing heating distribution: $p = 8.5 \text{ bar}$, $T_{\text{sub}} = 30 \text{ }^\circ\text{C}$, $Q = 1000 \text{ W}$ (step-wise increasing)

There are some oscillations of the pressure characteristic curve for the increasing heating power distribution in Figure 30 for the mass flux values from ca. $355 \frac{\text{kg}}{\text{sm}^2}$ to ca. $610 \frac{\text{kg}}{\text{sm}^2}$. This can possibly imply a negative slope in the pressure characteristic curve.

The effects of a step-wise decreasing heating distribution were analyzed by using the heat distribution showed in Figure 31. In Figure 31 the horizontal axis gives the number of the heater and the vertical axis gives the heating power in W . The heating power for Heater 1 was set to 300 W . The rest of the heaters were set to a heating power that is 50 W lower than the heater to their left, meaning that heater 5 had a heating power of 100 W .

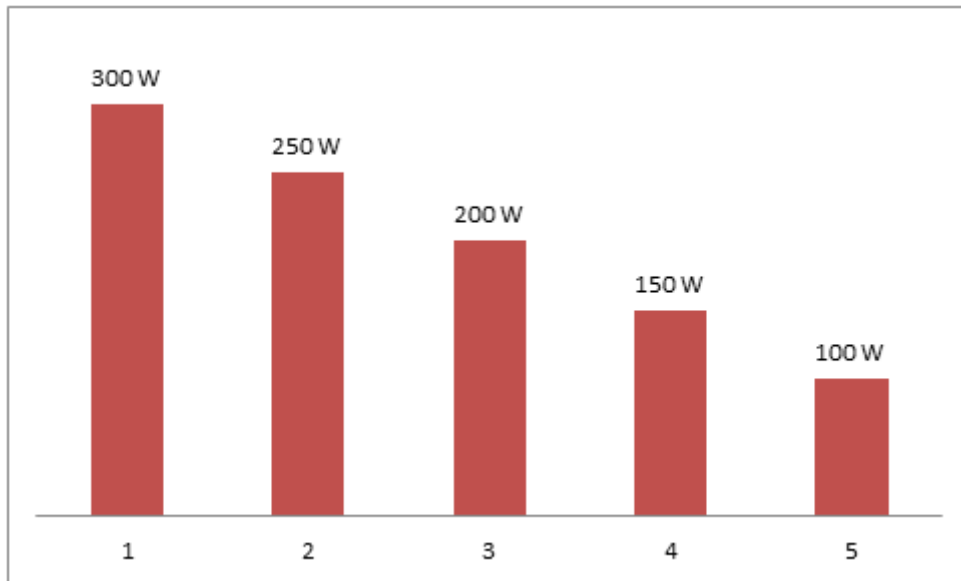


Figure 31: Step-wise decreasing heating distribution

Figure 32 shows the pressure characteristic curve for the step-wise decreasing heating power distribution. In Figure 32 the x-axis gives the mass flux and the y-axis gives the total pressure difference over the pipe.

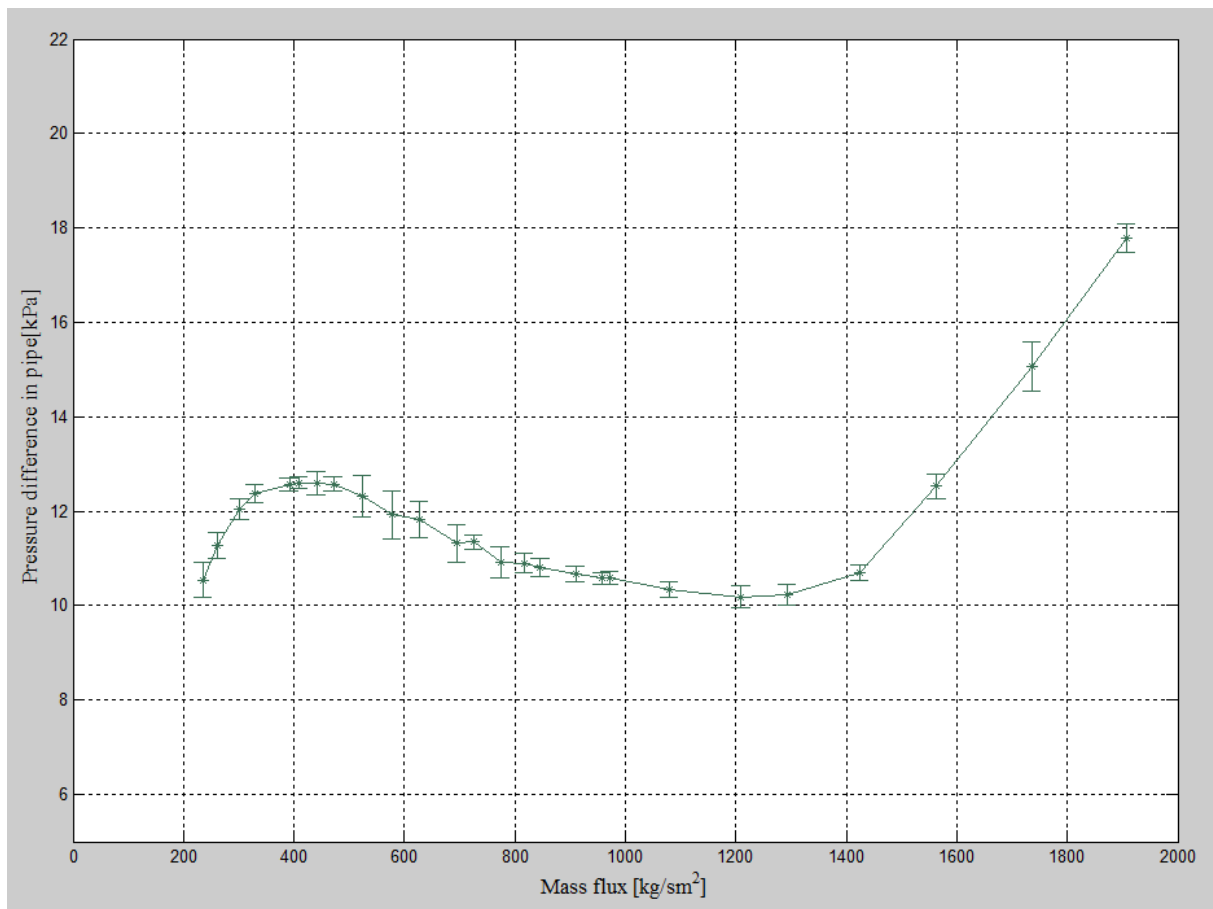


Figure 32: Step-wise decreasing heating power distribution: $p = 8.5$ bar, $T_{sub} = 30$ °C, $Q = 1000$ W (step-wise decreasing)

It can be seen from Figure 32 that there is a negative slope in the pressure characteristic curve for the decreasing heating power distribution for mass flux values from $440 \frac{kg}{sm^2}$ to $1360 \frac{kg}{sm^2}$.

In Figure 33 the cases for the step-wise increasing and step-wise decreasing heating power distributions of are compared with the reference case. In Figure 33 the x-axis gives the mass flux and the y-axis gives the total pressure difference over the pipe.

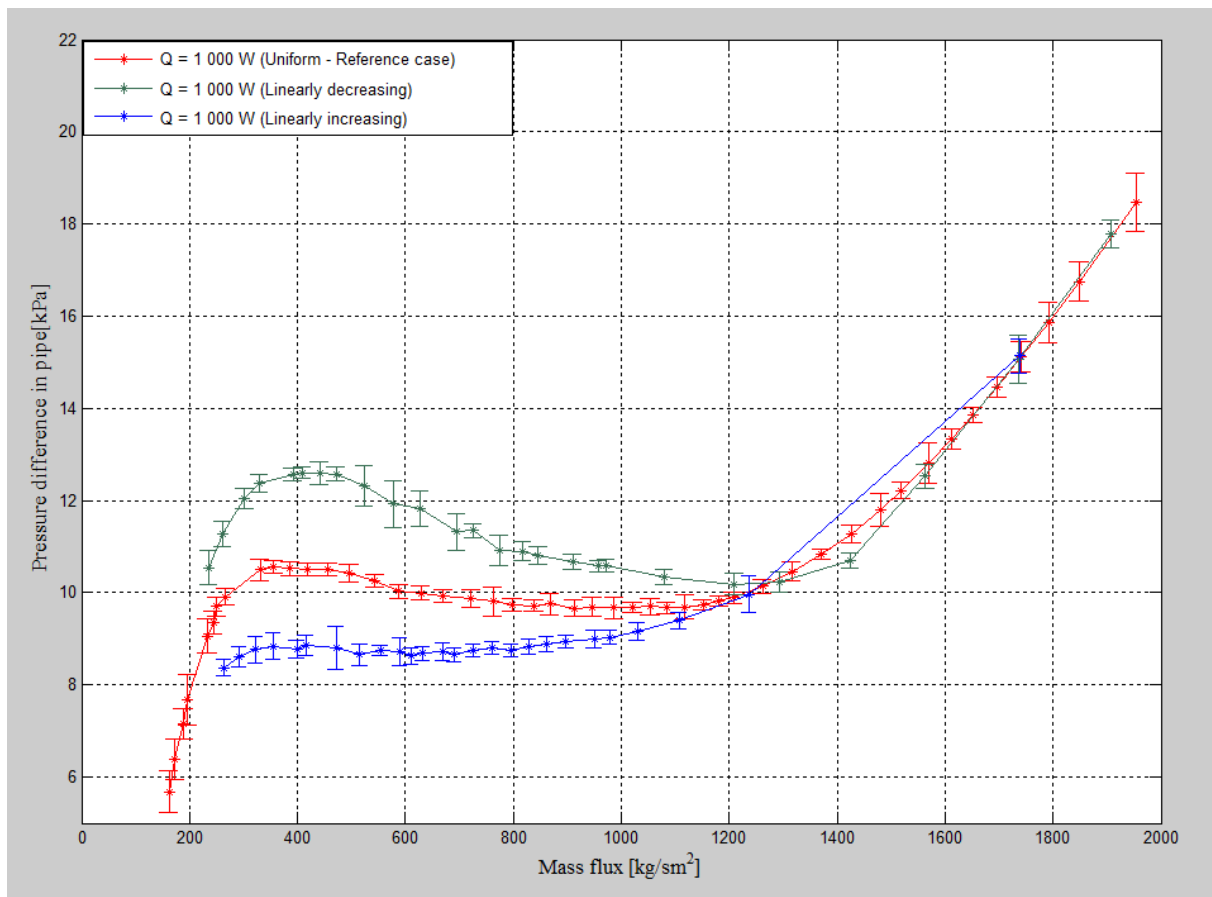


Figure 33: Comparing reference case with plots of step-wise increasing and decreasing heating power distributions

It can be seen from Figure 33 that a step-wise decreasing heating power distribution gives a steeper negative slope of the pressure characteristic curve, while step-wise increasing heating power distribution gives a flatter N-shape.

The reason for this behavior of the pressure characteristic curve is that more heating power applied at the beginning of the pipe results in a larger two-phase flow length. And as mentioned before a larger two-phase flow length results in a steeper N-shape of the pressure characteristic curve. The experimental results for the heating power distribution fit well with the numerical results from the numerical study [1].

7.6 Discussion of experimental work

This section summarizes and discusses the presented experimental results. The experimental work showed that all the parameters of the sensitivity analysis (inlet pressure, subcooling temperature, total heating power and heating power distribution) influence the behavior of the pressure characteristic curve.

The influence of inlet pressure is associated with the two-phase frictional factor, and the behavior of the density and viscosity of the phases. The influence of subcooling temperature is related to the rate of growth of the outlet mass quality with changes in the mass flux. For the total heating power it was shown that the lower heating power made the negative slope of the pressure characteristic curve flatter, while a higher total heating power made it steeper. The experimental results do not agree with the results from the numerical study. This sort of behavior of the pressure characteristic curve for the heating power is typical for vertical two-phase flow, where the elevation component of the pressure drop is relevant. The heating power distribution behavior is related to the relationship between the phase flow lengths in the pipe. Table 3 is a summary of the influence decreasing and increasing the parameters during the sensitivity analysis has on the slope of the pressure characteristic curve.

Table 3: Summary of the effect of the pressure characteristic curve

Parameter	Effect on the slope of pressure characteristic curve compared to reference case	Fits with existing numerical study
Lower inlet pressure (6.5 bar)	More negative	Yes
Higher inlet pressure (10.5 bar)	More positive	Yes
Lower subcooling temp. (20 °C)	More positive	Yes
Higher subcooling temp. (40 °C)	More negative	Yes
Lower total heating power (500 W)	More positive	No
Higher total heating power (1500 W)	More negative	No
Step-wise increasing heat dist.	More negative	Yes
Step-wise decreasing heat dist.	More positive	Yes

In the graphs of the experimental work it can be seen that the error bars vary in size. The main reason why some of the bars are larger than other is that subcooling temperature or inlet pressure was not kept at a constant value during the measurements. It was very challenging to always keep both the subcooling temperature and the inlet pressure at a constant value, especially at low mass flux value.

To analyze how large the influence of each parameter is on the behavior of the pressure characteristic curve, it is useful to consider how the representative slope of the pressure characteristic curve (for $0 \leq x_{out} \leq 1$), changes for each parameter compared to the slope of reference case. How the changes in the slope can be seen by considering Figure 34.

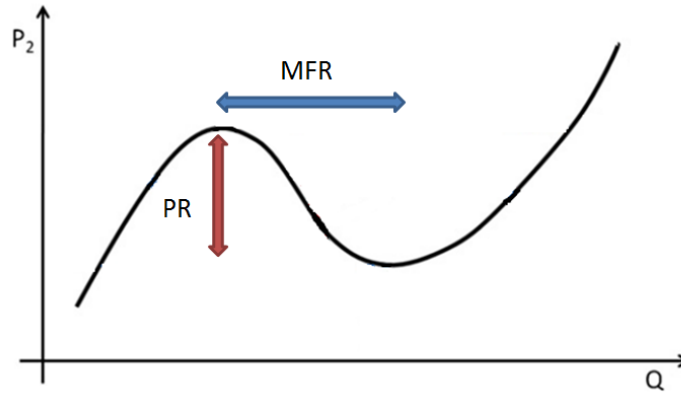


Figure 34: Typical pressure characteristic curve for two phase flow with indicated mass flux range (MFR) and pressure range (PR)

Figure 34 shows a typical pressure characteristic curve. The blue arrow indicates the range of the mass flux where the slope of the pressure characteristic is negative, and the range is called mass flux range (MFR). While the red arrow indicates the range of the pressure drop where the slope of the pressure characteristic curve is negative, and it is called pressure range (PR). For the cases from the sensitivity analysis where the slope of the pressure characteristic curve is negative MFR is found graphically as the distance between the zero gradient points in the graph. While for the cases where the slope becomes positive, MFR is defined as the range between $x_{out} = 0$ and $x_{out} = 1$. PR is found in the same way. Table 4 provides an overview of all the MRFs and PRs for all the analyzed cases.

Table 4: Mass flux ranges and pressure ranges for parameter slopes from the sensitivity analysis

	Mass flux [$kg/s\ m^2$]			Pressure [kPa]			Slope [$kg/s\ m^2\ kPa$]
	Min.	Max.	MFR	Min.	Max.	PR	
Reference case	335.0	986.0	631.0	9.6	10.5	0.9	0.0014
p: 6.5 bar	379.1	1235.3	856.1	11.1	14.4	3.3	0.0039
P: 10.5 bar	246.5	1136.9	890.4	7.7	8.9	1.2	0.0013(positive slope)
T_{sub}: 20 °C	255.8	1734.4	1478.6	10.6	19.6	9.0	0.0061 (positive slope)
T_{sub}: 40 °C	312.9	825.8	512.9	5.9	8.4	2.5	0.0049
Power: 500 W	119.1	577.6	458.5	2.9	3.2	0.3	0.000683(positive slope)
Power: 1500 W	550.0	1415.4	865.4	18.3	20.1	1.8	0.0021
Heat: Decreasing	409.8	1209.6	799.8	10.2	12.6	2.4	0.0031
Heat: Increasing	119.1	577.9	458.8	7.5	8.7	1.2	0.0026 (positive slope)

To clearly observe the results a graphical illustration of the effects the parameters have on MFR can be seen in Figure 35, 36, 37 and 38.

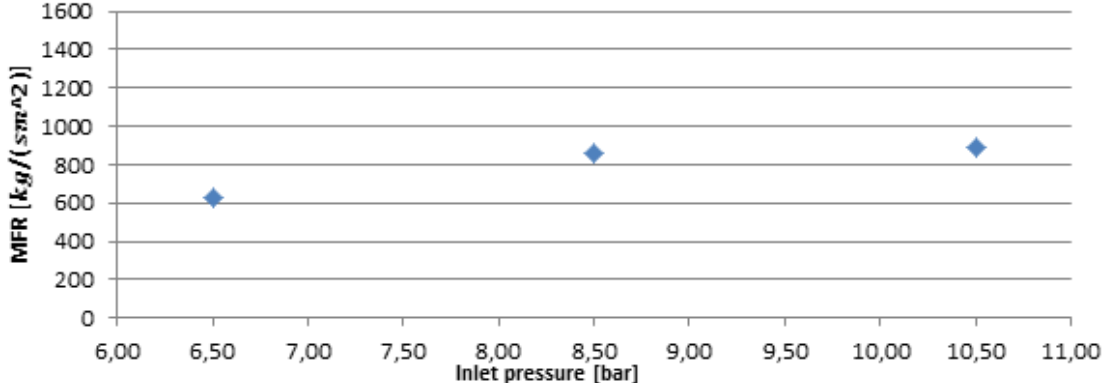


Figure 35: Inlet pressure effect on MFR

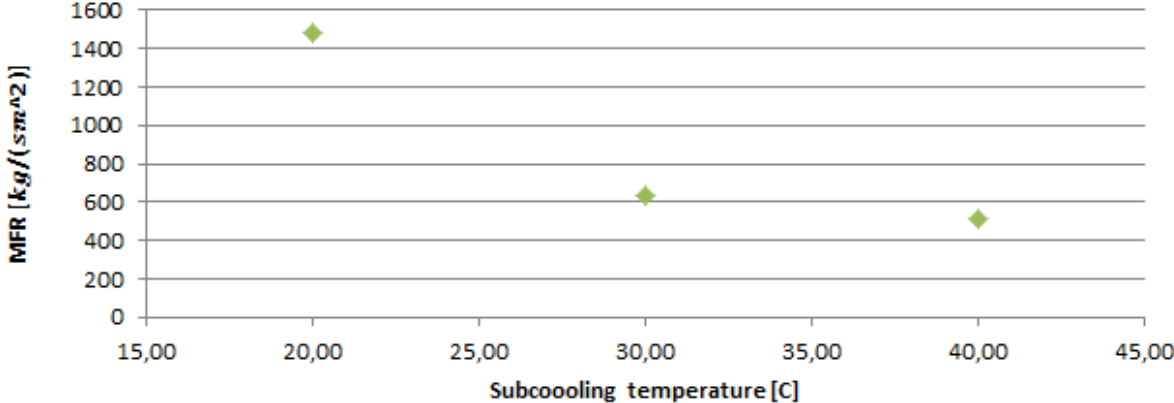


Figure 36: Subcooling temperature effect on MFR

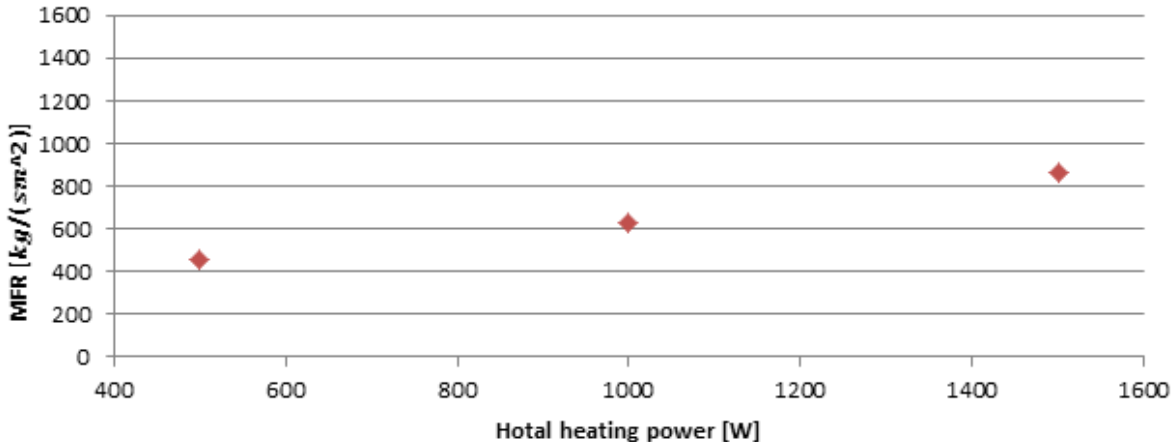


Figure 37: Total heating power effect on MFR

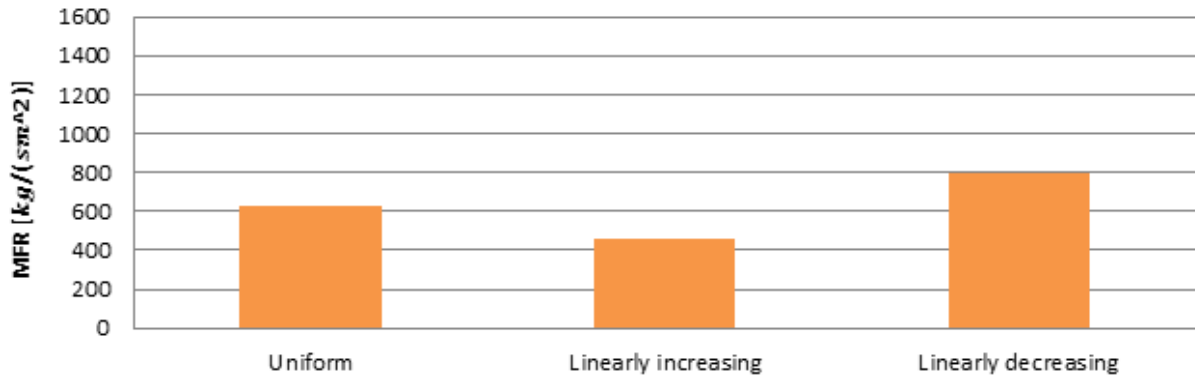


Figure 38: Heating power distribution effect on MFR

To investigate the influence each analyzed parameter has on the negative slope in pressure characteristic curve, we can compare how much the value of each parameter changes to that of MFR. The sensitivity analysis for MFR can be seen in Table 5.

Table 5: Sensitivity analysis for MFR

Parameters	Change in parameter compared to reference case	Change in MFR compared to the reference case	Sensitivity to the parameter
p: 6.5 bar	-23.53 %	+35.67 %	1.55
P: 10.5 bar	+23.53 %	+41.11 %	1.79 (positive slope)
T_{sub}: 20 °C	- 33.33 %	+134.33 %	4.03 (positive slope)
T_{sub}: 40 °C	+33.33 %	-18.72 %	0.56
Power: 500 W	-50 %	-27.34 %	0.55 (positive slope)
Power: 1500 W	+50 %	-37.15 %	0.74
Heat: Decreasing	-	-	-
Heat: Increasing	-	-	-

In Table 5 the column on the far right, called “Sensitivity to the parameter”, is defined as the absolute value of the ratio of the change in percentage of the MFR to the percentage change in the parameter. This ratio indicates how much a change in the parameter changes the MFR. It can be seen that lowering the inlet pressure has the largest effect on the range where the negative slope on the pressure characteristic curve can occur. Increasing the total heating power has the second largest effect, and increasing the subcooling temperature has the third largest. The other cases of the sensitivity analysis make the slope of the pressure characteristic positive, and are not considered.

Next, it is useful to analyze how the PR is influenced by the parameters. The PR indicates how unstable the system represented by pressure characteristic curve is. The sensitivity analysis for the PR can be seen in Table 6.

Table 6: Sensitivity analysis of PR

Parameters	Change in parameter compared to reference case	Change in PR compared to the reference case	Sensitivity to the parameter
p: 6.5 bar	-23 %	+266.67 %	11.69
P: 10.5 bar	+23 %	+33.33 %	1.45 (positive slope)
T_{sub}: 20 °C	-33.33 %	+900.00 %	27.0 (positive slope)
T_{sub}: 40 °C	+33.33 %	+177.78 %	5.33
Power: 500 W	-50 %	-66.67 %	1.33(positive slope)
Power: 1500 W	+50 %	+100 %	2.00
Heat: Decreasing	-	-	-
Heat: Increasing	-	-	-

In Table 6 the column on the far right, called “Sensitivity to the parameter”, is defined as the absolute value of ratio of the change in percentage of the MFR to the percentage change in the parameter. It can be seen that lowering the inlet pressure has the largest influence on how unstable the system represented by pressure characteristic curve is in the negative slope region. Increasing the subcooling temperature has the second largest influence, while increasing the total heating power has the third largest influence. Like with the MFR, the parameters leading to a positive slope of the pressure characteristic curve are not considered.

It should be noted from Table 5 and Table 6 that heating distribution is not accounted for in the sensitivity analysis of the parameters because it is not possible to quantify that parameter in the same way as the other parameters.

8 Conclusion

An experimental analysis of the pressure characteristic curve for two-phase flow has been performed in this study. The behavior of the pressure characteristic curve has been analyzed for inlet pressures of 6.5 *bar*, 8.5 *bar* and 10.5 *bar*, subcooling temperatures of 20°C, 30°C and 40 °C, total heating power of 500 *W*, 1000 *W* and 1500 *W*, and heating distributions which are uniform, step-wise decreasing and step-wise increasing. The experimental analysis was done for refrigerant R-134a through a single, horizontal pipe with an inner diameter of 5 *mm*. The experimental results have been compared with the results from an existing numerical study [1].

The experimental work showed that all the tested parameters during the sensitivity analysis affect the behavior of the pressure characteristic curve. Lower inlet pressure, higher subcooling temperature, higher total heating power and a step-wise decreasing heating power distribution made the negative slope in the pressure characteristic curve steeper compared to the reference case. While higher inlet pressure, lower subcooling temperature, lower total heating power and a step-wise increasing heating power distribution made the negative slope in the pressure characteristic curve flatter compare to the reference case. All the experimental results are in agreement with both the results from the existing numerical study [1] and the literature, except for the total heating power. However the impact these parameters have on the pressure characteristic curve is not the same.

The inlet pressure was found to be the parameter which has the largest relative influence on the pressure characteristic curve for the MFR and the PR. Decreasing the inlet pressure expands the mass flux range where instabilities can occur for the mass flux almost 3 times more than increasing the subcooling temperature, and 2 times more than increasing the total heating power. The pressure characteristic curve becomes approximately 2 times more unstable than increase in the subcooling temperature, and almost 6times more than when the total heating power is increased.

Since the measurements for the total heating power do not agree with neither the numerical study, nor the literature it requires further work to be done. The further work can consist of doing more refined measurements within the boundaries of the sensitivity analysis used in this study. High speed visualization can also be used to observe the flow patterns at the outlet of the pipe in the heated test section, and hence obtain a clearer understanding of the processes occurring when the total heating power is varied.

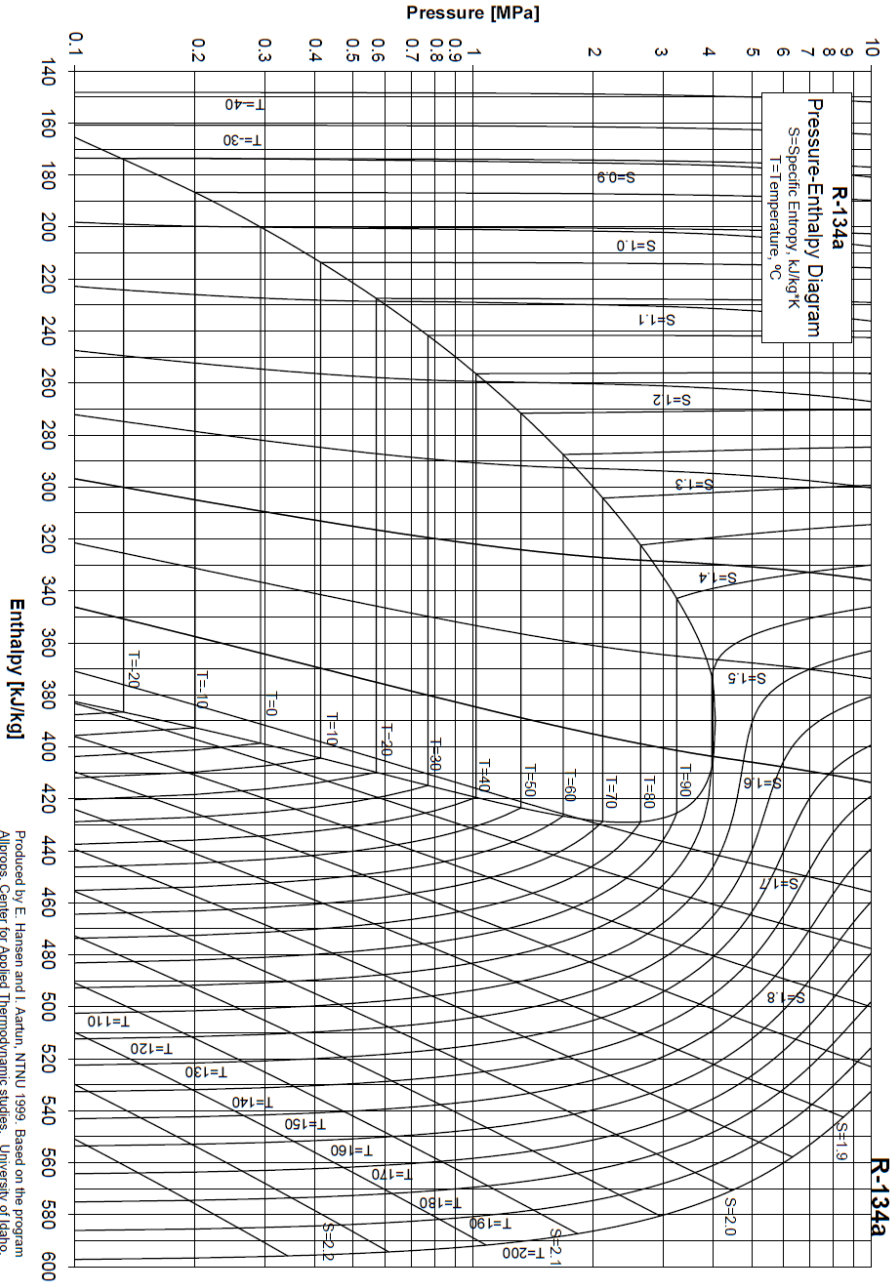
References

1. E. Manavela Chiaper, M.F., C.A. Dorao, *Parametric study of the pressure characteristic curve in a boiling channel*. Computational Thermal Science, 2011.
2. Ghiaasiaan, S.M., *Two-Phase Flow, Boiling and Condensation* 2008: Cambridge University Press. 613.
3. A.L. Souza, J.C.C., J.M.S. Jabardo, J.P. Wattelet, J. Panek, C. Christoffersen, N. Rhines, *Pressure Drop During Two-Phase Flow of Refrigerant in Horizontal Smooth Tubes*. 1992.
4. Thome, J.R., *Wolverine Tube Inc. Engineering Data Book 3*, 2010, Swiss Federal Institute of Technology Lausanne: Lausanne, Switzerland.
5. Incropera, D., Bergman, Lavine, *Fundamentals of Heat and Mass Transfer*. Vol. Sixt Edition. 2007: John Wiley & Sons.
6. E. Manavela Chiaper, M.F., C.A. Dorao, *Review on pressure drop oscillations in boiling systems*. Nuclear Engineering and Design, 2012.
7. T. Zang, T.T., J. Chang, R. Prasher, M. K. Jensen, J.T. Wen, P. Phelan, *Ledinegg instability in microchannels*. Science and Technology of Nuclear Installations, 2009.
8. J. Hass, M.D.W., G.B Thomas, *Calculus Part 2* 2008: Pearson Education.
9. J. A. Boure, A.E.B., L.S. Long, *Review of Two-Phase Flow Instability*. Nuclear Engineering and Design, 1972.
10. M. Yilmaz, O.C., S. Karsli, *The effect of inlet subcooling on two-phase flow instabilities in a horizontal pipe system with augmented surfaces*. International Journal of Energy Research, 2002.
11. S.Kakac, L.C., *Analysis of convective two-phase flow instabilities in vertical and horizontal in-tube boiling systems*. International Journal of Heat and Mass Transfer, 2009.
12. H.Yuncu, O.T.Y., S. Kakac, *Two-Phase instabilities in a horizontal single boiling channel*. Applied Scientific Research, 1990.
13. Carlson, G.A. *Experiemtnal Errors and Uncertainty*. 2000-2002; Available from: http://www.ece.rochester.edu/courses/ECE111/error_uncertainty.pdf.
14. Dimanek, D.R. *Error Analysis (Non-Calculus)*. Available from: <http://www.lhup.edu/~dsimanek/errors.htm>.
15. SUher, A. *Errors: What they are, and how to deal with them*. Available from: https://newton.ex.ac.uk/teaching/resources/au/1st_year_lab/errors_handouts.pdf.
16. White, F.M., *Fluid Mechanics*. McGraw-Hill Series in Mechanical Engineering Sixt Edition.
17. J. W. Nilsson, S.A.R., *Lectrical Circuits*. Vol. 8th Edition. 2008: Pearson Education Inc.
18. E. Hansen, I.A. *Pressure-Enthalpy Dagram R-134a*. 1999; Available from: http://www.nt.ntnu.no/users/haugwarb/Phase_diagrams_and_thermodynamic_tables/P_haseDiagrams/R134a.pdf.
19. <http://www.docstoc.com/docs/4195427/THE-MOODY-DIAGRAM-ABSOLUTE-ROUGHNESS-OF-PIPE-OR-DUCT>. *Moody diagram*.

Appendices

Appendix A

Appendix A gives a pressure-enthalpy diagram for refrigerant R-134a which can be seen in Figure 39.



Produced by: E. Hansen and I. Aarhus, NTNU 1999. Based on the program Allprops, Center for Applied Thermodynamic studies, University of Idaho.

Figure 39: Pressure-Enthalpy diagram for R-134a [18]

Appendix B

Appendix B contains a Moody-diagram which can be seen in Figure 40.

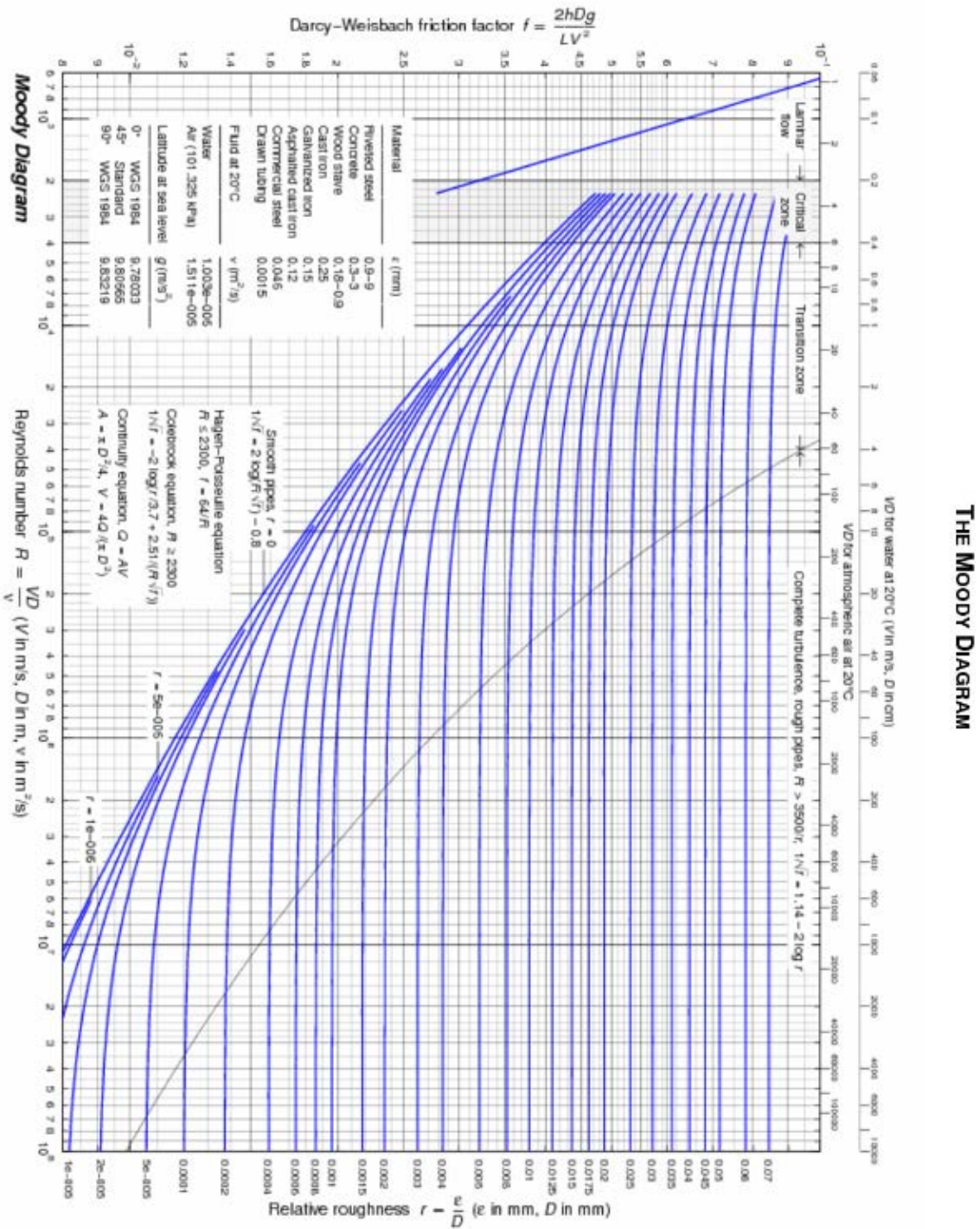


Figure 40: Moody diagram [19]

Appendix C

Appendix C contains a diagram of the complete two-phase experimental facility (not only the components described in Chapter 3). The complete experimental facility can be seen in Figure 41.

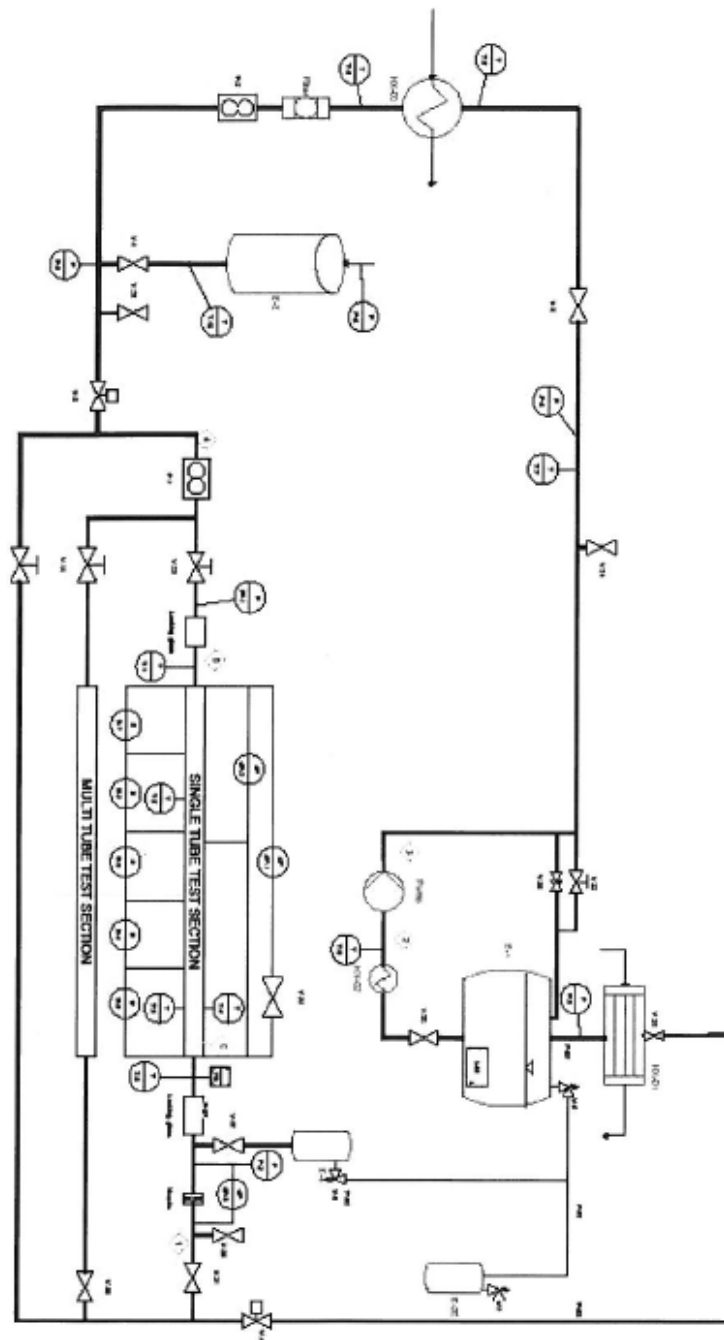


Figure 41: Diagram of complete two-phase experimental facility

Appendix D

Appendix D contains the results from the calibration of the heaters in the heating section. In Figure 42, Figure 43, Figure 44, Figure 45 and Figure 46 the x-axis is the value mean value obtained in LabVIEW, and the y-axis is the Root mean square (RMS) value measured with the oscilloscope. The red circles indicate the measurements points, and the black graph is the polynomial fit of 2 degrees.

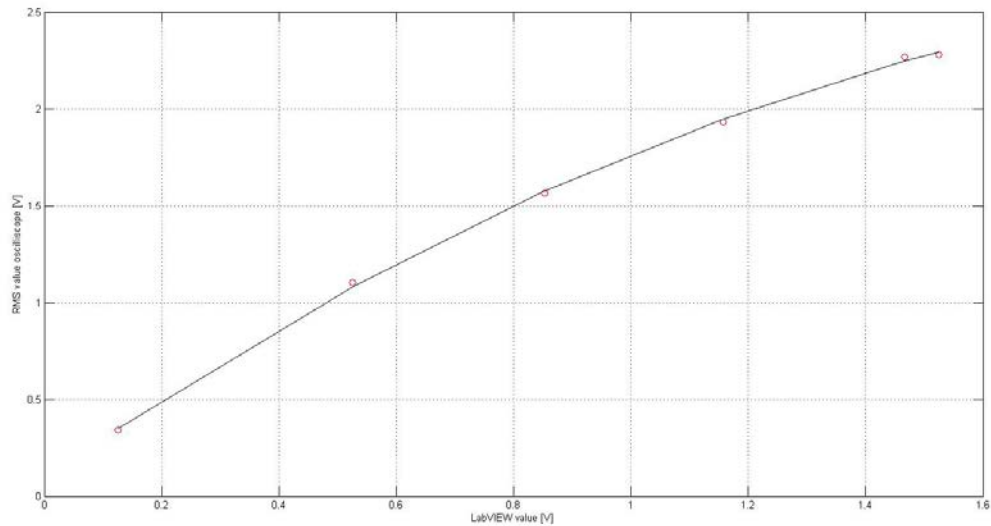


Figure 42: Voltage calibration of Heater 1

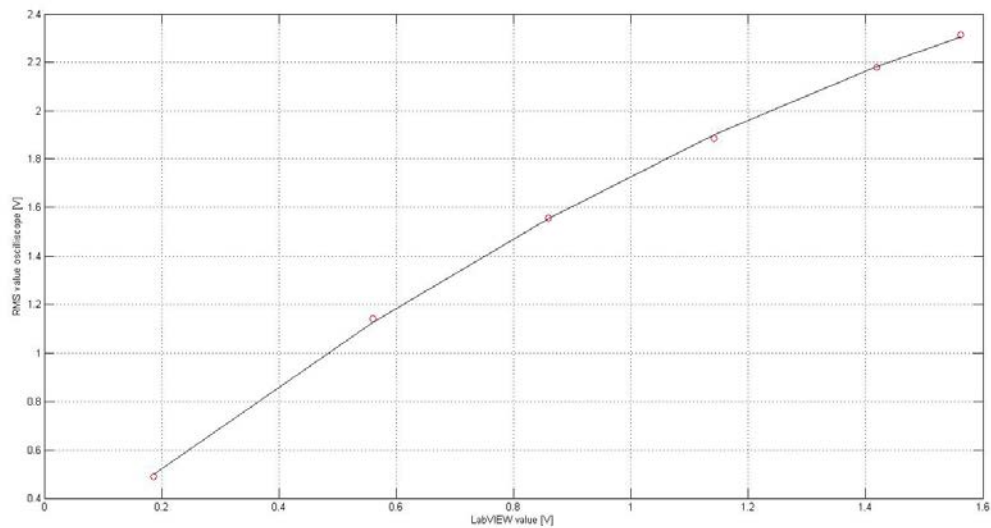


Figure 43: Voltage calibration of Heater 2

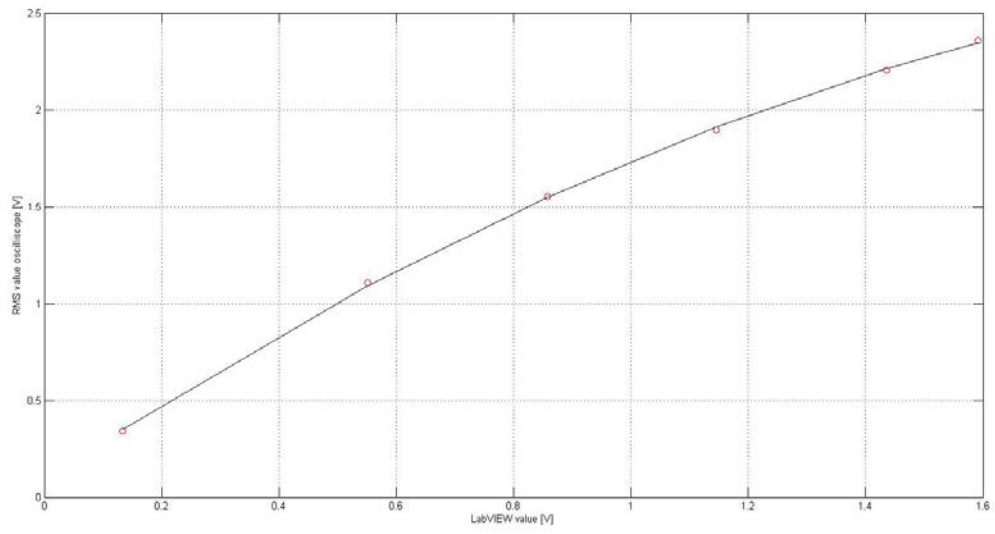


Figure 44: Voltage calibration of Heater 3

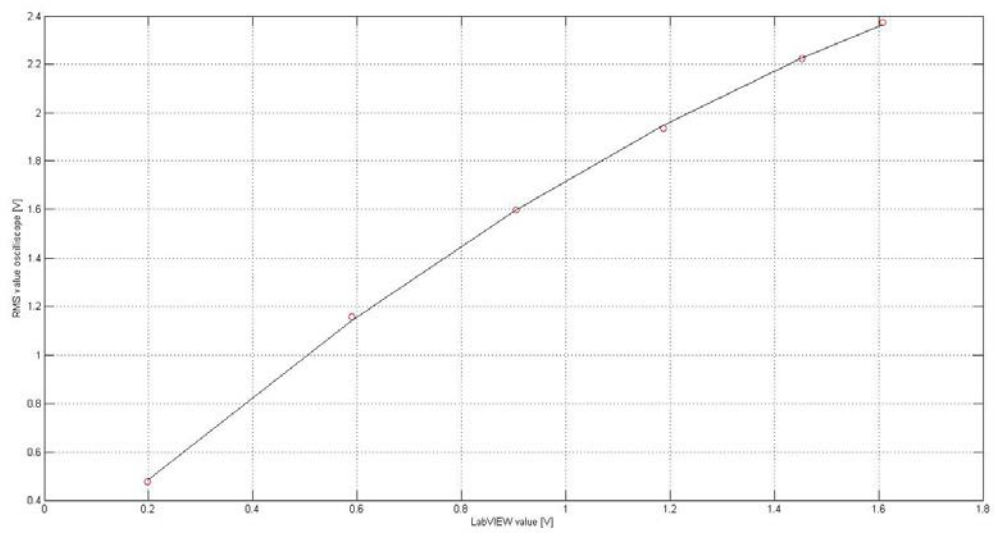


Figure 45: Voltage calibration of Heater 4

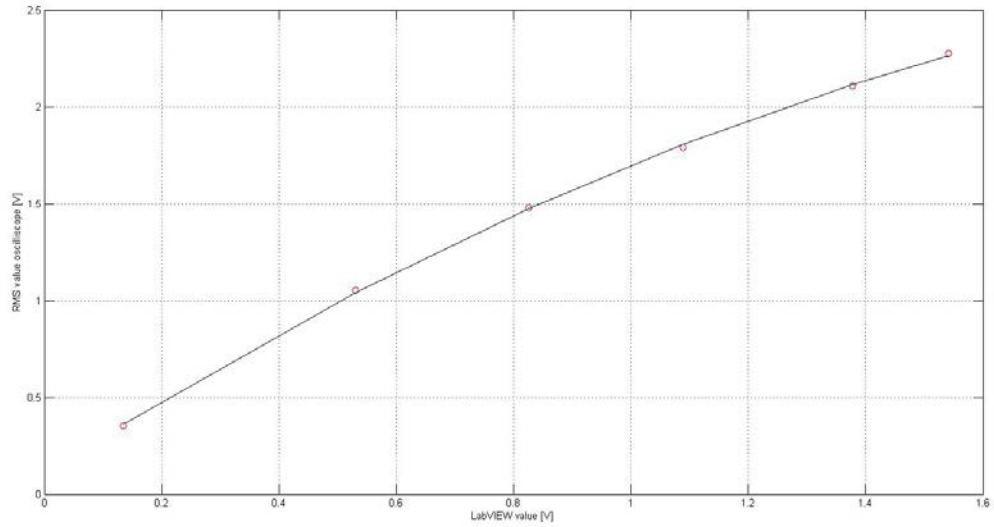


Figure 46: Voltage calibration of Heater 5

Table 7 contains the equations for the polynomial fit for the voltage calibration for Heaters 1-5.

Table 7: Polynomial equations from measurements from calibration of heaters

Heater	Polynomial fit for voltage calibration
1	$V_{rms} = -0.4366x^2 + 2.1081x + 0.0936$
2	$V_{rms} = -0.3666x^2 + 1.9558x + 0.1454$
3	$V_{rms} = -0.3909x^2 + 2.0415x + 0.0854$
4	$V_{rms} = -0.3485x^2 + 1.9591x + 0.1092$
5	$V_{rms} = -0.3618x^2 + 1.9601x + 0.1011$

Appendix E

Appendix E is a user manual for the experimental facility. It is divided into three parts: The first part contains information on the requirements for accessing the experimental facility, the second part is about the software used for controlling the experimental facility called LabVIEW and the third part provides information on how to start-up the experimental facility. This user manual has been developed with guidance from the co-supervisor of the project, Ezequiel M. Chiapero. All photographs used in this user manual have been taken by the author of this project.

Accessing the experimental facility

This section explains what needs to be done in order to get access to the laboratory at NTNU where the two-phase experimental facility is located. Before being allowed to access the laboratory at NTNU an online HSE (health, safety and environment) course must be passed. After passing the online HSE course one must also get a guided tour at the laboratory from an HSE coordinator from NTNU. Both the HSE course must be passed and the guided tour given for access to the laboratory to be granted. Before using the two-phase experimental facility without supervision, it is highly recommended that one gets proper training by the person responsible for the experimental facility. The training should be on both how to operate the facility and on how to use LabVIEW. When the training is completed, one must fill out a form together with the project leader (Carlos A. Dorao). This form is then placed in the yellow folder located next to the experimental facility.

LabVIEW

This section contains some information about the software used to control and monitor the experimental facility. The software is called LabVIEW (Laboratory Virtual Instrumentation Engineering Workbench) and it has been developed by National Instrument. All the thermocouples, flow meters, heaters and differential pressure transducers are connected to a computer next to the experimental facility. The computer has LabVIEW installed on it. A screenshot of LabVIEW can be seen in Figure 47. The experimental facility is controlled digitally by changing the values of the temperatures and the pump power in LabVIEW.

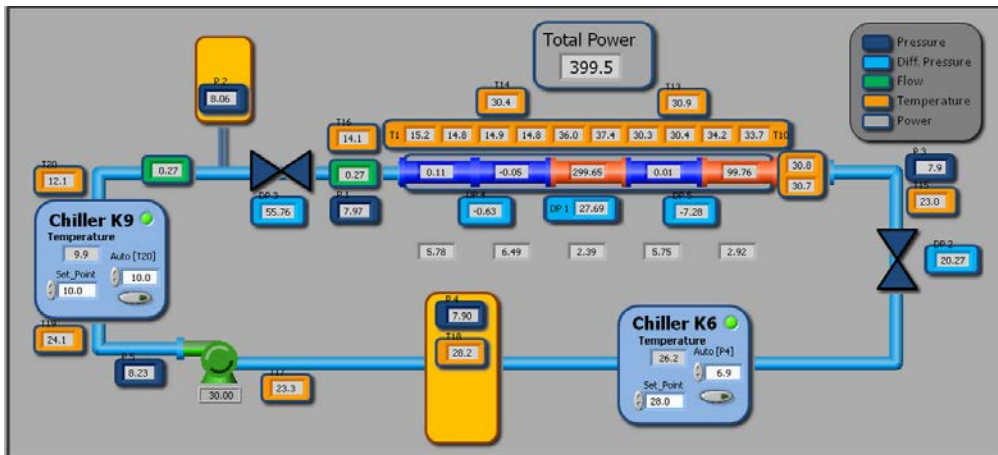


Figure 47: LabVIEW screenshot

It should be noted that the experimental facility can partly also be controlled manually, and this will be explained later.

Starting up the experimental facility

This section contains information on how to start-up the experimental facility. The procedure for starting up the experimental facility is presented in 10 chronological steps, numbered 1 to 10.

Below the 10 chronological steps which must be taken when starting the experimental facility are represented:

1. In order for the experimental facility and the PC to be supplied with power both the contactors, which can be seen in Figure 48, need to be switched on. The contactors are switched on when the black levers inside them are in the upper position. The contractor on the right side is for supplying power for everything except for the K9-heat exchanger, and the contractor on the left side is for supplying power to the K9-heat exchanger.



Figure 48: The contactors

2. The water tap over the water sink, which located next to the experimental facility, must be turned on to supply the K6-heat exchanger with water. The water tap is marked with the red circle in Figure 49. The water tap is turned on when it is in the vertical position with the “on” sign facing upwards. If the water is not turned on while operating the experimental facility, burnout might occur in the K6-heat exchanger.



Figure 49: The water sink

3. Next, the main power of the facility needs to be turned on. This is done by pushing the green button marked as “Start main power” on the door of the locker located next to the K6-heat exchanger. This button is marked with a red circle in Figure 50. When the main power is turned on, the light marked as “Main power ON” will be on.

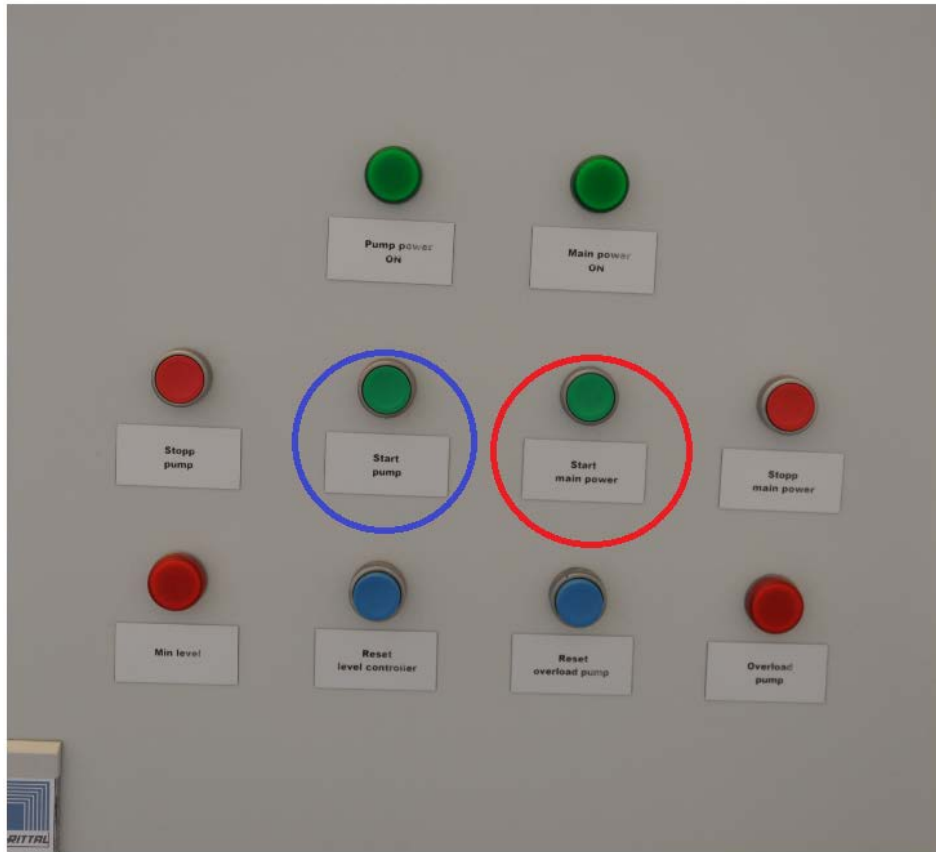


Figure 50: The locker

4. Both the heat exchangers (K6 and K9) in Figure 51 can now to be turned on. They are turned on by turning the round, red knob 90 ° clockwise, so that it is pointing upwards.



Figure 51: Heat exchangers (K6 on the left and K9 on the right)

5. The desired temperature for the heat exchangers can be set in two ways: Either digitally in LabVIEW, or manually on the panel (Figure 52) of the heat exchangers. If the temperature is set in LabVIEW, one should always check on the panel that the inserted value in LabVIEW corresponds to the value on the display of the panel. Setting the temperature on the panel is done by pressing “p” and the up or down arrow, and finally “p” again to confirm the temperature. The panel is identical for both heat exchangers, and the temperature can be adjusted with steps of 0.1 °C. On the display of the panels the temperature in red is the current temperature, and the temperature in green is the desired temperature. The difference between the two temperatures must not be larger than 5 °C when setting the desired temperature. The reason for this is that forcing the heat exchangers to adjust to too large temperature differences can damage them.



Figure 52: Heat exchanger panel

6. The by-pass valve of the pump, which also affects the flow rates in the facility, must be open. The by-pass valve is located next to the main tank (marked with red circle in Figure 53). First the valve should be turned in the clockwise direction until it is closed, meaning that it cannot be turned anymore, and then it should be turned 3-4 times counter clockwise. This will ensure that the valve is properly open.



Figure 53: By-pass valve for pump

7. The power to the pump can now be turned on. This is done by pressing the “Start Pump” button on the door of the locker located next to the K6- heat exchanger. This button is marked with a blue circle in Figure 50. The “Pump power ON” light is switched on when the power to the pump is turned on.

8. Next, the instrumentation panel can be turned on. This is done so that instrumentation such as thermocouples, flow meters and DP cells can be used. The instrumentation panel is located next to the K9- heat exchanger. It is turned on by pressing the “Start power” button marked with a red circle in Figure 54. A confirmation that the instrumentation panel is turned on is that the monitors on the DP cells are turned on. LabVIEW cannot be used unless the instrumentation is turned on.



Figure 54: Instrumentation panel

9. To apply heat to the test section the heating system must be turned on. The heating system is located in the locker under the heated test section. On the right door of the locker (Figure 55) first one must first check if the red “Emergency stop mode 2 activate” light is turned on. If it is turned on, then the knob called “Nødstop” (marked with the blue circle) must be depressed. When “Nødstop” is depressed, the blue button called “Reset safety relay” (marked with red circle) must be pressed. Pressing the “Reset safety relay” button will make the “Emergency stop mode 2 activate” light go off, and the green “Safety relay on” light be turned on.



Figure 55: Panel for heating section, right door

The door of the locker must then be opened with a key and inside a black lever in the right bottom corner must be lifted in the upward position. The blacker lever is marked with a red circle in Figure 56. The lever consists of 5 parts, each for one heating section.

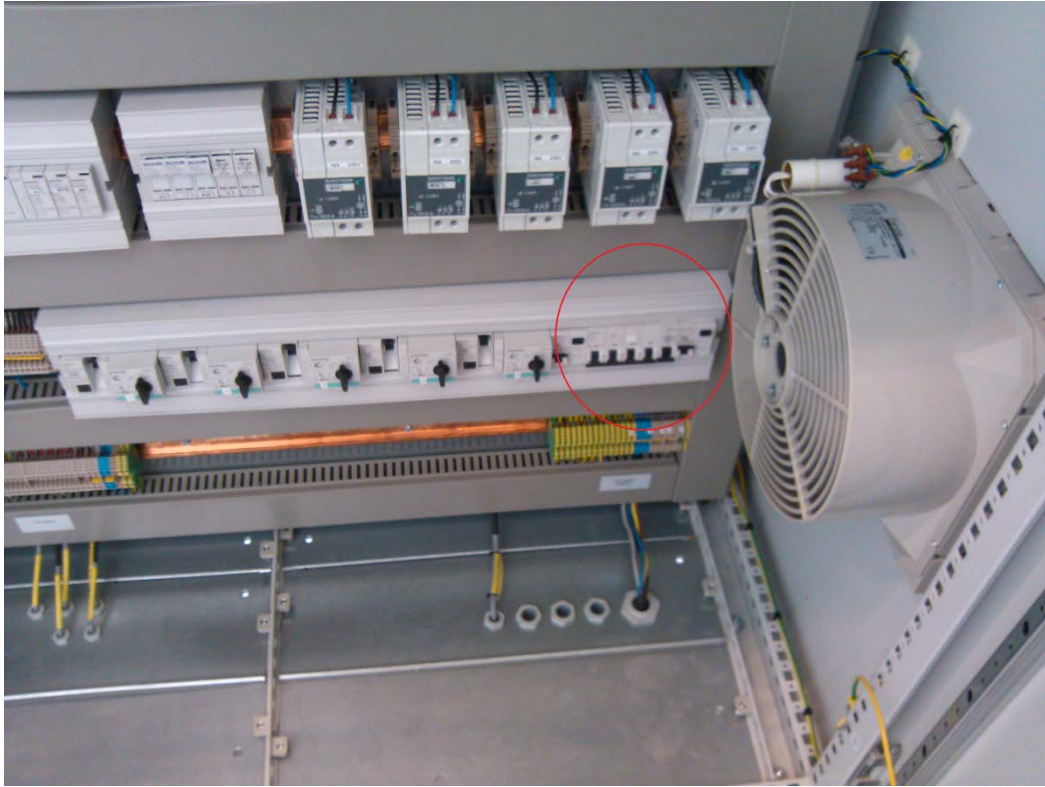


Figure 56: Inside heating locker

10. To apply heat to the test section the heaters must be turned on. The panel for turning on the 5 heaters is located on the door of the locker under the test section (same locker as the “Start main power” button, but left door). Each of the heaters has its own button (Start Zone 1-5) and all the 5 buttons are marked with the red rectangle in Figure 57. The buttons are marked in a counterintuitive way, meaning that heating section where the fluid enters in marked as Zone 5 and the heating section where the fluid exits is marked as Zone 1. The input values of the heaters are controlled in LabVIEW.

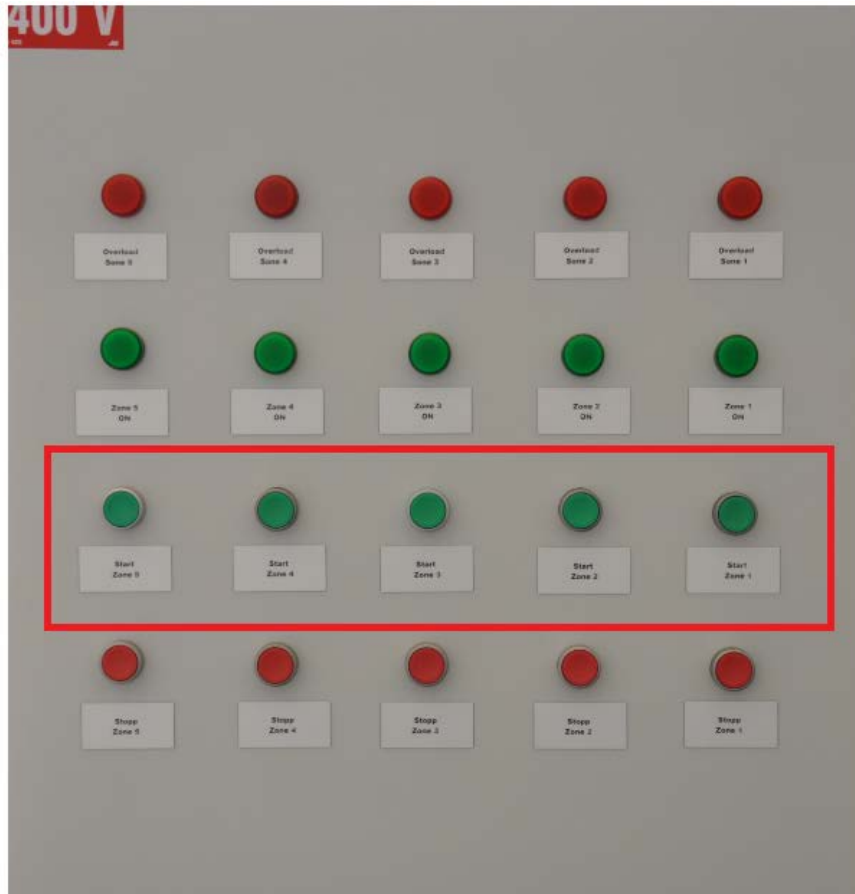


Figure 57: Panel for heating section, left door

Appendix F

The density as a function of pressure for the refrigerant R-134a can be seen in Figure 58.

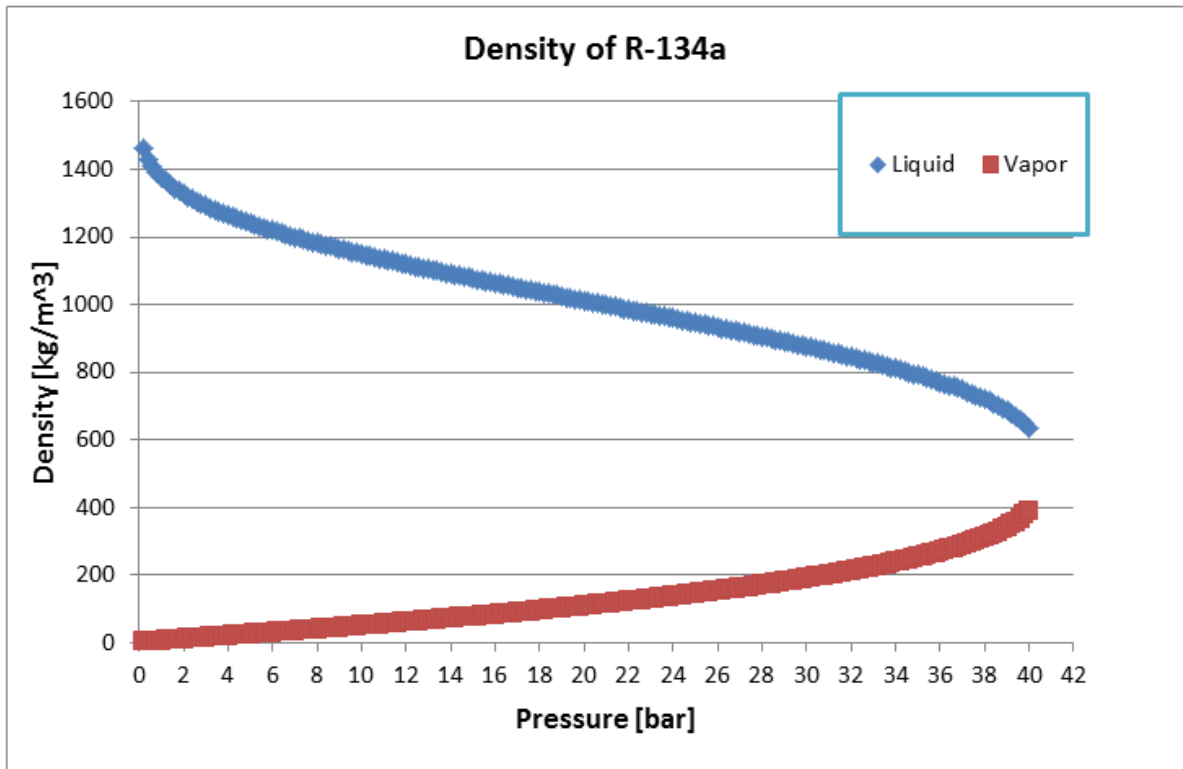


Figure 58: Density as function of pressure for R-134a (values from REFPROP)

Appendix G

The results for the verification of the mass flow meters are reported here. Figure 59 and Figure 60 show the results of the calibration. The x-axis gives the Reynolds number and the y-axis gives the friction factor. The red points are the experimental values obtained from the measurements, while the black points are theoretical values calculated from **(Equation 41)**. F1 is the flow meter before the surge tank, and F2 is the flow meter after the surge tank.

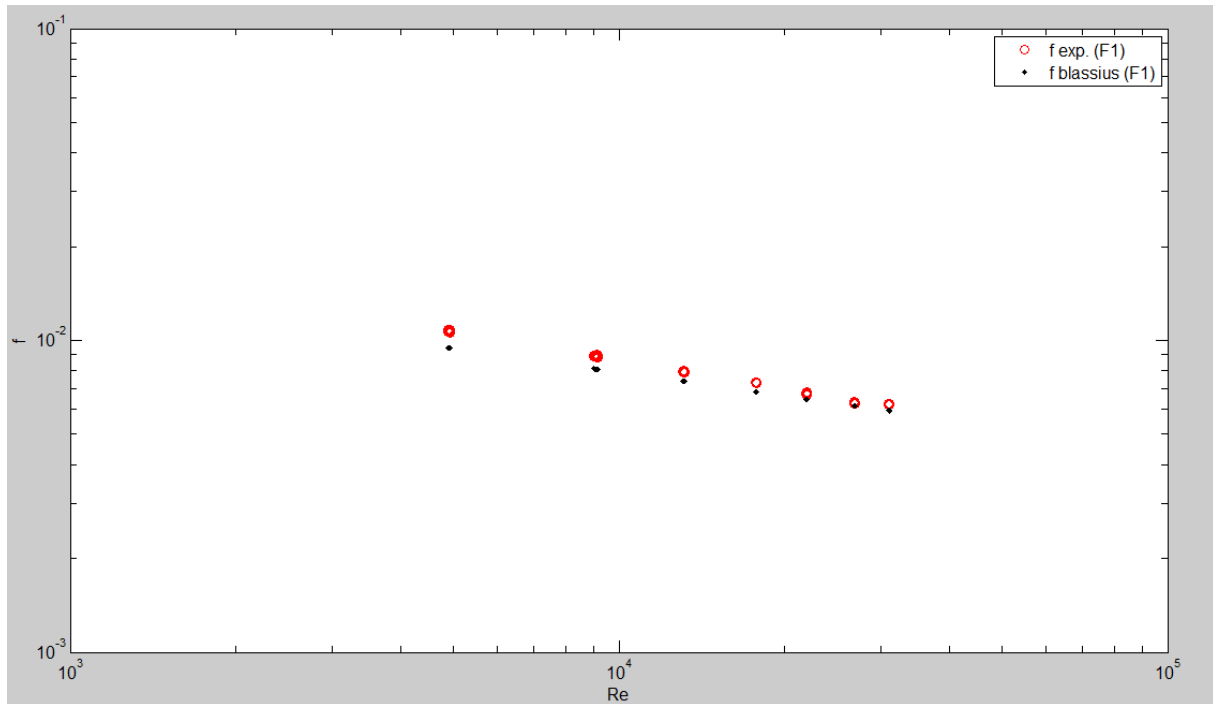


Figure 59: Verification of mass flow meter F1

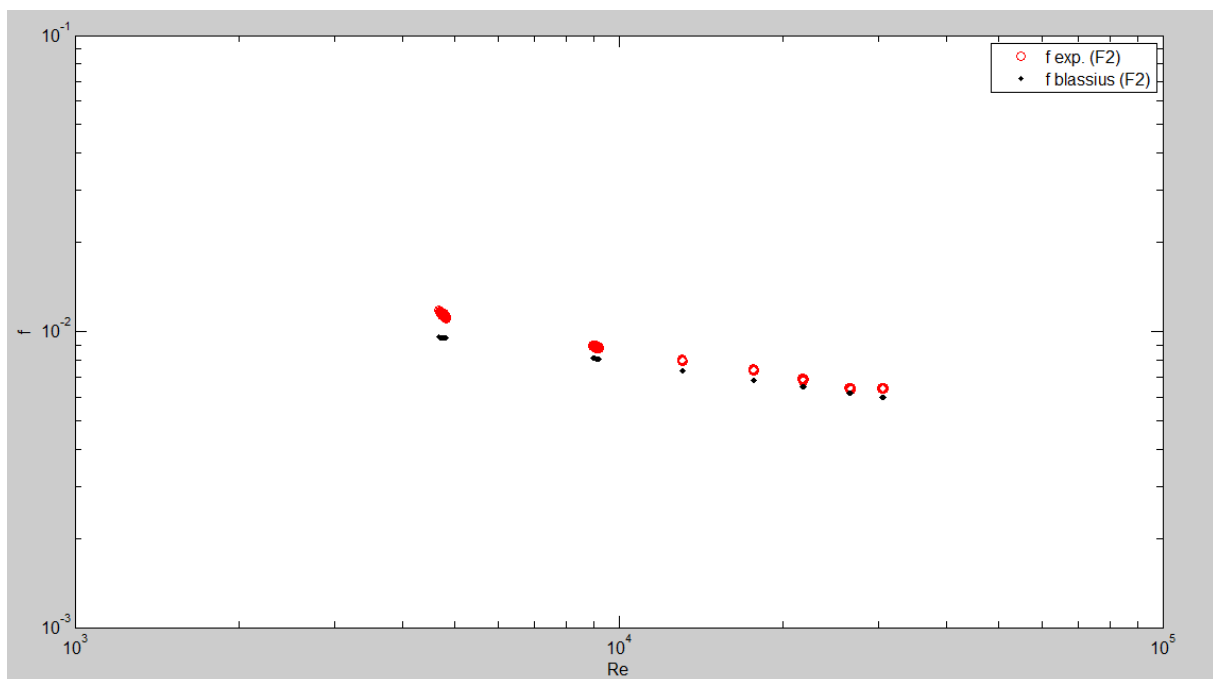


Figure 60: Verification of mass flow meter F2